Study of Ammonia Emissions in a Ventilated Pig Pen

Rong, Li

Publication date:
2011

Document Version
Publisher's PDF, also known as Version of record

Study of ammonia emissions in a ventilated pig pen

PhD thesis
Defended in public at Aalborg University

Li Rong

ISSN 1901-7294
DCE Thesis No. 25

AALBORG UNIVERSITY
Department of Civil Engineering

Aalborg University
Department of Civil Engineering
Indoor climate

DEC Thesis No. 25

Study of ammonia emissions in a ventilated pig pen

PhD thesis defended in public at Aalborg University

by

Li Rong

January 2011

Scientific Publications at the Department of Civil Engineering

Technical Reports are published for timely dissemination of research results and scientific work carried out at the Department of Civil Engineering (DCE) at Aalborg University. This medium allows publication of more detailed explanations and results than typically allowed in scientific journals.

Technical Memoranda are produced to enable the preliminary dissemination of scientific work by the personnel of the DCE where such release is deemed to be appropriate. Documents of this kind may be incomplete or temporary versions of papers—or part of continuing work. This should be kept in mind when references are given to publications of this kind.

Contract Reports are produced to report scientific work carried out under contract. Publications of this kind contain confidential matter and are reserved for the sponsors and the DCE. Therefore, Contract Reports are generally not available for public circulation.

Lecture Notes contain material produced by the lecturers at the DCE for educational purposes. This may be scientific notes, lecture books, example problems or manuals for laboratory work, or computer programs developed at the DCE.

Theses are monograms or collections of papers published to report the scientific work carried out at the DCE to obtain a degree as either PhD or Doctor of Technology. The thesis is publicly available after the defence of the degree.

Latest News is published to enable rapid communication of information about scientific work carried out at the DCE. This includes the status of research projects, developments in the laboratories, information about collaborative work and recent research results.

Published 2011 by
Aalborg University
Department of Civil Engineering
Sohngaardsholmsvej 57,
DK-9000 Aalborg, Denmark

Printed in Aalborg at Aalborg University

ISSN 1901-7294
DCE Thesis No. 25

PREFACE

This thesis is submitted in a partial fulfillment of the requirements for obtaining the degree of Doctor of Philosophy. The work was carried out from May 2007 to July 2010 at the Department of Civil Engineering at Aalborg University and supervised by Professor Peter V. Nielsen. The project was financed by the Ministry of Food, Agriculture and Fisheries under the project of "Reduction of Odor Source in and Emission from Swine buildings (ROSES)". The financial support is acknowledged indeed.

I would like to thank my supervisor, Professor Peter V. Nielsen, for giving me the opportunity to complete my PhD study at Aalborg University. I am especially grateful for his understanding, support and encouragement when I confronted difficulties and failure. I would also like to thank Professor Per Heiselberg for the help during the course of defense preparation.

My thanks also extend to Professor Guoqiang Zhang for the valuable discussions from experiment conductions to scientific paper writing during the whole PhD study. I would like to thank Professor B. Bjerg for the discussion about the full scale pig pen simulations. I am also grateful to all members at Air Physics Lab at Bygholm Research Center at Aarhus University for the help when I was doing experiments there. My sincere thanks are also given to Professor Qingyan Chen at Purdue University and Professor Zhongyi He at Harbin Institute of Technology for their advice and encouragement.

I would also like to thank Professor H. Ezzat Khalifa and Professor Basman Elhididi at Syracuse University for allowing me to visit Syracuse University, giving me the opportunity to join the PhD course 'Fluid Dynamics' and use the Fluent software. I especially appreciate their passion and guidance for the work completed there. I also thank Professor Tong Dang for the discussions and the other PhD students in the office.

I would also like to express my appreciation to all staff members and colleagues at Indoor Climate Group at the Department of Civil Engineering at Aalborg University for their help as well as to Helle Schrøder Hansen and Vivi Søndergaard for linguistic support.

Last but not least, I am deeply grateful to my husband for his love, support and encouragement all the time.

Li Rong

July 2010

ABSTRACT

Pig productions cause a wide emission of odors, such as ammonia (NH_3), hydrogen sulfide (H_2S), and methane (CH_4). Ammonia is one of the most important emissions for evaluating the air quality either in animal buildings or atmospheric environment. In studies of ammonia emission from animal buildings reported in literature, little effort has been made to investigate the accuracy of current Henry's law constant for modeling ammonia mass transfer process and study ammonia emissions in a full scale pig pen from fluid dynamics by CFD simulations. This will be the main objectives of this study.

The ammonia emission rate was measured in a wind tunnel under different airflow and ammonium solution temperatures. This investigation provides a general understanding for the influence of velocity, turbulence intensity and temperature on the ammonia emissions. The relationship between ammonia emissions and boundary layer thickness of velocity are shown linearly under different ammonium solution temperatures.

Using the experiment data measured in the wind tunnel including velocity, concentration and temperature profiles and emission rate, this study adopts computational fluid dynamics (CFD) to investigate the accuracy of Henry's law constants to determine the ammonia concentration in the air through the air-liquid interface. None of the present Henry's law constant models provide a respectable agreement between simulated and measured results. A simplified model to determine the ammonia concentration in the air through the air-liquid interface is suggested from vapor-liquid equilibrium properties of ammonia water. Furthermore, the effects of airflow and temperature on ammonia mass transfer coefficient are also analyzed under different concentration boundary conditions determined by various Henry's law constant models and vapor-liquid equilibrium properties.

The simplified model to determine the ammonia boundary condition on the emission surface has been further used to study the ammonia emissions in a full scale pig pen under different ventilation systems and slatted floor opening ratios as well as various solution temperatures. Under certain assumptions for CFD simulations, the results show that the diffusive ceiling ventilation system can provide a relative low velocity in the pig pen and decrease ammonia emissions from the pig pen, but this ventilation system causes high ammonia concentration distribution in the animal occupied zone. Further, our study shows the effects of slatted floor opening ratios and solution temperature on ammonia emissions and analyzes the influence of those factors on the ammonia mass transfer coefficient.

CONTENTS

Chapter 1

Introduction

Ammonia emission has been of a great concern in agricultural activities. This chapter reviews the problems associated with the ammonia emission and current methodology in measuring and modeling ammonia emissions from ammonium solutions and manure surfaces. The review indicates a need to validate the accuracy of the concentration boundary conditions on the emission surface to model the ammonia emissions by using Computational Fluid Dynamics (CFD) and predict ammonia emissions under different airflow and ammonium solution's temperature in a full scale pig pen, which comprises the major objective of this thesis.

1.1 Overview of problems associated with agricultural emissions

The increasing of odor emissions (e.g., organic acids) and trace gases (e.g., carbon dioxide (CO_2), methane (CH_4), NO_x, NH_3 and H_2S) in the atmosphere has been proved by growing evidence to be related to the increased size and geographical concentration of animal-feeding operations (AFOs) and agricultural crop production (NRC, 2003). Emissions of nitrogen and gaseous sulfur compounds from animal and crop agriculture have become a serious political and environmental problem. In Denmark, the agriculture has been subject to increased environmental requirements. A new environmental regulation for all livestock facilities larger than 3 livestock units (LU) came into force in January 2007. All producers with livestock farms larger than 75 LU must obtain environmental authorization if they wish to extend or modify their production (DPP, 2007). In USA, compliance with increasingly stringent federal and state air pollution regulations pose both economic and technical challenges to agricultural operations. The U.S. Department of Agriculture has taken several steps to respond to the growing need to increase the understanding of the current state of knowledge in this area and to develop socioeconomically beneficial policies (http://www.esa.org/AirWorkshop/issues.php).

Agricultural emissions in Europe are important to several atmospheric transport-related environmental issues. These include local and regional air quality problems, such as PM exposure, eutrophication and acidification, toxics and contribution to greenhouse gas emissions, resulting in a number of environmental impacts and more specifically air quality-related issues (Erisman et al., 2008). Air quality contributes to the condition of human health through exposure of ammonia, toxic organic compounds, pesticides and particulates as well as animal health (Chaoui et al. 2009). In a survey of about 8000 randomly selected farmers in some European countries, pig farmers were identified to be at the highest risk (27.3%) among agricultural workers for the development of symptoms of work-related respiratory illness (Radom et al., 1999). Air quality also contributes to climate change in the form of greenhouse gases and as cooling aerosols. For example, atmospheric nitrogen deposition has been

considered to be one of the top three causes for global biodiversity loss in this century following land use and climate change (Sala et al., 2000).

Among those agricultural emissions, the most important ones are ammonia (90%), PM (20%) and methane and nitrous oxide (both 5%) over Europe (Erisman et al., 2008). Particularly, around 50% of ammonia emissions from pig production stem from pig houses and slurry storage in Netherland, Denmark and France (Van der Peet-Schwering, 1999). In the USA, 90% of the atmospheric NH_3 emission also stem from animal production and emissions from slurries and manures (Davison and Cape, 2003). In livestock buildings, NH_3 is a health risk to animal and people because long term exposure to NH_3 combined with dust can cause severe lung diseases (Seedorf and Hartung, 1999) and high concentration of NH_3 may reduce animal performance (Portejoie et al., 2003). In a survey of ammonia concentration in 82 German livestock buildings, around 31% of the pig and poultry units exceeded the limitation of ammonia concentration and this indicated the need to improve the air quality in pig houses in the future (Seedorf and Hartung, 1999). In addition, NH_3 likely plays an increased role in $PM_{2.5}$ formation as the emissions of sulfur oxides (SO_x) and NO_x are reduced in the coming years (Zhang et al., 2008).

The review of the ammonia emission related problems indicated that it is important to control the ammonia concentration in animal houses as well as decrease the ammonia emissions to the atmosphere. In order to evaluate the amount of ammonia emissions, the methods to measure the ammonia emissions become very significant. Hence, the methods for measuring ammonia emissions from ammonium solution and manure surface are introduced in the next section.

1.2 Methods for Measuring Ammonia Emissions from Ammonium solutions and Manure Surfaces

Since ammonia emissions have such an effect on air quality, it is important to characterize its emissions and obtain reliable emission rate. One of the main problems in measuring the ammonia emission rate is the air sampling method. Table 1.1 lists three types of methods widely used for measuring ammonia emissions from ammonium solutions and manure surfaces in livestock buildings: wind tunnel studies, environmental chamber studies and field studies (Hudson and Ayoko, 2008). There are also other methods for measuring ammonia emissions from livestock buildings such as feed and manure nitrogen balance, summation of local ammonia sources and micrometeorological methods, static headspace analysis etc(Shah et al. 2006, Phillips et al. 2000). For example, in the headspace analysis a specimen of emission sources is placed in a small, airtight container (headspace vial) made of inert and emission-free material. Samples of the air inside the container are analyzed by gas chromatography (GC) with mass spectrometry to identify the compounds and determine the compound concentrations emitted from the emission sources. But these methods are more concerned with analyzing ammonia emissions using chemistry and cannot even provide emission data at all (Headspace analysis) and are therefore not discussed in

this chapter. We mainly focus on the methods for measuring ammonia emissions from fluid dynamics.

Table 1.1 Typical methods for measuring ammonia emissions

Methods	Description	Pros	Cons
Wind tunnel studies	Measure emissions in a wind tunnel	• Provide emission rate data under well controlled environmental conditions • Cheap compared to full scale chambers studies and field studies • Being able to compare the mass transfer coefficient with some classical studies before	• Limitations of transforming the emission data to actual pig pens
Environmental chamber studies	Measure emissions in small scale chambers	• Provide emission rate data under well controlled environmental conditions • Cheap compared to full scale chambers	• Limitations of transforming the emission data to actual pig pens
	Measure emissions in full scale chambers	• Provide emission rate data under actual environmental conditions	• Expensive compared to small scale chambers • Difficult to control local environmental parameters (e.g. local velocity)
Field studies	Measure emissions in actual pig houses	• Provide integrated emission profile affected by other emission gases under uncontrolled conditions	• Differentiating the coupled effects of environmental conditions and other gas releases on ammonia emissions extremely difficult

1.2.1 Wind tunnel studies

Using wind tunnel techniques, terrain and topographical features could be controlled and useful data translatable to real life situations could be obtained in a wide range of air pollution problems (Sharma et al. 2005). Wind tunnel has been used to estimate ammonia emissions from arable land (Loubet et al. 1999a, 1999b) as well as to estimate odour emissions from piggeries (Smith & Dalton, 1999) and feedlots (Smith &Watts 1994a, 1994b). During an investigation of odour emissions from feedlots, Smith and Watts (1994b) compared emission rates obtained from two wind tunnels. The odour emission rate to velocity relationships was very similar for both tunnels.

Smith (1993) also demonstrated that odour emission rates estimated from samples derived from wind tunnels were consistent with those derived from a simple Gaussian dispersion model. It was the first time a device-independent method had been used to validate odour emission rates derived from a wind tunnel. Loubet et al. (1999a, 1999b) evaluated the wind tunnel techniques for estimating ammonia volatilization from land and suggested that the wind tunnel sampling system could decrease the error to measure the ammonia emission rate due to sampling in a small percentage. Furthermore, wind tunnel studies can control the environmental conditions well and analyze the mass transfer process above the emission surface using boundary layer theory. Rong et al. (2009) studied the ammonia emissions from a wind tunnel and analyzed the effects of airflow and ammonium solution temperature on ammonia emissions. Besides, they also show the relationship between ammonia emissions and velocity boundary layer thickness using boundary layer theory.

Generally, the entire wind tunnel system includes a wind tunnel, a container for providing an emission surface, an environmental enclosure, air supply system and concentration sampling system. To avoid the ammonia sorption on the wall of the wind tunnel, the wind tunnel is usually made of stainless material or the inside of the wind tunnel is painted with a special epoxy which is chemically inert.

1.2.2 Environmental chamber studies

Environmental chambers are usually used to obtain emission data. Two types of chambers are commonly employed for emission testing: small-scale chambers and full-scale chambers. Compared to full-scale chambers, small-scale test chambers are less expensive and widely used. The entire chamber system includes an environmental test chamber, an environmental enclosure to house the chamber, equipment for supplying air to the chamber and outlet fittings for sampling the air from the chamber's exhaust. To avoid possible absorption and emission from the chamber itself, all the materials and components in contact with the emission sources should be chemically inert.

Small chambers have the advantages of being less expensive and well-controlled ambient environmental conditions while they also have obvious limitations. The flow and thermal conditions in a small-scale test chamber cannot adequately represent the whole range of conditions in a real building (Yang, 1999). Emission data measured using a small-scale chamber may not be applicable to buildings. Topp (1999) discussed the influence of scale on the evaporative emission processes and showed that different mass transfer coefficients are found in two geometries at the same velocity. It might be explained by the different velocity profiles and turbulence scale in those two geometry models.

A full-scale chamber usually consists of a full-size room and an HVAC system. Similar to small-scale chambers, a full-scale chamber also consists of a data acquisition system for sampling and analyzing the ammonia emitted from the

ammonium solution or manure surface. Hence, a full-scale chamber is much more expensive and difficult to operate than a small-scale chamber.

The measurement of ammonia emissions in small-scale or full-scale chamber can be either direct or indirect. An example of direct measurement is the use of an electronic balance to monitor the weight decay of an emission source as a function of time (Arogo et al. 1999). Although this measurement provides the most direct information on emissions, it also has limitations. For instance, the method is only applicable for sources that have a large emission rate and fast decay. For many components of odor the emission rates are so low that the weight decay cannot be accurately detected by an electronic balance even with a high resolution. In these cases, direct measurements are not applicable. Indirect measurement monitors time-dependent concentration change resulting from emissions of ammonia. The methods of calculating emissions based on the measured concentration data will be discussed in section 1.3.

1.2.3 Field Studies

While environmental chamber studies are useful for determining emission rates of ammonia under controlled conditions, they still cannot measure the contaminant exposures in actual livestock buildings. Field studies provide an opportunity to monitor the air pollution level and evaluate factors such as variable air exchange rates, manure temperature, pH value of the manure and animals' weight and activities on odor emissions.

Literally many field studies have been conducted to investigate the odor emissions from animal houses. Unfortunately, the emission sources in the animal houses share common emission profiles in terms of the compounds emitted. Thus, isolating the source of common indoor pollutants based on indoor measurements may be impossible. In addition, some compounds of odors can be absorbed by the structures and water inside the animal houses and then re-emits from those sources, for instance, ammonia. Hence, field study results generally only provide an integrated assessment of odor emissions from a multitude of sources and re-emitting sources under uncontrolled conditions.

1.3 Methods for Modeling Ammonia Emissions from Ammonium Solutions and Manure Surface

Before discussing the methods for modeling ammonia emissions from livestock buildings, it is worthwhile to briefly mention the factors that may affect ammonia emissions. Ammonia emissions from livestock buildings are affected by many factors such as the environmental conditions (airflow rate, temperature, humidity, turbulence etc.), ammonia concentration in the slurry, temperature of the slurry, the emission surface, head space below the slatted floor, pH value of the slurry etc (Griffing et al., 2007; Ni 1999; Aarnink and Elzing, 1998). In general, these factors can be classified into two categories:

(1) Internal factors: the properties of the solution or the manure such as the pH value, concentration, temperature;
(2) External factors (or environmental conditions): the surrounding conditions such as airflow, temperature, humidity and ammonia concentration in the bulk air. These factors exist independent of the manure.

Theoretically, the characteristics of odor emissions can be predicted with sufficient knowledge of each individual factor. However, this is very difficult in practice because the manure behaves like a black 'box'. Odor emissions observed by experiments reflect very few perspectives from outside the 'box', resulting from interactions of numerical internal and external factors. Therefore, an emission model should be developed based on the experimental data. The purpose of the experimental data is to provide some knowledge on the impact of influencing factors, either internal or external, on emissions. In general, two modeling approaches are usually employed.

The first approach is to derive a mathematical model based on the observation and statistical analysis of emission data obtained from environmental chamber testing or field measurements. The model derived from environmental chamber and scaled model could give a general understanding of the effects of airflow on the emissions, but the transformation of emissions from the chamber and scaled model to full scale model is almost impossible. Ye et al. (2009) developed an experimental model of ammonia emission in a scale model, which was a function of mean air velocity and turbulence intensity. The mean air velocity was represented by the value of points located 13mm above the manure surface. This definition for mean air velocity is controversial and random so that the application of this emission model can probably only be used in this specific geometry model. Cortus et al. (2008) developed a dynamic model of ammonia emission from urine puddles which considered the processes of evaporation, urea conversion, change in liquid concentration and puddle pH using an environmental chamber.

The model derived from the field studies can provide a comprehensive estimate of ammonia emissions on site but the impact of internal and external factors on emissions are all lumped together. Aarnink and Elzing (1998) developed a dynamic model to simulate the ammonia volatilization from pig housing with partially slatted floors. The input of the model included emitting surface temperature, air velocity, pH, TAN (Total Ammonia Nitrogen), emitting surface area etc. These empirical emission models are easy to use, but they are not able to provide insight into physical emission mechanisms.

The second approach is to develop models based on mass transfer theory. This type of model is developed in light of notion that ammonia emissions from manure surface are governed by well-established mass transfer principles and hence are predictable using mechanistic mathematical models. From a mass transfer point of view, two main mechanisms contribute to ammonia emissions: ammonia diffusion in the manure as a result of a concentration gradient which can be described by the Fick's law, and

interfacial mass transfer due to the interaction of the manure surface with the adjacent air. In general, external factors govern the interfacial mass transfer and the internal factors of the manure can be attributed to a few physical properties (e.g. diffusivity) and the equilibrium chemical actions among different compounds. The mechanisms of ammonia emissions are shown in Figure 1.1. Besides the internal diffusion mass transfer, equilibrium chemical actions and interfacial mass transfer process, the equilibrium of ammonia concentration at the gas-liquid interface also exists, which can be described by Henry's law constant. Unlike the empirical models, mass transfer-based models allow separation of internal and external factors. This allows scaling the model parameters developed from environmental chambers to actual buildings.

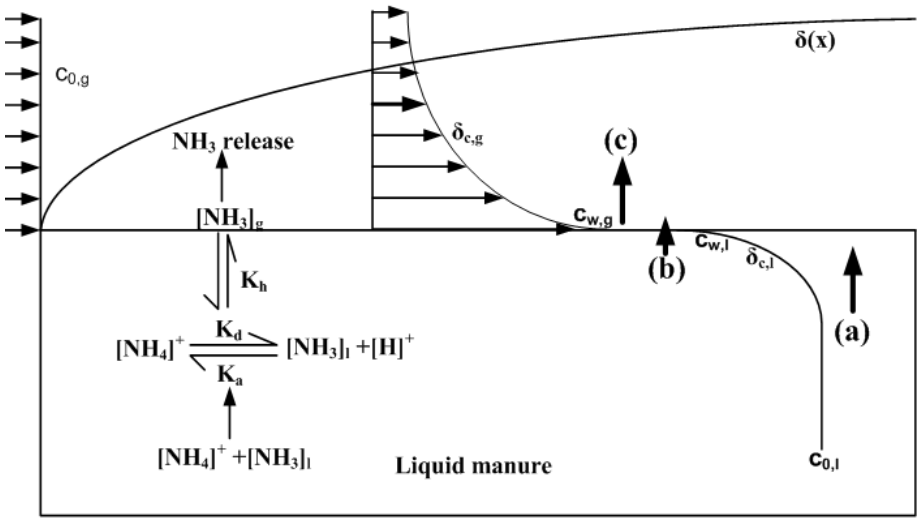

Figure 1.1 Illustration of ammonia emission mechanism from liquid manure to the air. (a) diffusion inside the liquid; (b) mass transfer through the gas-liquid interface; (c) evaporation.

Currently, the models of ammonia emissions based on the mass transfer theory can be found in literatures. Olesen and Sommer (1993) developed a mechanistic model for calculating ammonia emissions from stored slurry. The internal diffusion of ammonia was modeled by Fick's law and the interfacial mass transfer coefficient was modeled by a series of semi-experimental functions to estimate the resistance in the turbulent layer above the slurry, resistance in the laminar boundary between the gas-liquid interface and the turbulent layer and resistance of the slurry cover. Zhang et al. (1994) developed a computer model for predicting ammonia emission rates from manure pits in swine buildings. The model coupled ammonia diffusion and generation in the manure with ammonia emission from the manure surface. Ni et al. (2000) developed a dynamic mathematical model of Carbon-dioxide Accelerated Ammonia Release (CAAR) based on the known knowledge of the chemistry of ammonia in liquid solution, mass transfer inside and across liquid-gas interface. This model provided a quantitative description of some new understanding of the mechanism of ammonia

release in the pig house. Montes et al. (2009) reviewed the process modeling of ammonia volatilization from ammonium solution and manure surfaces and recommended the models to determine the parameters accordingly by validation of experiments data obtained from a flux chamber. They employed the mass transfer coefficient as a function of the flow Reynolds number (Re) and the ammonia Schmidt number (Sc). However, the validation of these models was based on a small scale flux chamber and may not be applicable to buildings in which the flow conditions usually cannot be represented by a single Reynolds number.

The above studies provided much information on ammonia emission mechanisms and theoretical analysis of parameters needed determining in models development even though they are only one-dimensional modeling. However, it was unavoidable to employ some empirical functions of ammonia mass transfer coefficient in the air, Henry's law constant to determine the ammonia concentration on the emission surface at the air side and ammonium dissociation constant in the solution/manure. Unfortunately, these mass transfer coefficient models were developed either from environmental chamber test or borrowed from the infinite plate using boundary layer theory analysis, which may not be applicable to the actual livestock buildings. Therefore, Computational Fluid Dynamics (CFD) is employed by some researchers to study the VOC emissions from office buildings and greenhouse gas emissions from animal houses. Besides, the definition of the Henry's law constant varies greatly in literature (Montes et al. 2009). Staudinger and Roberts (1996), Ni (1999) and Renard et al. (2004) have pointed out variations in the units used to quantify the value of Henry's law constant, as well as in the values obtained when the estimates are transformed to common units. The difference of the Henry's law constant can be three-fold. At present, the accuracy of applying Henry's law constant model to determine the ammonia concentration on the air side is seldom studied and we therefore do not know the error caused by Henry's law constant to predict the ammonia emissions from the manure.

Although there is general agreement that ammonia emissions from manure can be described by fundamental mass transfer theories, the above mentioned indicates that it is impossible (quite difficult at least) to develop a generalized model of mass transfer to predict the ammonia emissions from livestock buildings. Further, the accuracy of Henry's law constant to determine the ammonia concentration on the air side through the gas-liquid interface should also be studied. This suggests a need to apply CFD in order to predict the ammonia emissions at various environmental conditions and manure properties, which will not be limited by geometry scales and modeling dimensions, and to validate the boundary conditions of concentration on the emission surface determined by Henry's law constant.

1.4 Aim of the Present Work

As discussed above, ammonia emissions from pig productions in recent years have been the subject of considerable studies. However, due to the complexity of the emission processes, the studies are still mainly done by the experimental approach. In the past, many environmental chamber tests and field tests have been conducted to identify the effects of airflow and manure properties on ammonia emissions. The ultimate goal of such studies is to provide accurate and sufficient information for designing a healthy indoor environment. In order to realize this objective, the following questions have not been answered yet by present studies:

(1) What does the emission data measured from an environmental chamber or wind tunnel mean in actual buildings in which environmental and boundary conditions are usually significantly different from those of test chambers?
(2) What is the accuracy of present Henry's law constant models to determine the ammonia concentration in the air side through the gas-liquid surface?
(3) How can we reduce indoor contaminant levels using control or mitigation strategies, such as selecting effective ventilation system?

The purpose of this thesis is to address the three questions mentioned above. This thesis is organized as follows. In Chapter 2, the ammonia emissions from an ammonium solution surface in a wind tunnel are measured as well as the velocity, concentration and temperature profiles in the boundary layer above the emission surface. The purpose of the study is to understand the effects of environmental conditions (e.g. velocity, velocity fluctuation) on ammonia emissions. In Chapter 3, the accuracy of present popular Henry's law constant models is validated using CFD simulations. The experiment data obtained from Chapter 2 are used to validate the numerical models in CFD software and the accuracy of the concentration boundary condition on the emission surface determined by Henry's law constant. In Chapter 4, the effects of airflow rate, ventilation system and temperature on ammonia emissions are studied in a full-scale pig pen. The concentration boundary condition of the emission surface validated in Chapter 3 is applied in these studies. Chapter 5 provides general conclusions and recommendations based on the investigations in this thesis.

Chapter 2

Measurements of ammonia emissions from an aqueous solution in a wind tunnel

In this chapter, the ammonia emissions from an aqueous solution were measured. The purpose of this study was to systematically investigate the effects of environmental conditions (temperature, velocity and turbulence intensity) on ammonia emissions. The experiments were conducted in a wind tunnel with a cross section of 0.5m×0.5m. The results indicated that both the velocity and solution temperature had important effects on ammonia emissions while the turbulence intensity proved not to be important according to the ANOVA analysis. The measured data (e.g. ammonia emissions and profiles measured in the boundary layer) were used to validate the turbulence models and the concentration boundary conditions on the emission surface, which will be the focus of the next chapter.

2.1 Introduction

Ammonia emissions and deposition to terrestrial and aquatic ecosystems have increased nearly four-fold in the past 135 years. Much of the increase has been associated with an increase in agricultural activities, especially with respect to animal productions (Lynch and Kerchner, 2005). In Denmark, approximately 50% of ammonia emission from pig production is from pig housing and slurry storage (Van der Peet-Schwering et al. 1999). Hence, understanding the emission characteristics of ammonia is important in order to decrease the effects of ammonia emission on atmosphere environment and natural ecosystem as well as improving the indoor air quality in the pig houses.

The amounts of ammonia emitted from manure were usually measured using environmental chambers, wind tunnel and field test. To fully understand the emission characteristics of ammonia from liquid manure, the factors that affect emissions must be identified and evaluated. Using environmental chambers, previous studies have found that ammonia emissions from liquid solutions are likely to depend on environmental conditions (e.g. temperature, air velocity, turbulence, humidity) and liquid properties (e.g. diffusivity, pH value, Total Ammonium Nitrogen (TAN) concentration) (Arogo et al. 1999; Ni 1999). Currently, a wide variety of experimental data on emission characteristics of ammonia from environmental chamber, wind tunnel and scaled model can be found in the literature. However, most of the data were obtained by isothermal cases from a small-scale environmental chamber. Although some investigations have either measured or addressed the impact of environmental parameters such as temperature and airflow on ammonia emission from aqueous solution, detailed information on airflow and boundary conditions of ammonia concentration on the emission surface are not available to validate the model using Computational Fluid Dynamics (CFD) simulations in the following chapters.

Therefore, experiments to measure ammonia emission using a wind tunnel (0.5m×0.5m) were conducted under different airflow conditions and ammonium solution temperatures. Data obtained from the wind tunnel measurements are used to validate the turbulence models and boundary conditions of concentration on the emission surface.

The following section discusses the experimental methods for measuring ammonia emissions, a description of the testing results and analysis.

2.2 Experimental Method

According to the discussion of the ammonia emission mechanism from manure in chapter 1, it is indicated that the mass transfer process from the manure to the air is complex. In order to avoid the ambiguity of the ammonia mass transfer process caused by other gases, the solution made for the measurements was simplified. It was introduced in the section 2.3.1.2. In this section, the test facility, test conditions and cases, along with the test procedure are presented sequentially. An analysis of the measured data is presented at the end of this section.

Experiments were conducted in a wind tunnel with cross section of 0.5m×0.5m, see Figure 2.1. The wind tunnel provided the control for velocity and turbulence intensity over the emission surface during testing. The air was supplied through perforated plate at the belt mouth and exhausted by the fan unit at the end of the wind tunnel through the tube to another room. Two perforated plates were used to generate different turbulence intensity. The airflow rate was controlled by the orifice and monitored at a computer. The computer was used to monitor and/or control the test conditions, including the air-exchange rate, temperature and relative humidity at the inlet and outlet. The evaporable components were ammonia and water. They evaporated from an ammonia aqueous solution. The emission surface was located at 2.05m downstream from the belt mouth.

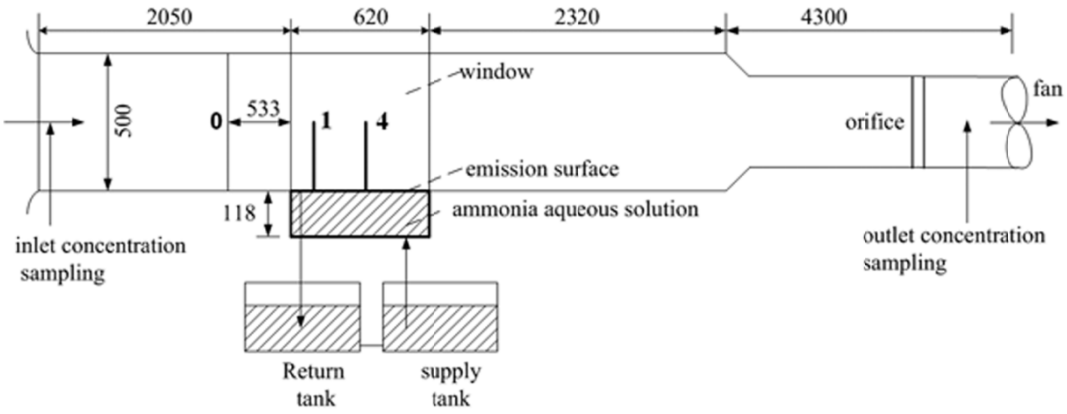

(a) sketch of wind tunnel

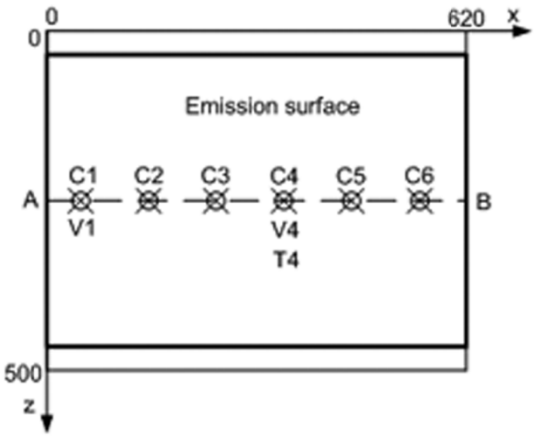

(b) top view of the emission surface

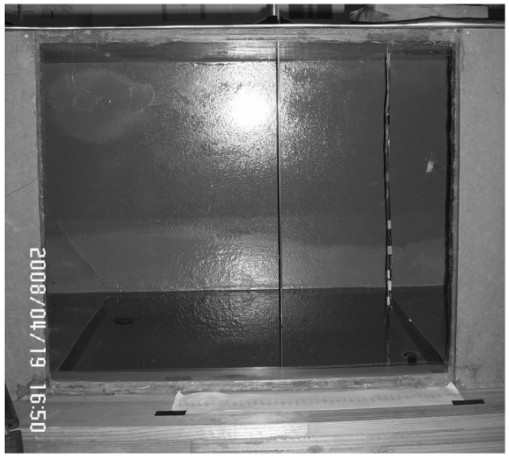

(c) photo of emission surface

Figure 2.1 the wind tunnel for emission measurements. '⊠' represented the measuring location, 'V', 'T' and 'C' represented velocity, temperature and concentration respectively.

2.2.1 Tested parameters

2.2.1.1 Velocity and velocity fluctuation

Velocity and velocity fluctuation have been measured at inlet and boundary layer by Laser Doppler Anemometry (LDA). LDA measures velocity using light beams at a point in the flow seeded by small particles which could follow the turbulent motion of the flow. It senses true velocity component and measures the component in a sequence of near instantaneous samples. The signal is time series and this allows common statistical data analysis to the velocity information. The integration time of velocity measurement varied according to the value of velocity fluctuation in a range from 6 min to 20 min. Data was recorded by a computer that was connected to the signal processor and analyzed by LDA software package. The seed particles were generated by a fogger generator (FOG 2010) using standard liquid. The instrument and inlet combination were shown in Figure 2.2. The turbulence intensities representative of the cases are 10%, 16% and 35% from the left to the right

respectively in Figure 2.2(b). The definition of the turbulence intensity was given in section 2.2.4.3.

(a) photo of LDA

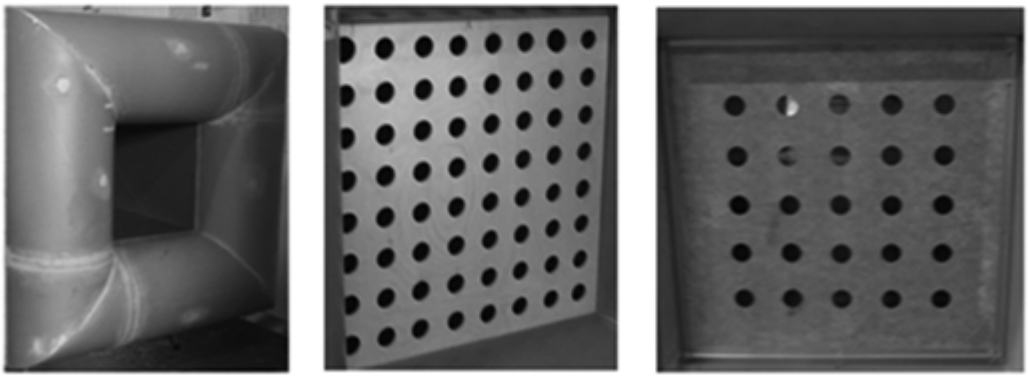

(b) photo of inlet set-up

Figure 2.2 photo of LDA and inlet set-up

2.2.1.2 Ammonia aqueous solution and ammonia concentration

Ammonia aqueous solution was made of NH_4Cl, Na_2CO_3 and $NaHCO_3$. NH_4Cl was the source of the emitted ammonia while Na_2CO_3 and $NaHCO_3$ buffered the solution to keep the solution's pH value constant. Two tanks stored 180L aqueous ammonium solution and the solution was circulated at a low flow rate (0.5L/min) between these two connected tanks. The 'Total Ammonia Nitrogen' (TAN), pH and solution temperature were measured before and after measurements were performed each day. Meanwhile, the stability of ammonium solution was also studied for case that the velocity was 0.3m/s and turbulence intensity was 35%, shown in Figure 2.3. The results demonstrate that the solution could generate ammonia emission under steady state condition.

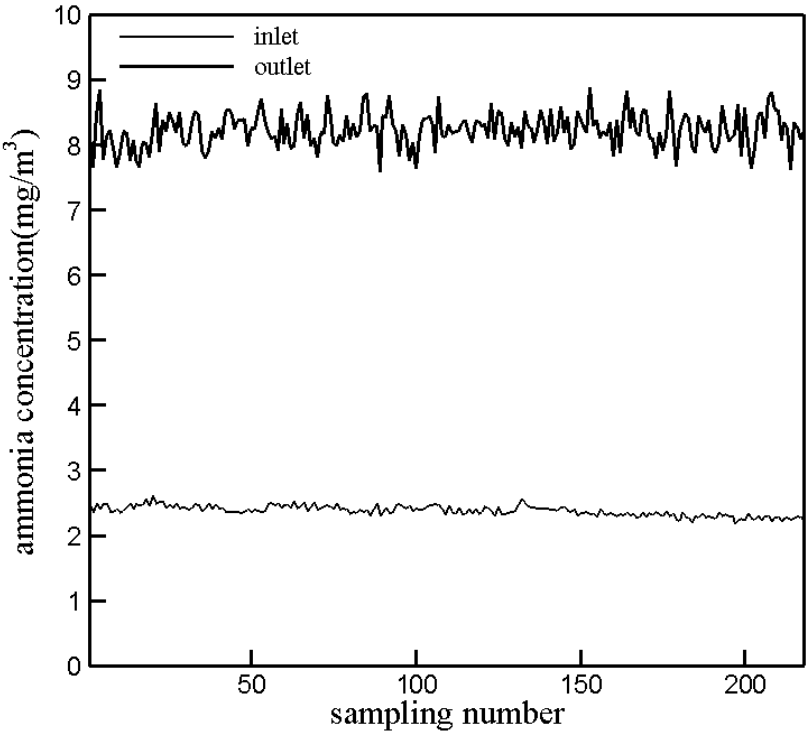

Figure 2.3 Stability study of ammonium solution for one day measurement

TAN was measured according to ISO 7150/1. The samplers were diluted in proportion of 1:100 with distilled water in a test tube. One level of blue micro-spoon of reagent NH_4^{-2} was added into the test tube and the tube was vibrated vigorously until the reagent was completely dissolved. The test tube was then put in a Spectraquant NOVA 30A to measure the TAN after leaving the test tube to stand for 15 min. The pH value and temperature of the samples were measured by a standard electrode of pH meter (Sension 1, HACH-LANGE). The TAN was 6800mg/l and pH value was 8.98 with liquid temperature in 22.3℃. During the course of experiments, the TAN was kept the same while the pH value changed with the solution temperature, summarized in Table 2.1. However, it should be mentioned that the pH value and TAN in experiments were a little higher than the value in pig manure in order to obtain higher ammonia concentration in the air to increase the accuracy of the measurements. On the other hand, the higher pH value can eliminate the effects of CO_2 release on ammonia emissions (Ni et al. 2000) because CO_2 can hardly exist in the solution at this pH value (9.0 or higher).

The ammonia concentration at inlet, outlet and boundary layer were measured by Photoacoustic Multi-gas Monitor 1312 and a Multiplexer 1309 (*INNOVA* Air Tech Instruments A/S), seen in Figure 2.4, which was connected to another computer to monitor the concentration continuously. The instruments were calibrated by the company before the measurements. The sample integration time was 20s and the measuring time for every point was 45 min. The concentration of ammonia was measured sequentially at the inlet, outlet and along the boundary layer profiles.

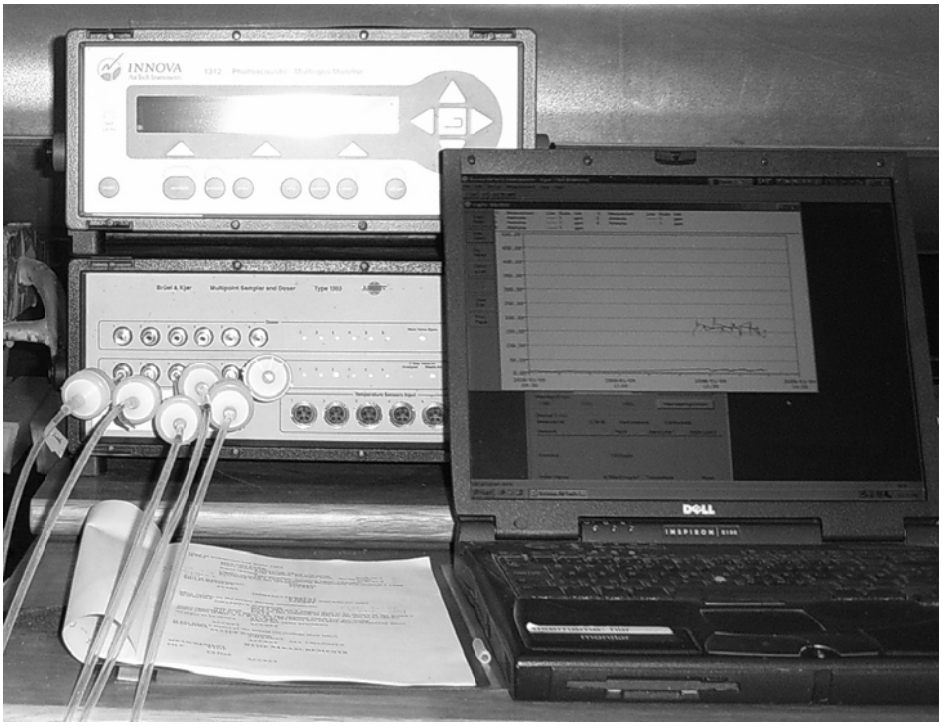

Figure 2.4 photo of Innova instruments

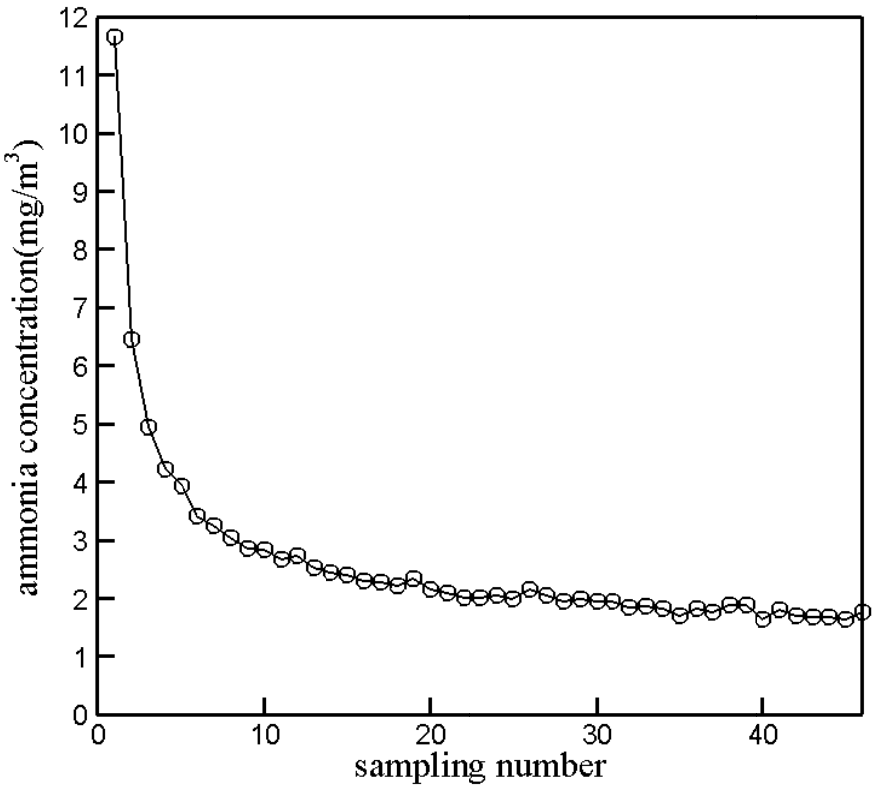

Figure 2.5 Inlet concentration sampling after switched from outlet concentration sampling

Measurements were made continuously at each location for 45 min before being switched to another measuring point. It was noticed that at least 15 min were needed for concentration value to stabilize following measurement of high concentration samples, see Figure 2.5. This can be explained by the time it took to assure that the chamber was completely replaced by the 'new' air before the 'old' air was flushed out, especially when the concentration of the 'old' air was high.

2.2.1.3 Temperature, humidity and pressure

When the ammonia solution was cooled, the supply tank and return tank were isolated by polyphenyl board. The tubes connected to the tanks, container and the cooling machine were isolated with Aeroflex closed cell insulation tubes. The temperature and humidity at inlet and outlet were measured by Testo 400 multi-parameter instrument with system accuracy of ±0.5℃. The data was sampled every one minute. The temperature profiles in boundary layer were measured by thermocouples (Type T, copper-constantan). These data were recorded by a data logger (Squirrel module M25, Eltek Ltd.) and sampled every five seconds and averaged every two minutes. The pressure difference through the orifice was recorded by a data logger (CR215, Campbell Scientific, Inc.) and monitored on the computer simultaneously.

2.2.2 Test conditions and cases

The experiments were designed to study the effects of velocity, turbulence intensity and ammonium solution temperature on ammonia emissions. The wind tunnel was operated at four velocities, i.e., 0.4m/s, 0.3m/s, 0.2m/s and 0.1m/s; four temperatures, i.e., 22.0±0.5℃, 15.0±0.5℃, 10.5±0.5℃ and 6.5±0.5℃; and three turbulence intensity levels, i.e., 35%, 16% and 10%. The air temperature was the same through the experiments as 22.0±1.0℃. The humidity of the air in the lab was 37%±3%. Table 2.1 summarizes the total 48 test cases.

Table 2.1 Test cases

Case	Environmental conditions				Liquid conditions		
	u (m/s)	T_{air} (℃)	Turbulence intensity (%)	Relative humidity (%)	T_{liquid} (℃)	TAN (mg/l)	pH
Tu10T22u4	0.4	22.0±1.0	10	37±3	22.0±0.5	6800± 300	8.98
Tu10T15u4					15.0±0.5		9.12
Tu10T10.5u4					10.5±0.5		9.22
Tu10T6.5u4					6.5±0.5		9.31
Tu16T22u4			16		22.0±0.5		8.98
Tu16T15u4					15.0±0.5		9.12
Tu16T10.5u4					10.5±0.5		9.22
Tu16T6.5u4					6.5±0.5		9.31
Tu35T22u4			35		22.0±0.5		8.98

Tu35T15u4					15.0±0.5		9.12
Tu35T10.5u4					10.5±0.5		9.22
Tu35T6.5u4					6.5±0.5		9.31
Tu10T22u3					22.0±0.5		8.98
Tu10T15u3			10		15.0±0.5		9.12
Tu10T10.5u3					10.5±0.5		9.22
Tu10T6.5u3					6.5±0.5		9.31
Tu16T22u3					22.0±0.5		8.98
Tu16T15u3	0.3		16		15.0±0.5		9.12
Tu16T10.5u3					10.5±0.5		9.22
Tu16T6.5u3					6.5±0.5		9.31
Tu35T22u3					22.0±0.5		8.98
Tu35T15u3			35		15.0±0.5		9.12
Tu35T10.5u3					10.5±0.5		9.22
Tu35T6.5u3					6.5±0.5		9.31
Tu10T22u2					22.0±0.5		8.98
Tu10T15u2			10		15.0±0.5		9.12
Tu10T10.5u2					10.5±0.5		9.22
Tu10T6.5u2					6.5±0.5		9.31
Tu16T22u2					22.0±0.5		8.98
Tu16T15u2	0.2		16		15.0±0.5		9.12
Tu16T10.5u2					10.5±0.5		9.22
Tu16T6.5u2					6.5±0.5		9.31
Tu35T22u2					22.0±0.5		8.98
Tu35T15u2			35		15.0±0.5		9.12
Tu35T10.5u2					10.5±0.5		9.22
Tu35T6.5u2					6.5±0.5		9.31
Tu10T22u1					22.0±0.5		8.98
Tu10T15u1			10		15.0±0.5		9.12
Tu10T10.5u1					10.5±0.5		9.22
Tu10T6.5u1					6.5±0.5		9.31
Tu16T22u1					22.0±0.5		8.98
Tu16T15u1	0.1		16		15.0±0.5		9.12
Tu16T10.5u1					10.5±0.5		9.22
Tu16T6.5u1					6.5±0.5		9.31
Tu35T22u1					22.0±0.5		8.98
Tu35T15u1			35		15.0±0.5		9.12
Tu35T10.5u1					10.5±0.5		9.22
Tu35T6.5u1					6.5±0.5		9.31

2.2.3 Test procedures

When the velocity was measured, the released particle to measure the velocity would seriously affect the accuracy of concentration measurement. Because of this limitation of INNOVA instruments, ammonia concentration couldn't be measured at the same time with the velocity measurement. Therefore, the procedures for tests were as follows:

(1) The pure water was used when the velocity was measured. The water was pumped into the container connected with the wind tunnel and adjusted the flow meter to 0.5L/min when the container was filled with water.
(2) When the ammonia concentration was measured, the wind tunnel was flushed with clean air for around 40 min until the inlet ammonia concentration is as the same as the value in the indoor air. Even though the inside of the wind tunnel was painted with a special epoxy to be resistant to ammonia absorption and the liquid in the container was pumped back to the returning tank after completing measurements each day, there was still a little liquid left in the container. At the same time, the airflow rate was adjusted to the pre-defined values as given in Table 2.1.
(3) In order to cool the ammonia solution, the cooling machine was started first. The liquid temperature could arrive at the pre-defined values after the cooling machine had run for approximately two hours. Then the fan in the wind tunnel was started and the liquid was pumped to the container. After that, the ammonia concentration and air flow rate were measured accordingly.

2.2.4 Test data analysis

2.2.4.1 Ammonia emission from an aqueous solution surface

Generally, the emission from an aqueous solution surface is determined by convective mass transfer coefficient and the concentration difference of the volatile substance at the surface and in the bulk air:

$$E = h_c A\left(c_{w,g} - c_0\right) \tag{2.1}$$

where E is the emission rate, kg/s; h_c is the convective mass transfer coefficient, m/s; A is the emission surface area, m^2; $c_{w,g}$ is the concentration of volatile substance on the emission surface, kg/m^3; c_0 is the concentration in the bulk air, kg/m^3.

On the other hand, the emission rate can also be calculated by airflow rate and concentration difference between the outlet and inlet under steady state conditions, as expressed in the following function:

$$E = Q\left(c_r - c_i\right) \tag{2.2}$$

where Q is the airflow rate, m^3/s; c_r is the concentration at the outlet, kg/m^3; c_i is the concentration at the inlet, kg/m^3. In this chapter, the ammonia emission rate was calculated by equation (2.2).

2.2.4.2 Turbulent boundary layer

In these experiments, the flow was turbulent. The turbulent boundary layer usually consists of a thin laminar sub-layer, a buffer layer and a turbulent layer when the solid surface is plane. In laminar sub-layer, the velocity is linear with the distance to the solid surface. In turbulent layer, a universal profile exists (the so-called wall-laws and wall functions) and the description for the velocity can be expressed as:

$$u_* = \sqrt{\frac{\tau_w}{\rho}} \tag{2.3}$$

$$y^+ = \frac{\rho y u_*}{\mu} \tag{2.4}$$

$$u^+ = \frac{u}{u_*} = \frac{1}{k}\ln y^+ + B \tag{2.5}$$

where τ_w is the wall shear stress, N/m^2; ρ is air density, kg/m^3; μ is dynamic viscosity, kg/ms; u_* is the friction velocity m/s; y^+ is dimensionless distance; u^+ is dimensionless velocity; u is the velocity in main flow direction, m/s; and y is distance from the wall, m. White (1991) suggests $B \approx 5.0$ for turbulent flow past smooth impermeable walls and the Karman constant $k \approx 0.41$.

As mentioned above, there is a buffer layer between laminar sub-layer and turbulent layer. In these experimental data analysis, the transition region from laminar sub-layer to fully turbulent layer has been ignored. Thus it assumed that there is a direct transition from the laminar sub-layer to the turbulent layer and these two velocity curves intersect at $y^+ \approx 11.06$ (Davies, 1972), as seen in Figure 2.6. In laminar sub-layer, there is:

$$u^+ = y^+ \tag{2.6}$$

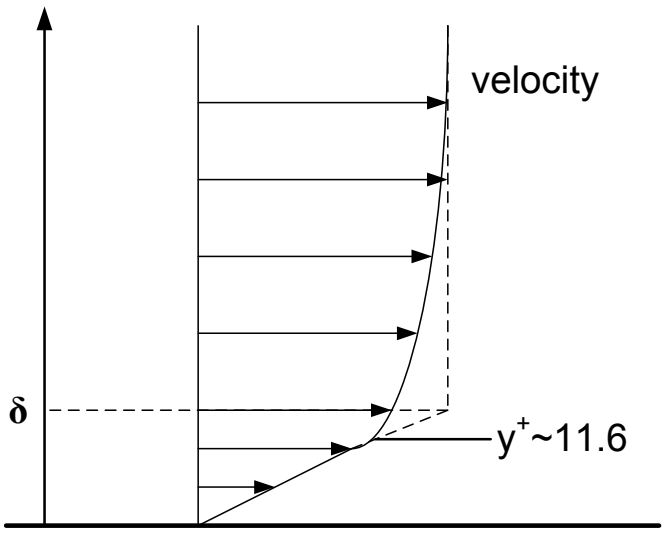

Figure 2.6 velocity profiles for turbulent flow

There are several definitions for boundary layer thickness of velocity such as δ_{99} and displacement thickness (Schlichting and Gersten, 1979). In Figure 2.6, the boundary layer thickness for velocity profile, δ, is defined as the distance from the wall where the velocity is equal to the bulk air velocity calculated by the linear relationship between velocity and wall distance in laminar sub-layer.

2.2.4.3 Turbulence intensity

The turbulence intensity was generated by different perforated plates and was defined as:

$$Tu = \frac{\sqrt{\overline{u'^2}}}{u_{center}} \cdot 100\% \tag{2.7}$$

Where Tu was the turbulence intensity; $\sqrt{\overline{u'^2}}$ was the Root Mean Square (RMS) of velocity fluctuation—u', m/s; u_{center} was the velocity measured at the point, which was located at the position '4' (see Figure 2.1b) and 0.25m above the emission surface. The velocity and velocity fluctuation were measured by LDV and the RMS was analyzed by the LDV software package.

2.3 Results and discussions

The emission rate presented in the following graphs was calculated by Eq. (2.2). The velocity boundary layer thickness was determined by the velocity profiles measured in experiments. The friction velocity was achieved by equation (2.5) to fit the measured velocity profiles. Then the velocity boundary layer thickness was obtained by equation (2.6) and linear relation between velocity and the distance from the wall in the laminar sub-layer.

2.3.1 Effects of velocity and turbulence intensity on ammonia emissions

The effects of air velocity and turbulence intensity on ammonia emission rate were illustrated in Figure 2.7. The results show that the emission rate increased with higher velocity, which is expected and in accordance with the mass transfer theory—larger air velocity generate bigger mass transfer coefficient so that the emission rate increases. In addition, the emission rate increased 9.5% when velocity increased from 0.3m/s to 0.4m/s while it increased 35.5% when velocity increased from 0.1m/s to 0.2m/s. Therefore, the ammonia emission rate was more sensitive to the change of velocity at the low velocity range compared to the change of velocity at a higher value. ANOVA testing indicated a significant effects of velocities on ammonia emission rates (p-value<0.001). The results also show that the emission rate increased slightly with higher turbulence intensity. However, ANOVA test did not show an important effects of turbulence intensity on ammonia emissions (p-value>0.3).

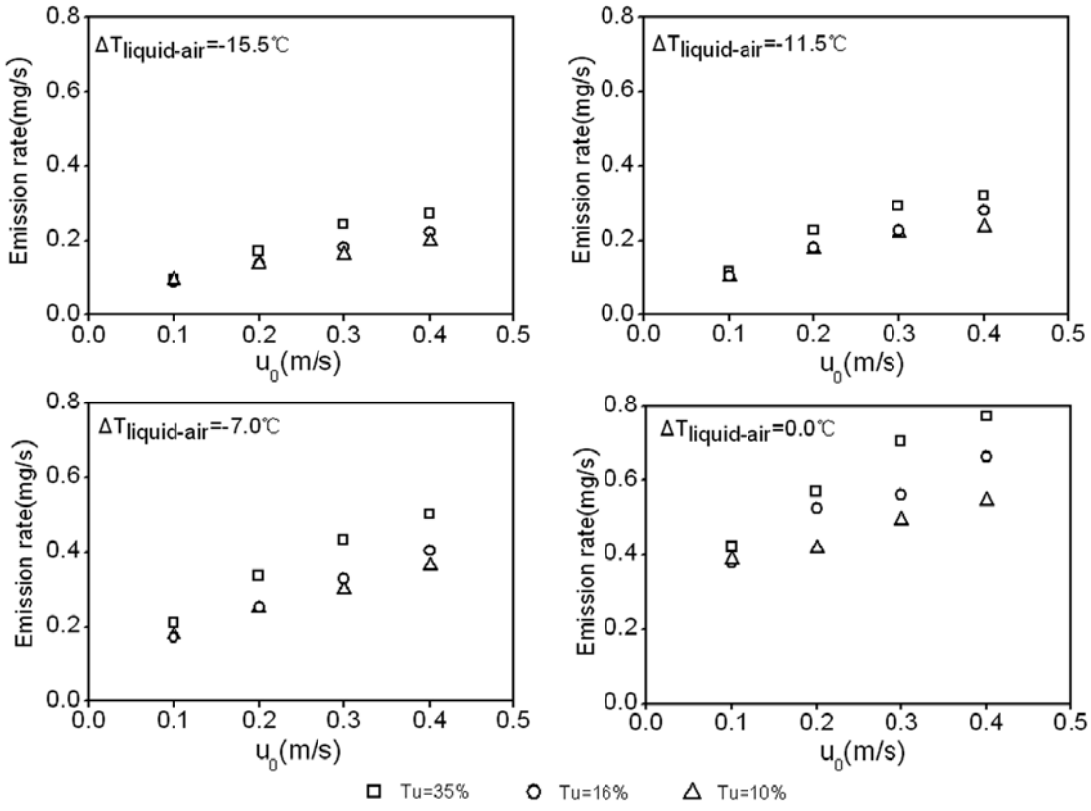

Figure 2.7 Effects of air velocity and turbulence intensity on the ammonia emission rate

2.3.2 Effects of liquid-air temperature difference on ammonia emissions

The effects of liquid-air temperature difference on ammonia emission rate were illustrated in Figure 2.8. The results show that the ammonia emission rate increased with higher liquid temperature. Meanwhile, the emission rate decreased 5% per degree when liquid-air temperature difference decreased from 0℃ to -7.0℃ while the

ammonia emission rate decreased 3.7% per degree when liquid-air temperature difference decreased from -11.5℃ to -15.5℃. This indicated that the emission rate was more sensitive to change of liquid temperature when it was exposed to high temperature conditions compared to low temperature conditions. ANOVA test showed a very significant influence of liquid temperature on ammonia emission rates (p-value<0.0001). It was known that the liquid temperature has an important effect on the liquid properties such as dissociation constant and Henry's constant of ammonia in the liquid. Both the dissociation constant and Henry's constant increased with higher liquid temperature so that the ammonia concentration above the liquid surface increased.

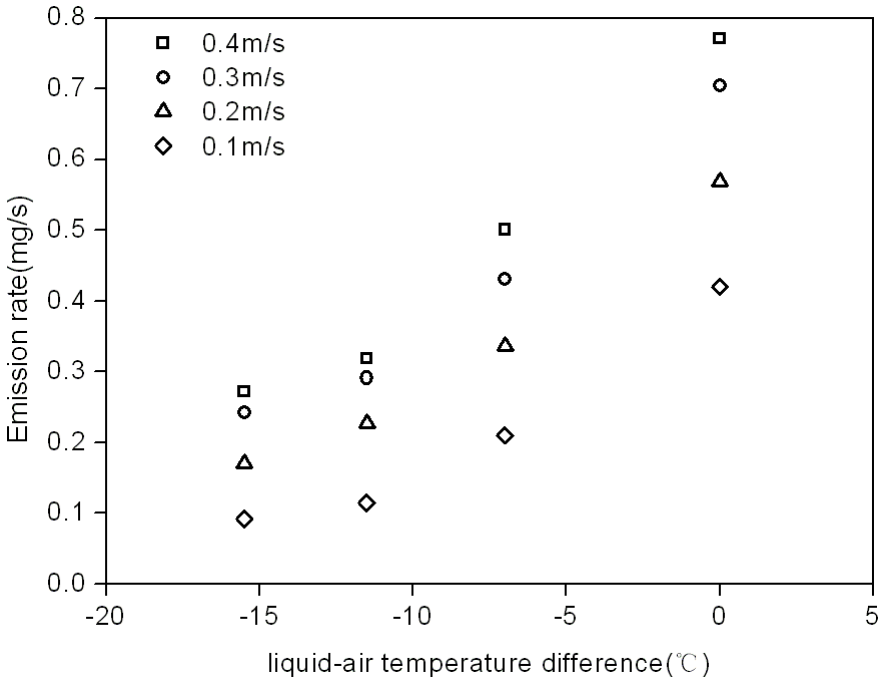

(a) Tu=35%

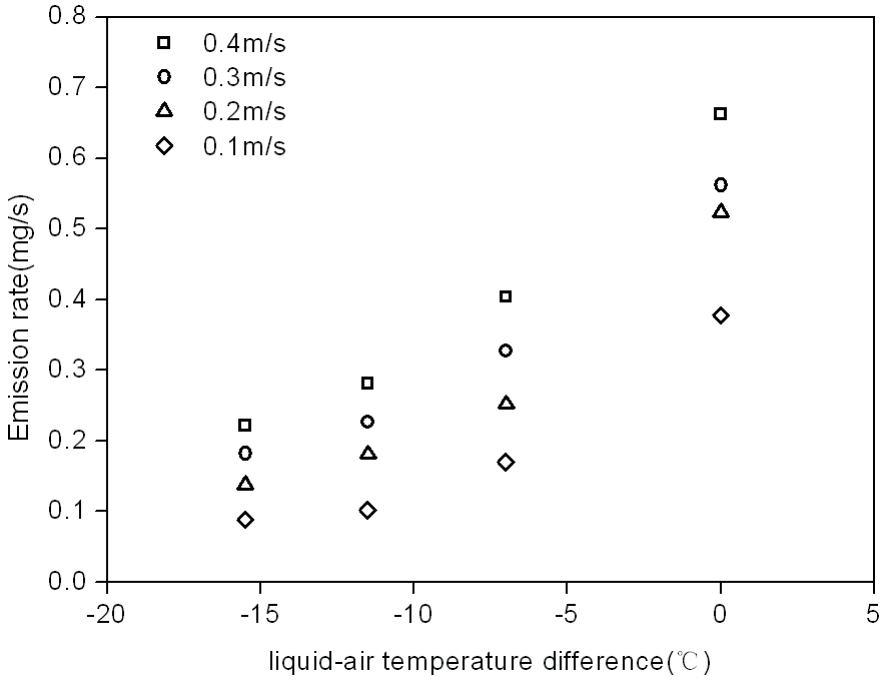

(b) Tu=16%

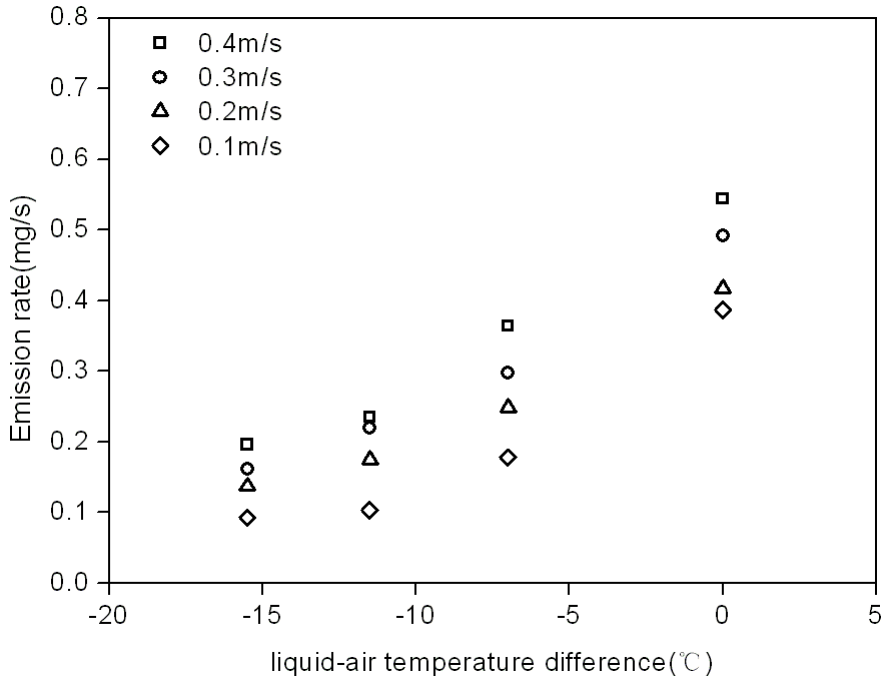

(c) Tu=10%

Figure 2.8 Effects of liquid-air temperature difference on ammonia emission rate

2.3.3 Effects of velocity and liquid-air temperature difference on boundary layer thickness of velocity

The velocity profiles measured in the experiments were shown in Figure 2.9. It was seen that the velocity profiles were distributed alike the logarithm law except that the solution temperatures were lower than the air temperature with velocity at 0.1m/s. The boundary layer thickness of velocity was calculated based on these velocity profiles.

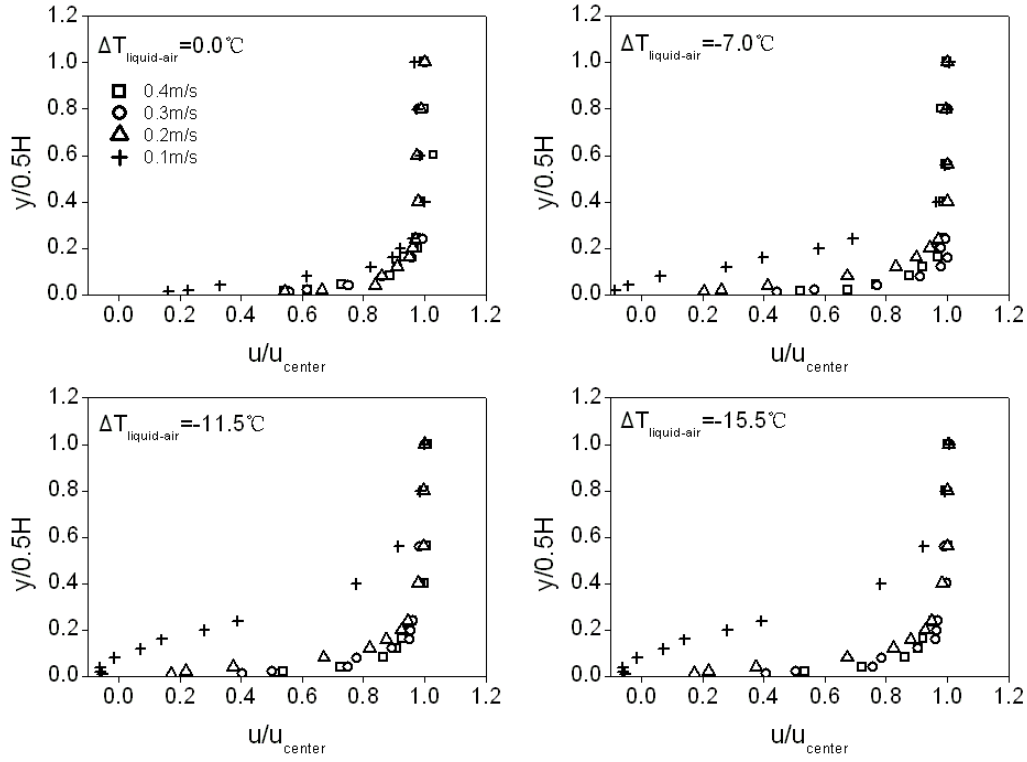

(a) Tu=10%

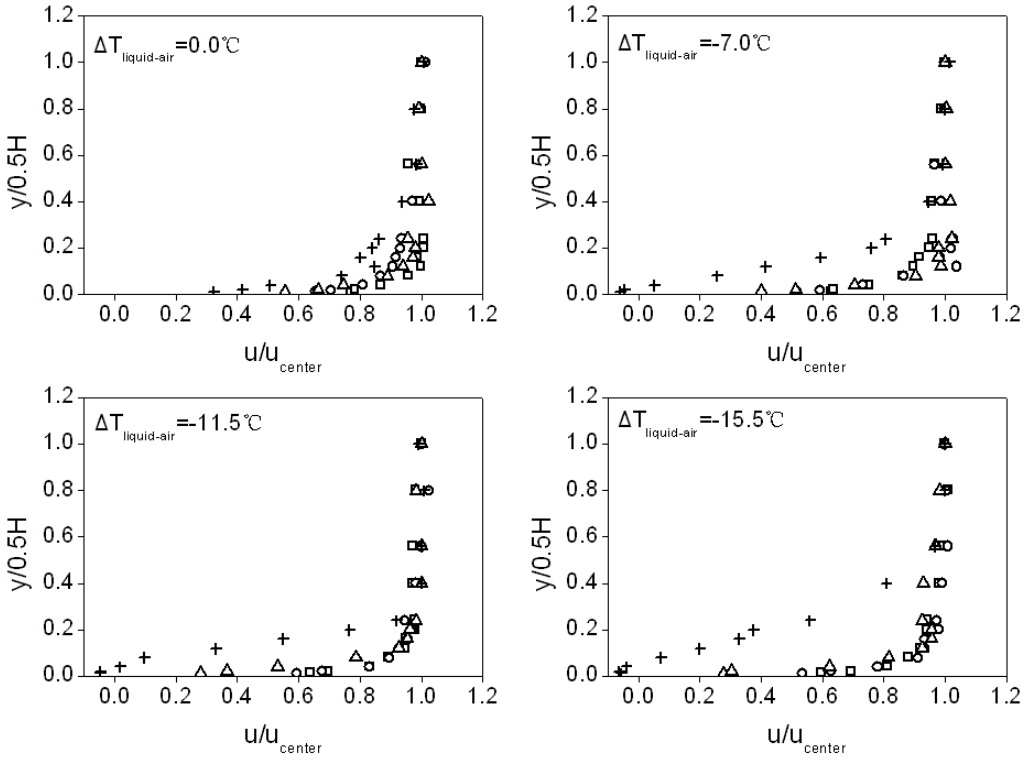

(b) Tu=16%

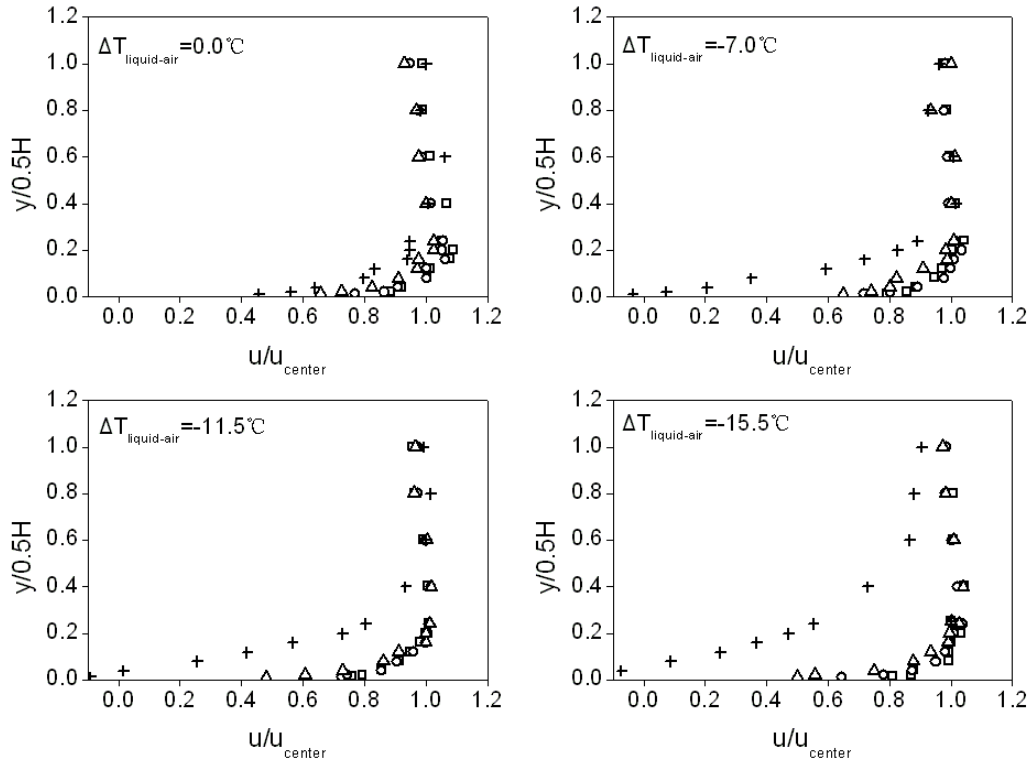

(c) Tu=35%

Figure 2.9 Velocity profiles along the wind tunnel height. '□', '○', '△' and '+' represented velocity of 0.4, 0.3, 0.2 and 0.1m/s respectively.

The relation between average velocity and boundary layer thickness of velocity was illustrated in Figure 2.10. The boundary layer thickness of velocity increased slightly over a velocity ranging from 0.4m/s to 0.2m/s and increased significantly over a velocity ranging from 0.2m/s to 0.1m/s, which could also be seen in Figure 2.7. This could be one of the reasons which explain why the ammonia emission rate was more sensitive to the change of the velocity at a low velocity range. On the other hand, the boundary layer thickness of velocity decreased sharply with higher turbulence intensity when velocity was 0.1m/s. When the turbulence intensity was low, the airflow tended to be laminar, which could significantly decreased the effects of turbulence on the diffusion area close to the emission surface.

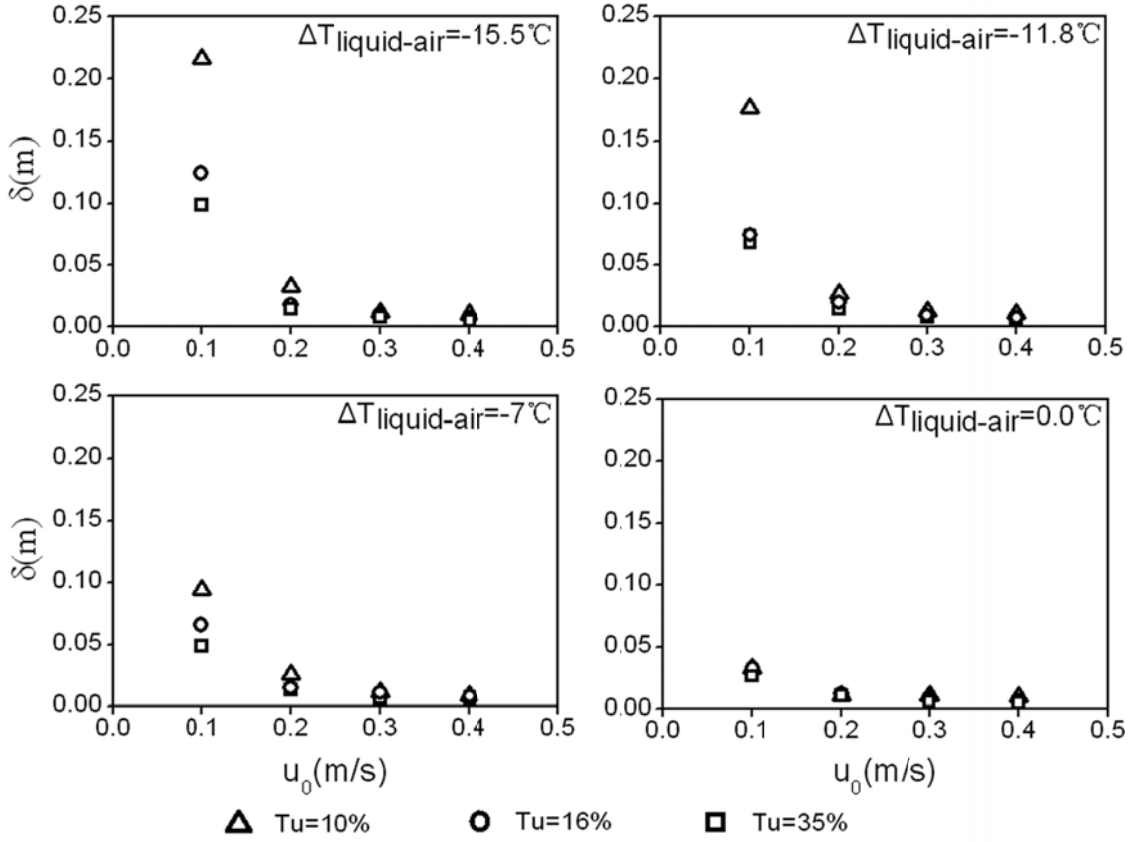

Figure 2.10 Relation between boundary layer thickness and average velocity.

The relation between liquid-air temperature difference and boundary layer thickness of velocity was presented in Figure 2.11. The results show that the boundary layer thickness of velocity varied little when liquid-air temperature difference ranges from -15.5℃ to 0.0℃ over velocity ranging from 0.4m/s to 0.3m/s. It indicated that lower surface temperature hardly had effects on the boundary layer thickness of velocity, especially under higher velocity and turbulence intensity. When the velocity was 0.1m/s, the boundary layer thickness of velocity changed significantly with liquid-air temperature difference.

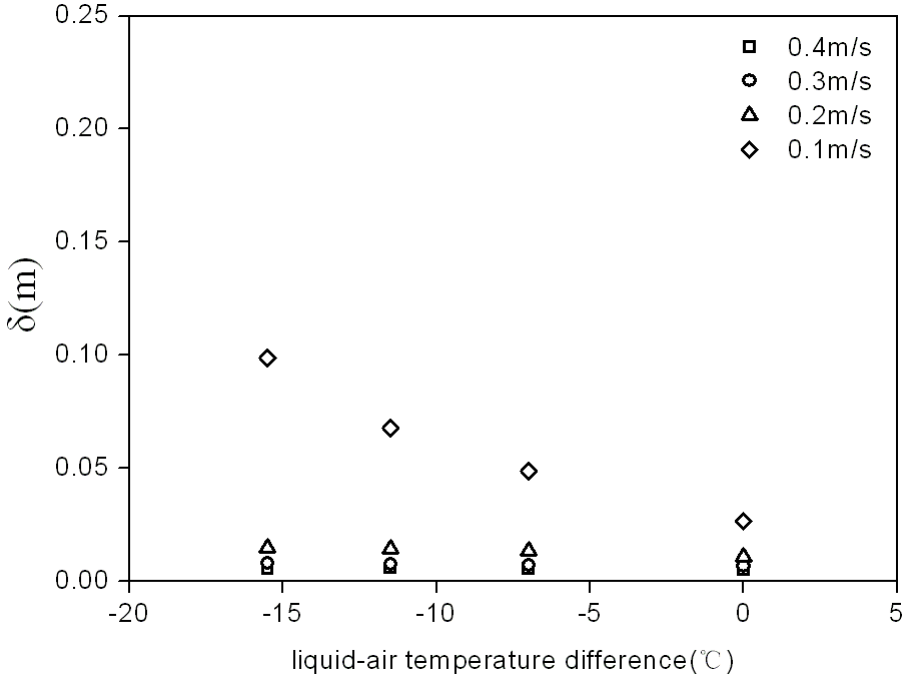
0.25
0.20
0.15
0.10
0.05
0.00
δ(m)
-20
-15
-10
-5
0
5
liquid-air temperature difference(℃)
0.4m/s
0.3m/s
0.2m/s
0.1m/s

(a) Tu=35%

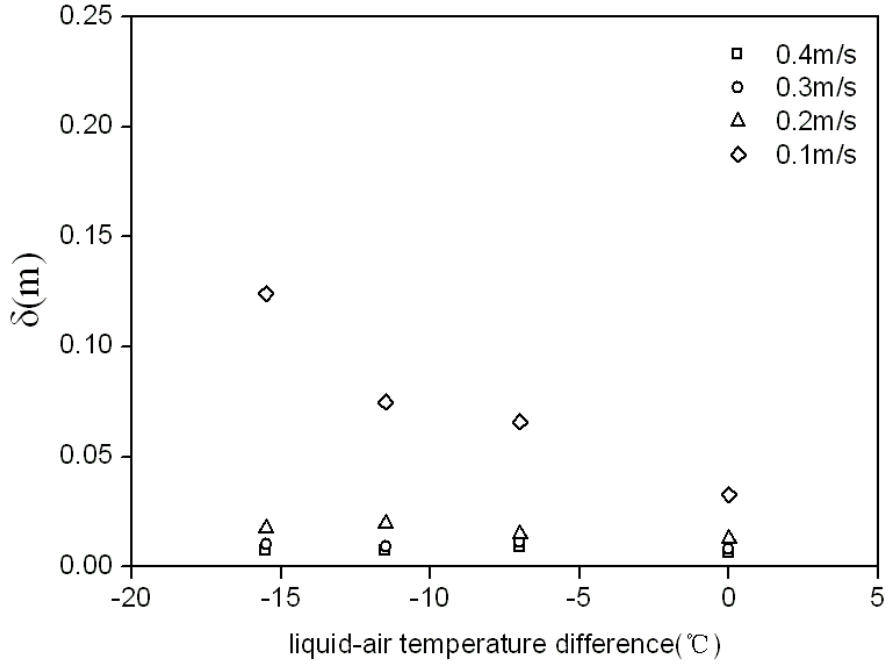
0.25
0.20
0.15
0.10
0.05
0.00
δ(m)
-20
-15
-10
-5
0
5
liquid-air temperature difference(℃)
0.4m/s
0.3m/s
0.2m/s
0.1m/s

(b) Tu=16%

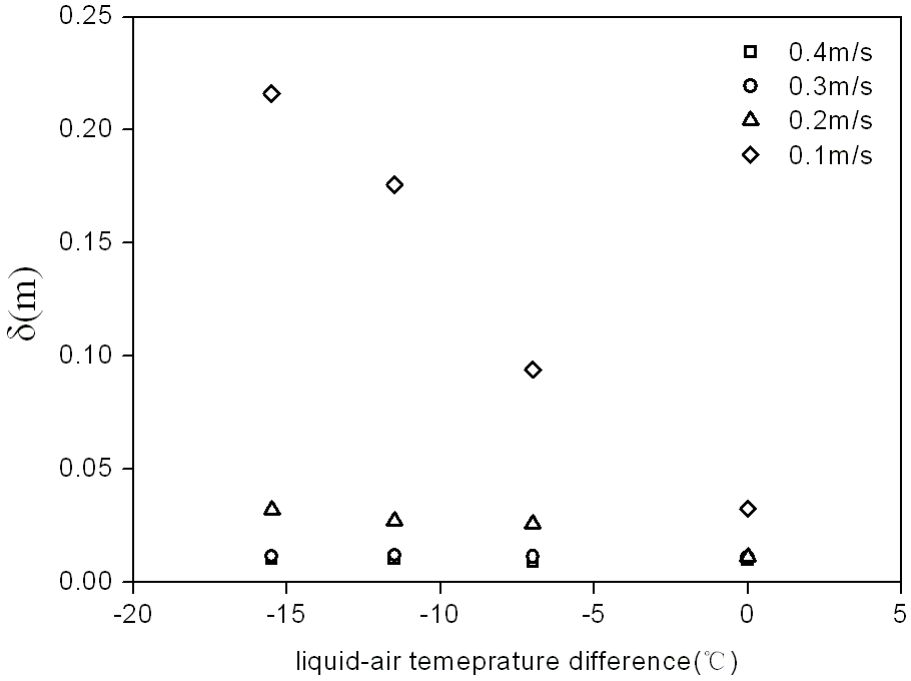

(c) Tu=10%

Figure 2.11 Relation between liquid-air temperature difference and boundary layer thickness of velocity

2.3.4 Relation between ammonia emission rate and boundary layer thickness of velocity

The relationship between ammonia emission rate and boundary layer thickness of velocity was shown in Figure 2.12. The ammonia emission rate increased with thinner boundary layer thickness. This was due to the boundary layer thickness of velocity which decreased with higher velocity and thereby resulting in higher emission rate. It was interesting to see that the emission rate was linear to the reverse of the boundary layer thickness of velocity.

The results from the experimental measurements indicated that both the environmental conditions (air velocity and turbulence intensity) and the solution properties (temperature) had effects on ammonia emission rate. Because the flow and thermal conditions in the wind tunnel study are usually different from those in the buildings, the emission rates obtained from the wind tunnel may not be applied directly to analysis of indoor air quality in buildings. Therefore, the experimental results obtained from the wind tunnel measurements will be served as the primary data for developing and validating the model for the CFD simulations including the turbulence models and models used to define the boundary conditions on the emission surface.

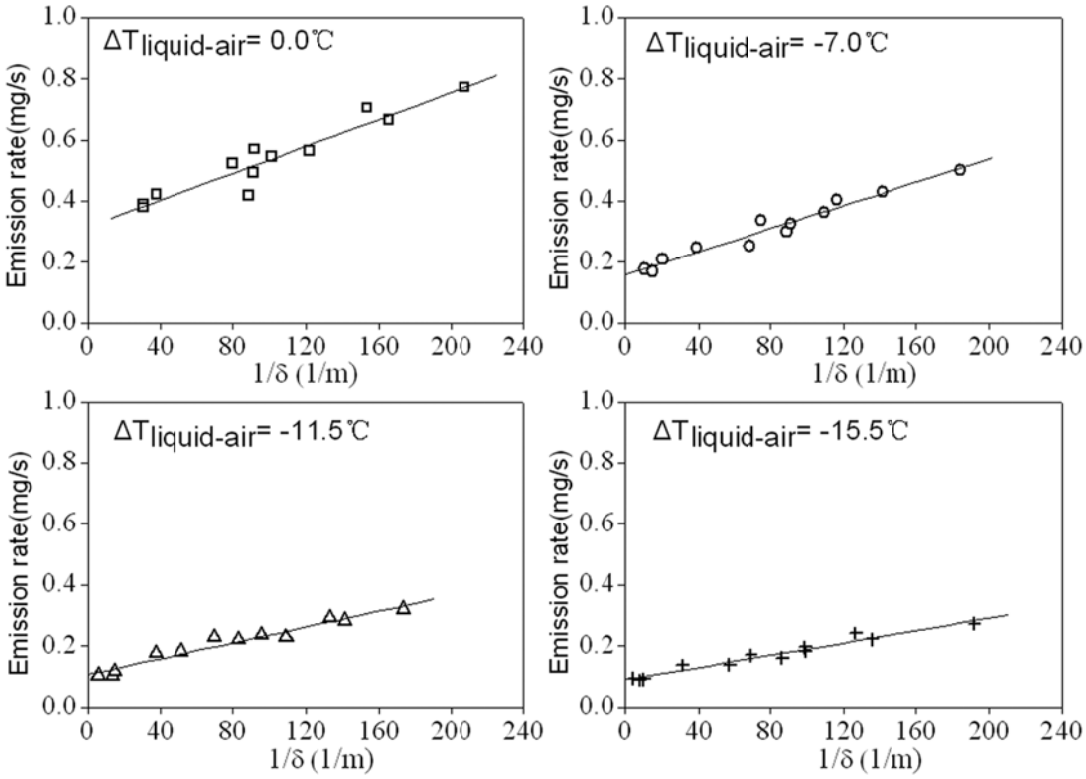

Figure 2.12 Relation between ammonia emission rate and boundary layer thickness of velocity

2.4 Conclusions

This Chapter has presented the results of an investigation of the emission characteristics of an ammonium aqueous solution measured using a wind tunnel. Emission rates were measured by monitoring the airflow rate and sampling the ammonia concentration at the inlet and outlet. The effects of the environmental conditions (air velocity and turbulence intensity) and ammonium solution properties (temperature) on ammonia emission rate were investigated by comparing the measured emission data between different cases. The following conclusions can be made based on the experimental measurements:

(1) Airflow (velocity and velocity fluctuation) affected the ammonia emission rate. The higher velocity and velocity fluctuation generated larger ammonia emission rate as expected. The ammonia emission rate was more sensitive to the change of velocity at a low range comparing to the change of velocity at a high range. Velocity fluctuation had slight effects on the ammonia emission rate comparing to the air velocity. When the velocity was low, there was almost no difference of ammonia emissions between various turbulence intensities.

(2) Ammonium solution temperature had a significant effect on the ammonia emission rate according to the ANOVA test analysis. The larger ammonia emission rates were observed when the liquid temperature was higher. It was also

observed that the ammonia emission rate was more sensitive to the change of temperature at a high range comparing to the change of temperature at a low range.

(3) The relationship between ammonia emission rate and the boundary layer thickness of velocity was also presented. It was interesting to observe that the ammonia emission rate was linear to the boundary layer thickness of velocity. Could this help to transfer the experimental data from the wind tunnel measurements to the full scale buildings? Further investigations are needed to answer this question.

Chapter 3

Modeling of ammonia emission from an aqueous solution

Ammonia emissions from an aqueous solution result from evaporation and internal diffusion. In this chapter, only the evaporation process was considered. The internal diffusion process was ignored because the ammonia aqueous solution was mixed and the ammonia concentration in the solution was assumed to be constant. Several boundary conditions of concentration on the emission surface were applied and validated using experimental data obtained from Chapter 2, including using Henry's law constant (HLC), vapor-liquid equilibrium (VLE) properties and constant flux to define the concentration boundary conditions on the emission surface. The results show that the HLC models generally over-predicted the ammonia emission rate and gave worse agreement of concentration profiles between numerical results and measurements while VLE model predicted the ammonia emission rate well, actually as well as the concentration profiles in the boundary layer.

3.1 Introduction

The experimental measurements presented in chapter 2 revealed that ammonia emissions can be affected by environmental conditions (velocity and velocity fluctuations) and ammonium solution properties (temperature). However, the emission data from the wind tunnel or environmental chambers under defined standard conditions may not be applied directly in full scale buildings, in which the environmental conditions may significantly differ from those in the test wind tunnel. However, it would be too expensive to study the ammonia emissions under the full scale livestock buildings. Hence, a feasible way to investigate the ammonia emissions could be to employ the Computational Fluid Dynamics (CFD) to simulate and study the emission processes in buildings using the boundary conditions of concentration on the emission surface validated by the inexpensive wind tunnel or chamber measurements.

The accuracy of CFD modeling depends on several factors, such as discretization scheme, numerical methods, boundary conditions, and turbulence models (Soerensen et al. 2003). In this study, one of the difficult boundary conditions to be determined is the ammonia concentration in the gas phase. Researchers usually employed Henry's law to relate the concentration in the gas phase to the concentration in the liquid (Cortus et al. 2008; Ye et al. 2008). Henry's law is well-known to be one of the theories used for vapor liquid equilibrium when the solution is diluted. At an expected low concentration (less than 1000mg/l in the solution) no serious error would be caused if the partition is considered to obey the Henry's law (Anderson et al., 1987). Furthermore, Henry's law constant holds for dilute solutions that do not react, ionize or dissociate with the solvent liquid (Mortimer, 2008). Ni (1999) reviewed the models of Henry's constant developed to determine the ammonia concentration in the gas phase. It showed that Henry's constants for NH_3 release from manure or the solutions

had appreciably diverse forms and adopted different definitions and units even using the same theory. In this chapter, the boundary condition of concentration on the emission surface determined by Henry's law constant was validated by experimental data using CFD simulations. Then the validated boundary condition of concentration will be applied to predict the ammonia emission under different environmental conditions and liquid properties in a full-scale pig pen in chapter 4.

The following section (3.2) introduced the various models to determine the boundary condition of concentration on the emission surface as well as the mathematical model and numerical methods for simulating ammonia emissions. Section (3.3) presented the effects of inlet entrance length, inlet turbulent parameters, boundary condition of concentration for the emission surface on the ammonia emission rate and the effects of airflow and ammonium solution temperature on ammonia mass transfer coefficient. Finally, section 3.4 summarized the findings from those processes.

3.2 The Mathematical models

In chapter 1, the ammonia emission mechanism was discussed in and from manure. The solution made for the measurements was already simplified to avoid the effects of other gases on ammonia emissions. The following assumptions were made for the numerical modeling:

(1) The solution in the container connected to the wind tunnel was assumed to provide a constant ammonia concentration in the solution by circulating the solution slowly between the container and tanks. The ammonia diffusion in the liquid was therefore not considered in the CFD simulations.
(2) During the emission process, ammonia in the liquid film and the ammonia vapor pressure were in thermodynamic equilibrium at the gas-liquid interface.
(3) The ammonia was passive contaminants and had no impacts on airflow.
(4) The effect of humidity in the air on ammonia emissions was not considered.

3.2.1 Gas-liquid interface

3.2.1.1 Henry's law constant

At the gas-liquid interface, the ammonia is transferred from the liquid to the air. Henry's law constant (HLC) is usually applied to relate the volatile compound concentration in the liquid to that in the air. HLC represents the air-liquid equilibrium partition coefficient for a particular chemical compound in a dilute aqueous solution (dilute typically defined as less than 0.001-0.01 mole fraction, corresponding to less than 5-50 g/l for a compound with a molecular weight of 100 g/mol) (Staudinger and Roberts, 2001) and represents a key physical property with respect to the compound's behavior in the environment. In the literature, one can encounter a multitude of forms for HLC based on the selection of different sets of associated units. When the same units are used for both concentration in the liquid and concentration in the air, HLC can be expressed as:

$$K_h = \frac{c_{w,l}}{c_{w,g}} \tag{3.1}$$

where

K_h —Henry's law constant of ammonia (air-to-liquid ratio)

$c_{w,l}$ —ammonia concentration in the liquid, mg/m^3 or mol/m^3

$c_{w,g}$ —ammonia concentration in the air, mg/m^3 or mol/m^3

Besides, HLC can also be expressed as:

$$K_h = \frac{p}{c_{w,l}} \tag{3.2}$$

where

p —ammonia partial pressure in the air, atm.

In this paper, three different HLC models to determine the boundary conditions of concentration for the emission surface are used, seen in Table 3.1.

Table 3.1 Different HLC forms applied in this Chapter

Definition and units	Equations	Note
$K_h = \frac{[NH_3]_l}{[NH_3]_g} = \frac{\text{mol/m}^3}{\text{mol/m}^3}$	$\log K_h = -1.69 + \frac{1477.7}{T}$ (Hales and Drewes, 1979)	HLC1
$K_h = \frac{c_{w,l}}{c_{w,g}} = \frac{\text{kg/m}^3}{\text{kg/m}^3}$	$K_h = 1384 \times 1.053^{(293-T)}$ (Ni, 1999)	HLC2
$K_h = \frac{p}{[NH_3]_l} = \frac{\text{atm}}{\text{mol/l}}$	$K_h = 160.559 - \frac{8621.06}{T} - 25.6767 \ln T + 0.035388T$ (Beutier and Renon, 1978)	HLC3

3.2.1.2 Thermodynamic vapor liquid equilibrium (VLE) of ammonia water system

Ammonia-water system has been studied numerously in design of absorption processes. The source of vapor-liquid equilibrium data can be found in literature (Patek and Klomfar, 1995). Patek and Klomfar developed a set of equations describing the vapor-liquid equilibrium properties of the ammonia-water system necessary for absorption cycle design. The data used to develop these equations were

taken from over 13 references in a range of -80℃<T<180℃, 0.002MPa<p<2MPa. These equations were as followings:

$$T(p,m_x)=T_0\sum_i a_i\left(1-m_x\right)^{m_i}\left[\ln\left(p_0/p\right)\right]^{n_i} \tag{3.3}$$

$$T(p,m_y)=T_0\sum_i a_i\left(1-m_y\right)^{m_i/4}\left[\ln\left(p_0/p\right)\right]^{n_i} \tag{3.4}$$

$$m_y(p,m_x)=1-\exp\left[\ln\left(1-m_x\right)\sum_i a_i\left(p/p_0\right)^{m_i} m_x^{\,n_i/3}\right] \tag{3.5}$$

where T, p, m_x and m_y are temperature(K), pressure(MPa), mole fraction in the liquid phase and mole fraction in the gas phase respectively; T_0 is 100K; p_0 is 2MPa; a_i, m_i and n_i are constants (i=1,2,……14). The Eq. (3.3) reproduces the $T(p,m_x)$ relation over the full concentration range from about 0.002MPa to 2MPa. Similarly, the data range of Eq. (3.4) for $T(p,m_y)$ relation is from 0.02MPa to 2MPa and the development of Eq. (3.5) has been based on the data of ammonia molar fractions in the liquid phase greater than 0.05 and pressures above 0.05MPa. The numerical consistency of $T(p,m_x)$, $T(p,m_y)$ and $m_y(p,m_x)$ was checked by the data used to develop these equations and found not to be worse than 5% when m_x was smaller than 20%. Technically speaking, not all the partial pressure of ammonia in measurements of chapter 2 is in the range of the data for the validity of these equations. One of the reasons that the data at low pressure did not fit the Eq. (3.4) and Eq. (3.5) is because of the greater difficulty encountered in measuring vapor composition. Therefore, these equations were extrapolated for application in this chapter.

3.2.2 Ammonia mass transfer in the air

The ammonia transport in the air is determined by the diffusion through the boundary layer at the gas-liquid interface and environmental conditions such as airflow. This part of the work was performed using CFD commercial software (Fluent 6.3). For an incompressible Newtonian flow, the general conservation equations for continuity, momentum, energy and species are as follows:

$$\frac{\partial}{\partial\tau}\left(\rho\Phi\right)+\frac{\partial}{\partial x_j}\left(\rho u_j\Phi\right)=\frac{\partial}{\partial x_j}\left(\Gamma_\Phi\frac{\partial\Phi}{\partial x_j}\right)+S_\Phi \tag{3.6}$$

Where Φ presents the independent variables: time-averaged velocity component u_i (i =1,2,3), turbulent kinetic energy k, dissipation of turbulent kinetic energy ε, specific dissipation rate ω, species C and temperature T. Γ_Φ is the effective diffusion coefficient for Φ and S_Φ is the source term for Φ. In this chapter, three turbulence models—Low Reynolds number $k-\varepsilon$ model (LRN), Renormalization group $k-\varepsilon$

model (RNG) and shear stress transport $k-\omega$ model (SST) — were used. The introduction of these models can be found in Fluent 6.3 User guide and text books (Wilcox 2004) as well as attached in Appendix A of this thesis.

It is known that the near-wall modeling significantly impacts the fidelity of numerical solutions since walls are the main source of mean vorticity and turbulence. Numerous experiments have shown that the near-wall region can be largely subdivided into three layers—viscous sub-layer, buffer layer where flow transits from laminar to turbulent flow and fully developed turbulent layer. In viscous sub-layer, the flow is almost laminar, in which viscosity plays a dominant role in momentum and heat or mass transfer. Traditionally, there are two approaches to modeling the near wall region. One approach is to not resolve the viscous sub-layer instead of using a semi-empirical formulas called 'wall functions' to bridge the viscosity affected region between the wall and the fully-developed region. This approach is inadequate in situations where the low-Reynolds-number effects are pervasive. Another approach is to modify the turbulence models to enable the viscosity-affected region to be resolved with a mesh all the way to the wall. It is given the name of near wall modeling.

The turbulence models used in this chapter handles the near wall region using the near wall modeling method since it is important to simulate the transfer process down to the emission surface. SST model is a combination of $k-\omega$ model (in the inner boundary layer) and $k-\varepsilon$ model (in the outer region of and outside of the boundary layer) developed by Menter (1994). The use of a $k-\omega$ formulation in the inner parts of the boundary layer makes the model directly usable all the way down to the wall through the viscous sub-layer and hence the SST model can be used as a low-Reynolds-number without any extra damping functions. RNG model was used with enhance wall treatment, which is a near wall modeling method that combines a two-layer model with enhanced wall functions. If the near-wall mesh is fine enough to be able to resolve the laminar sub-layer (typically $y^+ \approx 1.0$), then the enhanced wall treatment will be identical to the traditional zonal model and the enhanced wall treatment allows RNG $k-\varepsilon$ model to resolve the laminar sub-layer without using a wall function (Fluent, 2006). LRN model can predict the transport process in the laminar sub-layer and the log-law zone in contrast to the standard $k-\varepsilon$ model where this part of the flow is given by analytical wall functions.

3.2.3 Boundary conditions

Appropriate boundary conditions for velocities, temperature and ammonia species are needed in order to close the governing equations. The common velocity and temperature boundary conditions, including inlet, outlet, and walls were specified as the values measured in the experiments. The principles to define these boundary conditions can be found in the literature (Nielsen et al. 2007). However, it should be mentioned that the liquid was circulated through the container connected with the wind tunnel. A non-slip condition was applied to the velocities of all solid walls, and the liquid-air interface as a solid interface was further assumed since the flow rate of

the liquid was 0.5L/min, which was around the order 0.0002m/s (This is based on a uniform one dimensional velocity in the liquid container with the emission surface) of the liquid velocity on the emission surface.

The boundary condition for ammonia concentration in the air side has been introduced in 3.2.1 using HLC or vapor-liquid equilibrium to relate the ammonia concentration in the air with the ammonia concentration in the liquid. Therefore the assumed constant ammonia concentration in the liquid side should be determined even thought the mass transfer of ammonia in the liquid was not modeled in the numerical simulations. In ammonia-water system or ammonia solutions, NH_3 is a base that reacts in the acid-base reaction because of the asymmetric structure. This can be expressed as an acidic dissociation (Ni, 1999):

$$\mathrm{NH_4^+} \leftrightarrow \mathrm{NH_3} + \mathrm{H^+} \tag{3.7}$$

The reactions are effectively instantaneous so that NH_3 and NH_4^+ are at equilibrium at all points in the liquid. By assuming the activity coefficient of all the species involved in the reaction to be equal to unity, the dissociation constant is expressed as:

$$K_d = \frac{[NH_3][H^+]}{[NH_4^+]} \tag{3.8}$$

Like the HLC, the dissociation constant is also a function of temperature. It can be calculated from the following semi-empirical equation (Ni 1999):

$$\log_{10} K_d = -0.09018 - \frac{2729.92}{T} \tag{3.9}$$

In experiments, TAN was measured and it can be expressed as:

$$[\mathrm{TAN}] = [\mathrm{NH_4^+}] + [\mathrm{NH_3}]_l \tag{3.10}$$

The equations of (3.7)—(3.10) were used to determine the ammonia concentration in the liquid. The boundary conditions for numerical simulations were summarized in Appendix B.

3.2.4 Numerical methods

A Cartesian coordinate system with a structured mesh was applied to the geometry. The computational domain was truncated before the orifice and the fan at the exit. The flow was steady state and the SIMPLE algorithm was applied. Second-order accurate upwind schemes were employed for momentum equations, energy equation and species equation as the Peclet number was bigger than 2.0 in these simulations. A body weighted scheme was used for the pressure interpolation. The 'Incompressible Ideal Gas Law' was applied to compute the density. To resolve the boundary layer at the wall and maintain a $y^+<1$, the first node was placed at y<1mm from the wall and

an expansion ratio less than 1.2 was maintained to ensure that the results were second order accurate. The convergence criteria was set as 10^{-6} of residual for all solved equations and the convergence was not assumed to be reached until the velocity magnitude at a specific point above the emission surface had stabilized.

3.3 Results and discussions

It has been mentioned that the inlet velocity and turbulence intensity was measured at the location of 0.533m upstream from the emission surface while the belt mouth was 2.05m upstream from the emission surface (see Figure 2.1). It is known that the inlet entrance length affects flow development of both laminar flow and turbulent flow (Kays and Rawford 2005). In order to predict accurate velocity profiles above the emission surface, the influences of inlet entrance length and inlet turbulence parameters on the flow and ammonia emission rate were tested by three cases respectively. Then the appropriate inlet entrance length and turbulence intensity was used for other validation simulations. To qualify the differences of the simulated and measured results, the ratio of ammonia emission rate was used and defined as:

$$ERR = \frac{E_{CFD}}{E_{Exp}} \tag{3.11}$$

where E_{CFD} is the ammonia emission rate achieved from CFD simulations, kg/s and E_{Exp} is the ammonia emission rate obtained from experiments, kg/s. The purpose of these simulations was to validate the various models used to define the boundary conditions of ammonia concentration on the emission surface and CFD techniques being applied for further simulations.

3.3.1 Effects of inlet entrance length on ammonia emission rate

In order to identify the sensitivity of the numerical results to the inlet entrance length, the selected cases were Tu10T10u2, Tu10T10u3 and Tu10T10u4. The test conditions for the cases were summarized in Table 3.2. The ammonia mass fraction was defined by vapor-liquid equilibrium model. Two inlet entrance lengths—2.05m and 0.533m—were examined using SST and RNG turbulence models.

Table 3.2 Boundary conditions for test cases

case	Inlet			Emission surface	
	U(m/s)	Tu(%)	T(℃)	NH_3 mass fraction	T(℃)
Tu10T10u2	0.2	17.1	21.5	4.99E-04	10.6
Tu10T10u3	0.3	14.5	22.0	2.97E-04	9.7
Tu10T10u4	0.4	10.0	22.1	2.97E-04	9.7

The results in Figure 3.1 show that the ammonia emission rate is generally 3% ~10% higher with short inlet length than those with long inlet length. This could be

explained by the boundary layer theory. With the inlet length of 2.05m, the boundary layer is more developed and thicker which provided larger resistance to the transport process. On the other hand, the turbulence intensity decayed along the centerline of the wind tunnel as the domain was extended, which could also contribute to this reduction in ammonia emission. This effect is addressed in next section. Since the inlet entrance length affected the ammonia mass transfer from the emission surface, the following simulations are performed with the inlet length of 2.05m, which was more realistic and comparable to the experimental setup.

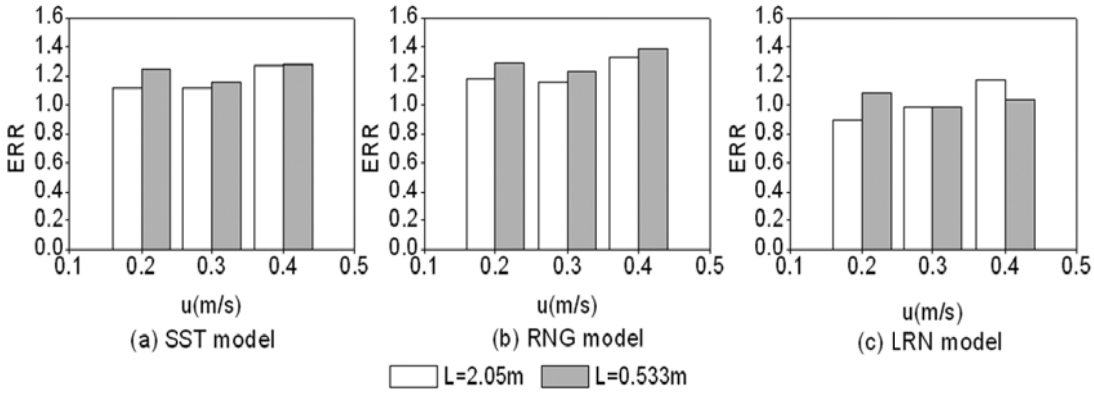

Figure 3.1 Effects of inlet length on ammonia emission rate ratio

3.3.2 Effects of inlet turbulence intensity on ammonia emission rate

To fully account for the boundary layer growth and mimic the experiment, the computational domain was extended to the edge of the bell mouth of the tunnel. At this location, there was no measurement for turbulence intensity and the value must be assumed and verified by the measurements downstream of the inlet. In order to qualify the effect of turbulence intensity at the inlet, we specify four different turbulence intensities at the inlet in simulations, ie. 14.5%, 25%, 35% and 45%. The turbulence intensity of 14.5% was measured at location '0' (0.533m upstream from the emission surface, see Figure 2.1) and the other three values were specified to match the velocity and velocity fluctuation profiles measured downstream. The tested conditions for the cases were the same as Tu10T10u3 in Table 3.2 except setting different turbulence parameters at the inlet.

To compare the turbulence intensity profiles, some assumptions have been made. As known in CFD simulations, the RANS models assumed the turbulence isotropic, i.e., the turbulent fluctuations in all directions are equal. However, in experiments only the horizontal component of the velocity and its fluctuating component was measured. To match the results obtained from the measurements, two methods to calculate the velocity fluctuation contributing to the turbulent kinetic energy in CFD simulations were therefore considered. The value of k in CFD simulations was only contributed by u' ($\sqrt{\overline{u'^2}} = \sqrt{2k}$) and the other two components v' and w' were approximately zero. This could be justified near the wall since one of the component, v', was damped by

the wall and the other component, w',was damped by virtue of symmetry (we are presenting results along the center plane of the tunnel). This was also shown in experimental results by Reichart (Schlichting, 1979). Nevertheless, the flow was considered as isotropic and the turbulent kinetic energy was contributed by velocity fluctuations at three directions ($\sqrt{\overline{u'^2}} = \sqrt{2k/3}$). This assumption is supposed to make the CFD simulation agree better with the experiments along the centerline of the wind tunnel.

Figure 3.2 and 3.3 presented the comparison of dimensionless velocity and Root Mean Square (RMS) between simulated and measured results. Numerical simulations did not show difference of velocity profiles between two turbulence intensity settings at the inlet and two turbulence models from Figure 3.2(a) and 3.3(a). Figure 3.2(b) and 3.3(b) show that the RNG model captured the peak better than SST model in the boundary layer. Figure 3.3(c) illustrated that the SST model gave good agreement in the core flow where turbulence was more or less isotropic in case of larger inlet turbulence intensity. The numerical results also indicated that changing the turbulence parameters at the inlet only had effects on the velocity fluctuation at the core flow and hardly affected the velocity fluctuation at the boundary layer.

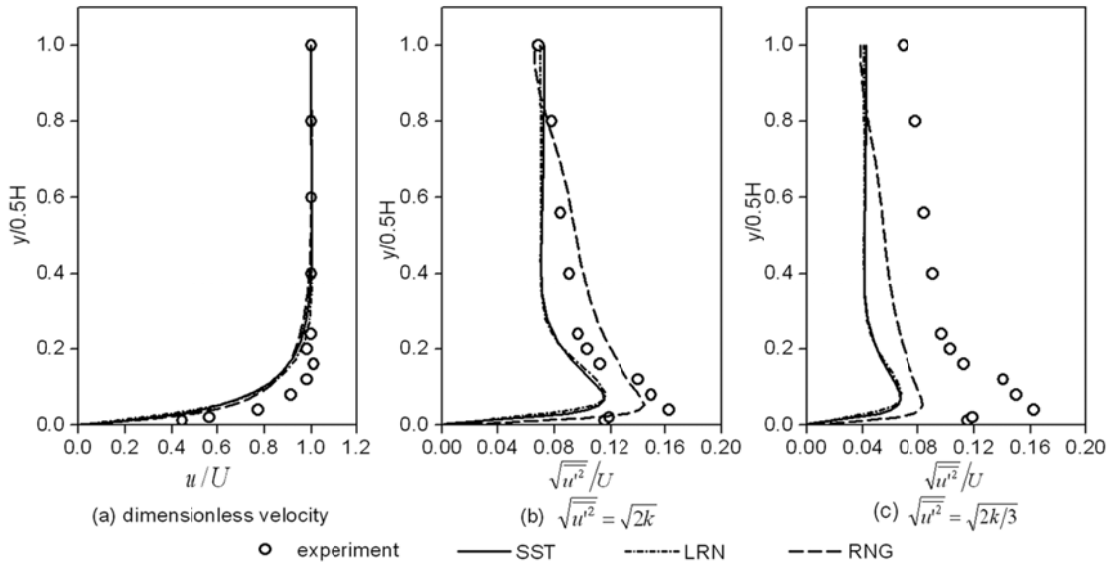

Figure 3.2 Comparison of dimensionless velocity and RMS profiles between simulations and measurements with inlet turbulence intensity of 14.5%

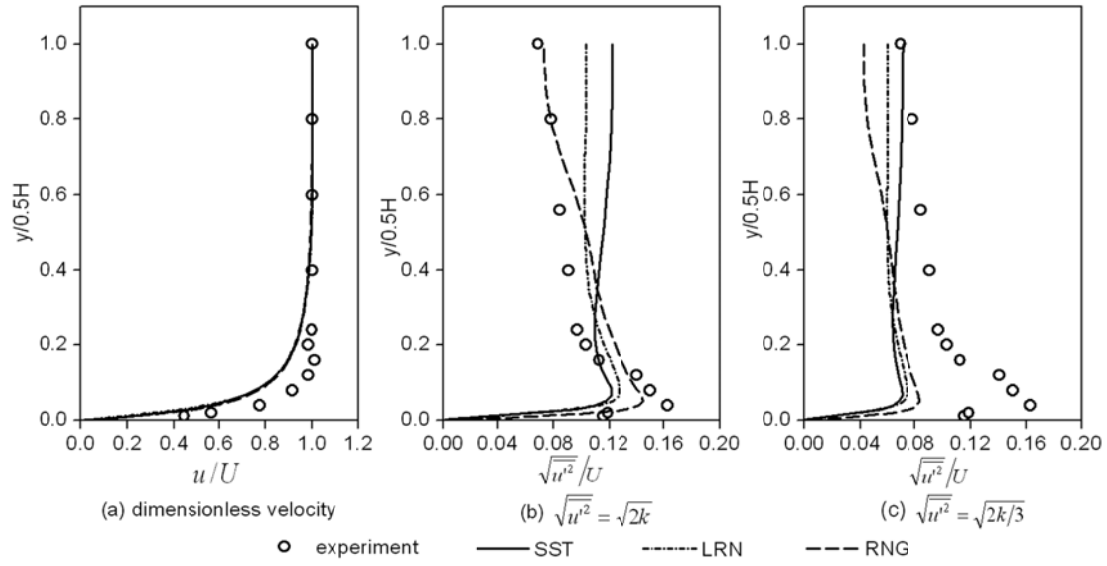

Figure 3.3 Comparison of dimensionless velocity and RMS profiles between simulations and measurements with inlet turbulence intensity of 45%

The variation of kinetic energy along the centerline for case Tu10T10u3 is presented in Figure 3.4. The kinetic energy decreased rapidly downstream. When the turbulence intensity at the center of the wind tunnel was 10%, it was possible to match the data measured downstream by increasing the turbulence intensity at the inlet. However, we found it was very hard to match the turbulence intensity downstream for the cases that the turbulence intensity at the center of the wind tunnel was 35%. It was mentioned that the turbulence intensity of 35% at the center of the wind tunnel downstream was generated by a perforated plate at the inlet (Figure 2.2b, the right one). We thought it might be the reason that we didn't model the inlet appropriately so that we also simulated a case with the inlet perforated plane modeling.

The case Tu35T22u3 was chosen to be simulated in a 2D model as the purpose was only to investigate the effects of the inlet perforated screen. The results presented in Figure 3.5 show that there was still a big difference of kinetic energy at the center of the wind tunnel between simulated and measured results even though the turbulence intensity at the inlet was set at 100%. At the same time, the kinetic energy increased sharply at a very short distance and then decayed rapidly downstream, which was also demonstrated by Said et al. (1993). Above the emission surface (from 2.05m to 2.67m at x direction), the difference of kinetic energy existed between inlet perforated screen modeling and inlet non-screen modeling. Even though the difference of kinetic energy was relatively small, only 13 cases were used to validate the turbulence models and the accuracy of concentration boundary condition determined by Henry's constant law and vapor liquid equilibrium properties. These 13 cases were that the turbulence intensity at the center of the wind tunnel was around 10%, see Appendix B of boundary conditions for CFD validation.

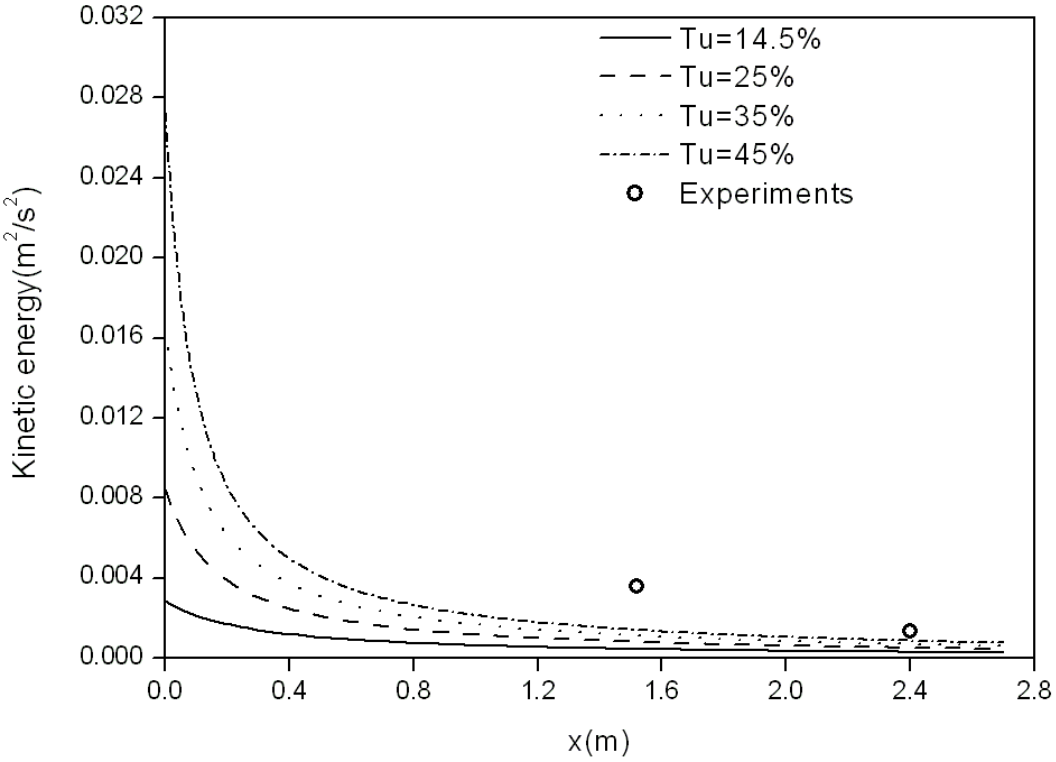

Figure 3.4 Kinetic energy distribution along the centerline (y=0.25m, z=0.25m) for case Tu10T10u3

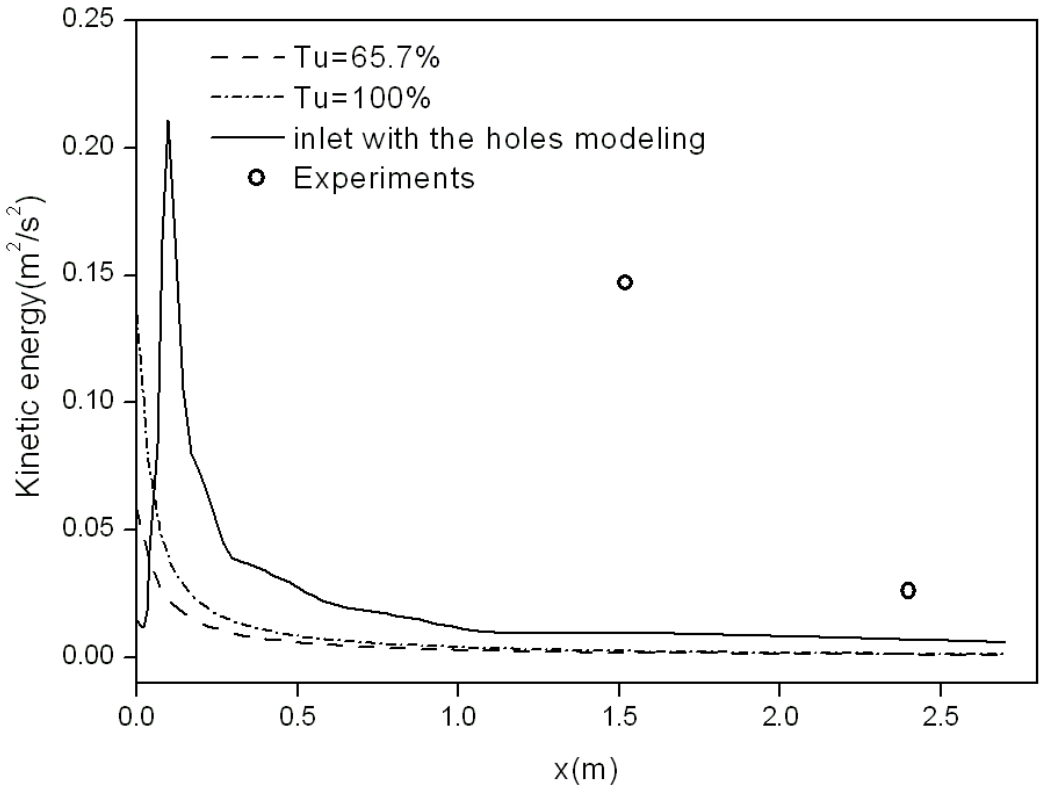

Figure 3.5 Kinetic energy distribution along the centerline (y=0.25m, z=0.25m) for case Tu35T22u3

The results exemplified in Figure 3.6 presented the effects of turbulence intensity at inlet for case Tu10T10u3. The turbulence intensity at inlet had little effects on the ammonia emission rate when using RNG model and it had slight effects on the ammonia emission rate (1%) when using SST model and 1%~4% with LRN model. From the above analysis, it was concluded that using the turbulence intensity measured in the experiments to define the inlet boundary conditions even though the inlet entrance length was extended in the following simulations.

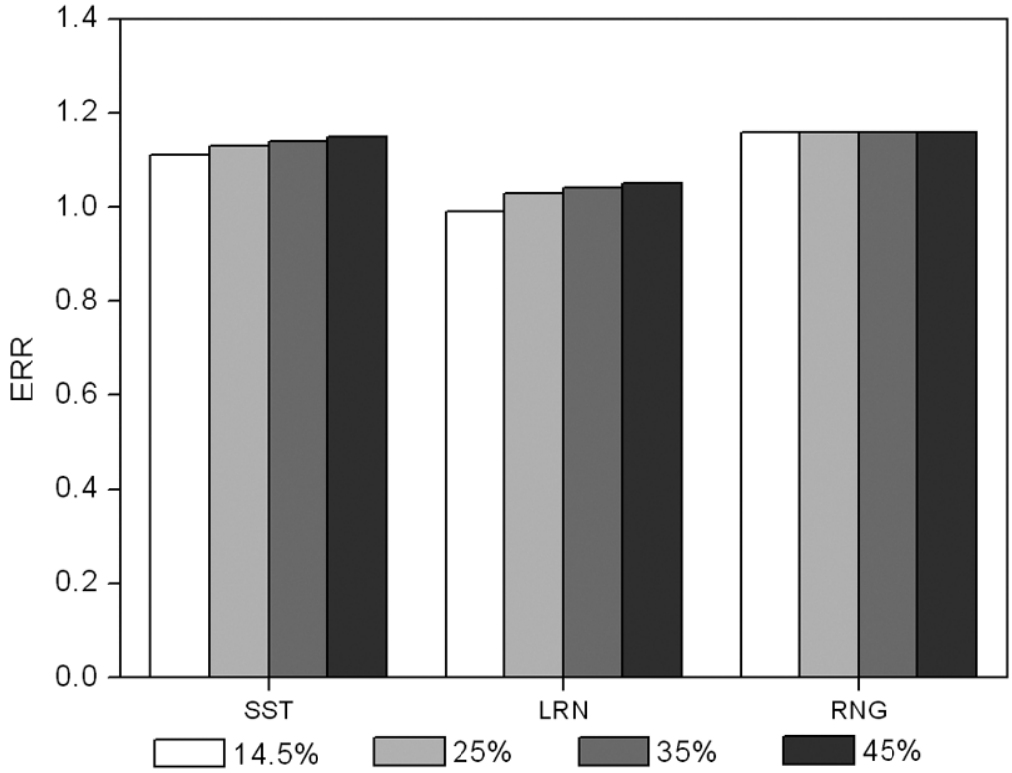

Figure 3.6 Effects of turbulence intensity at inlet on the ammonia emission rate ratio for Tu10T10u3

3.3.3 Validation of turbulence models

The effects of inlet entrance length and turbulence intensity at inlet have been studied above. It was important to realize that even if the governing equations of a given problem were solved accurately, the results could be wrong if the governing equations (including boundary conditions) did not model the physics appropriately. In this section, the turbulence models were validated using ammonia emissions measured for 13 cases (Turbulence intensity at the center of the wind tunnel is around 10%) in the wind tunnel experiment. Figure 7 presented the comparison of ammonia emission between simulated and measured results using three turbulence models with VLE model to determine the concentration boundary condition on the emission surface. The results illustrated that the difference of predictions among these three turbulence models were small. It is difficult to conclude which turbulence model was better or not.

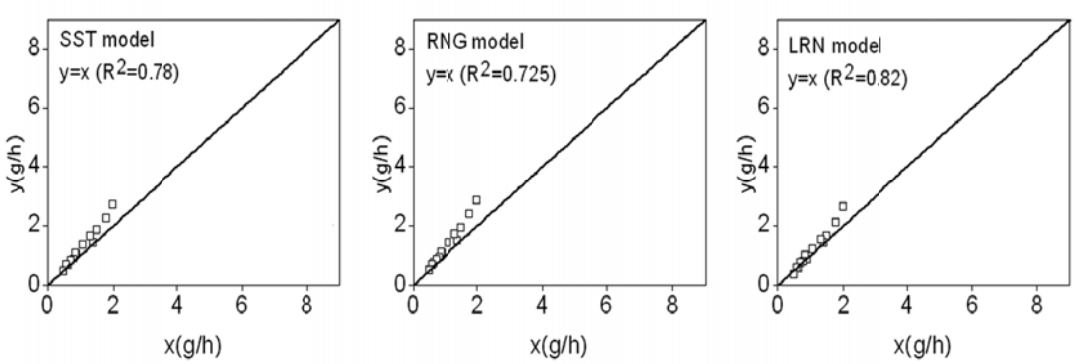

Figure 3.7 Comparison of ammonia emissions between simulated and measured results under three turbulence models with VLE model to determine the concentration boundary condition for emission surface. y is CFD results and x is experiment.

3.3.4 Validation of concentration boundary condition

As stated in previous sections, it is important to model the concentration on the emission surface correctly in order to predict ammonia emissions. The concentration of ammonia through the gas-liquid surface can be modeled by Henry's law constant and vapor liquid equilibrium properties. In this section, the accuracy of HLC models and VLE model to determine the ammonia concentration on the emission surface was validated by comparing the simulated and measured ammonia emissions and profiles measured in the boundary layer.

Figure 3.8 compared the numerical results and measurements of ammonia emissions when using various models to define the boundary conditions of ammonia concentration on the emission surface. The results show that the simulated ammonia emissions were over-predicted when HLC models were used to determine the concentration boundary condition while the simulated ammonia emissions were in better agreement with measurements when VLE model was used to determine the concentration boundary condition on the emission surface.

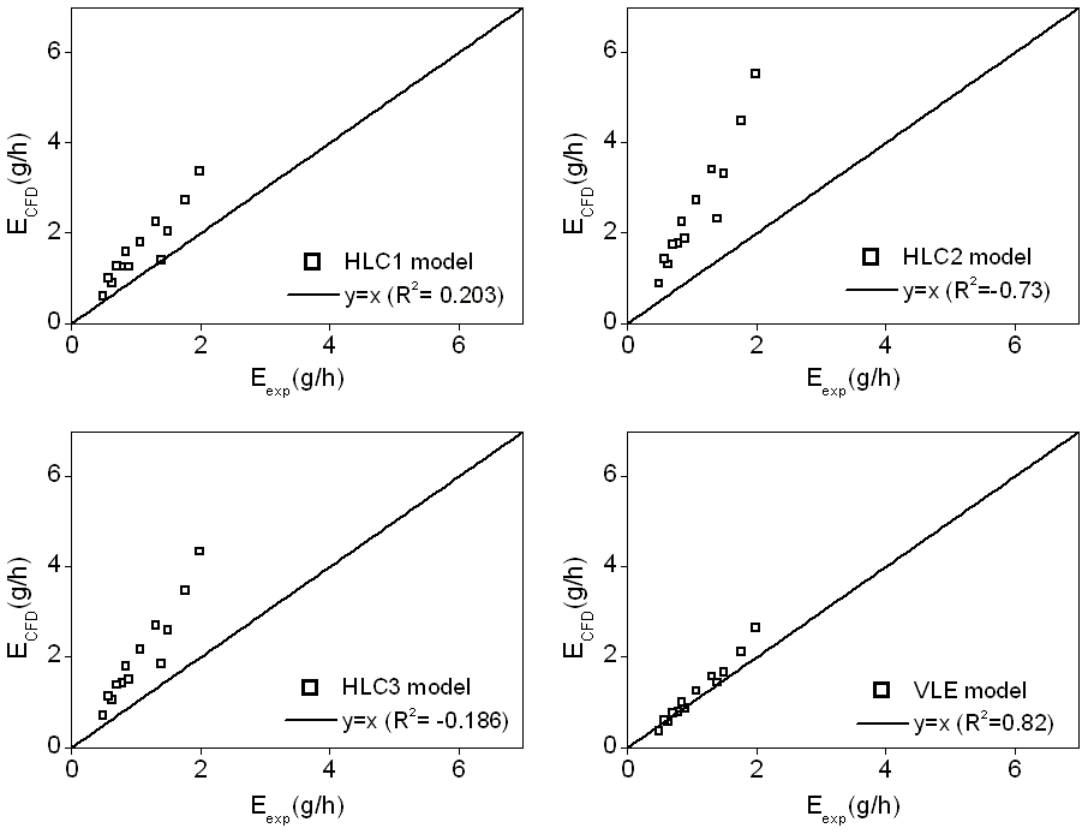

(a) LRN model

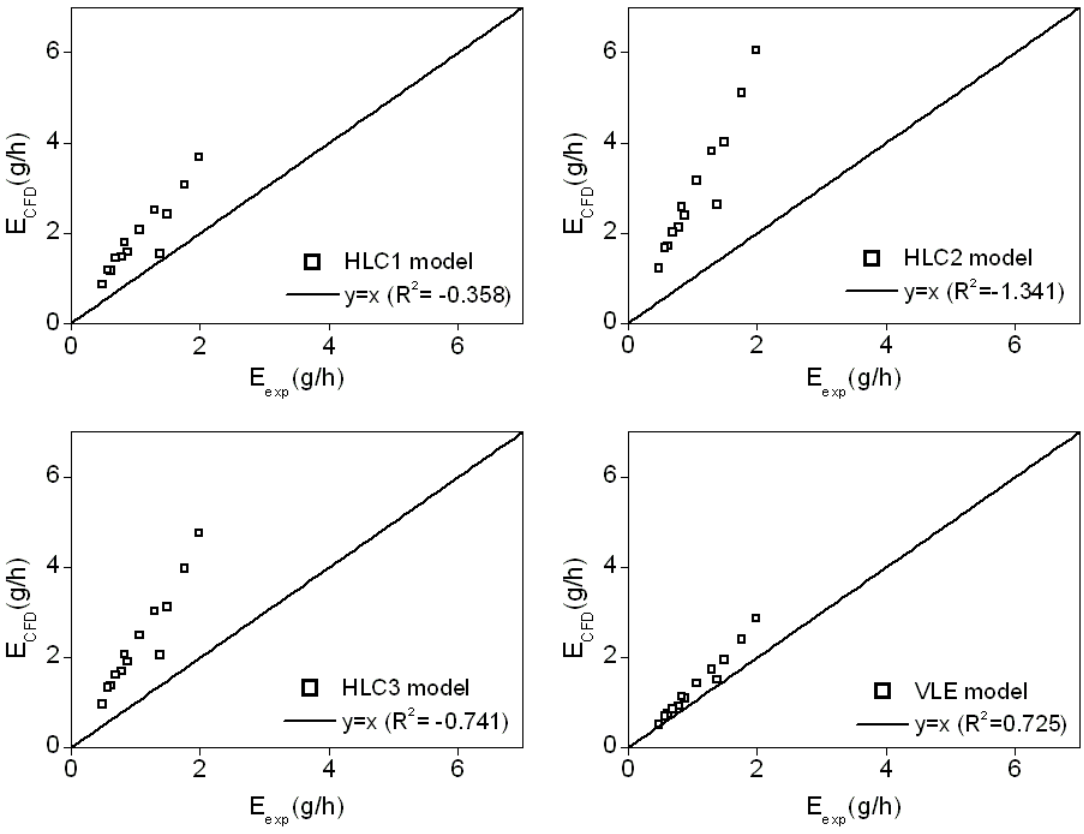

(b) RNG model

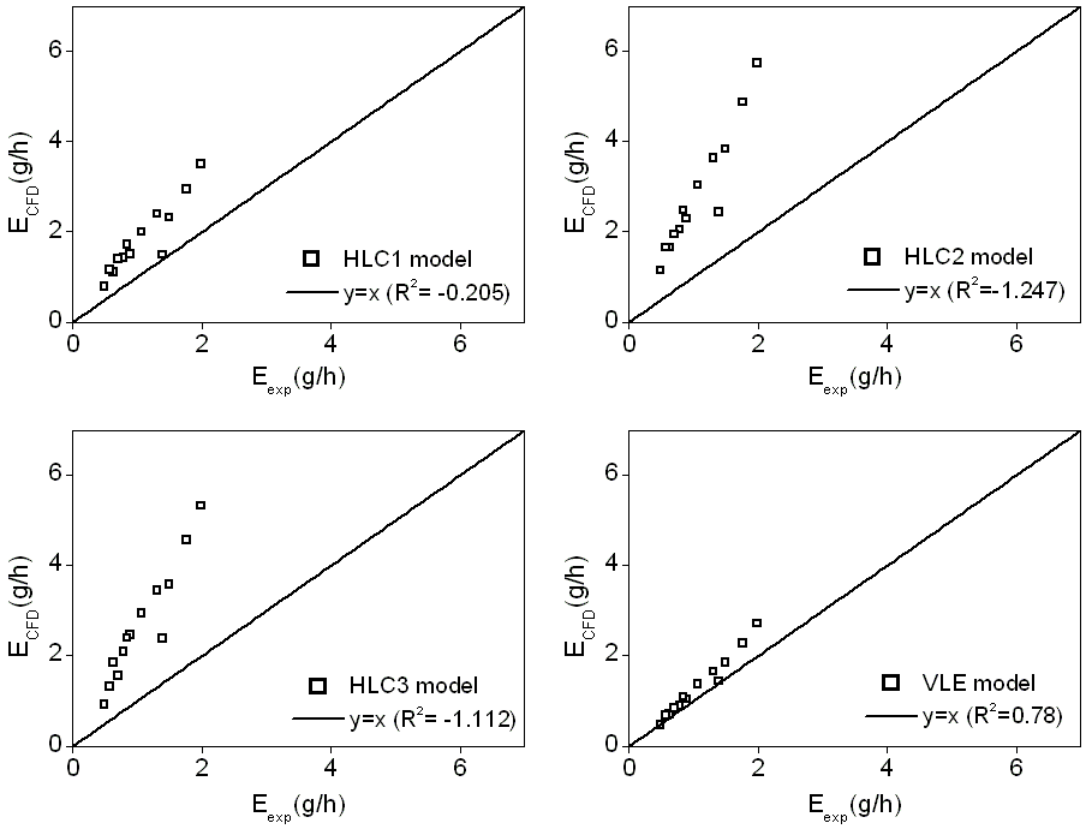

(c) SST model

Figure 3.8 Comparison of ammonia emissions between numerical results and measurements using different HLC models and VLE model to determine the concentration on the emission surface.

Figure 3.9 and Figure 3.10 presented the comparison of concentration, velocity and temperature profiles in the boundary layer for cases Tu10T10u3 and Tu10T22u3 using SST model (The comparison of profiles between simulated and measured results was presented in Appendix C using RNG model and LRN model). The results show that the simulated concentration profiles were in good agreement with measurements when VLE model was used to determine the concentration boundary condition on the emission surface for case Tu10T10u3 and Tu10T22u3, except that there was discrepancy of the concentration (The simulated ammonia concentration is around 1.5 times of measurements) at the point closest to the emission surface for case Tu10T22u3. The difference of ammonia concentration in the boundary layer was big and the simulated ammonia concentrations at some points are four times of the measurements when the HLC models were applied to define the concentration boundary conditions on the emission surface. The HLC2 model provided the worst predictions.

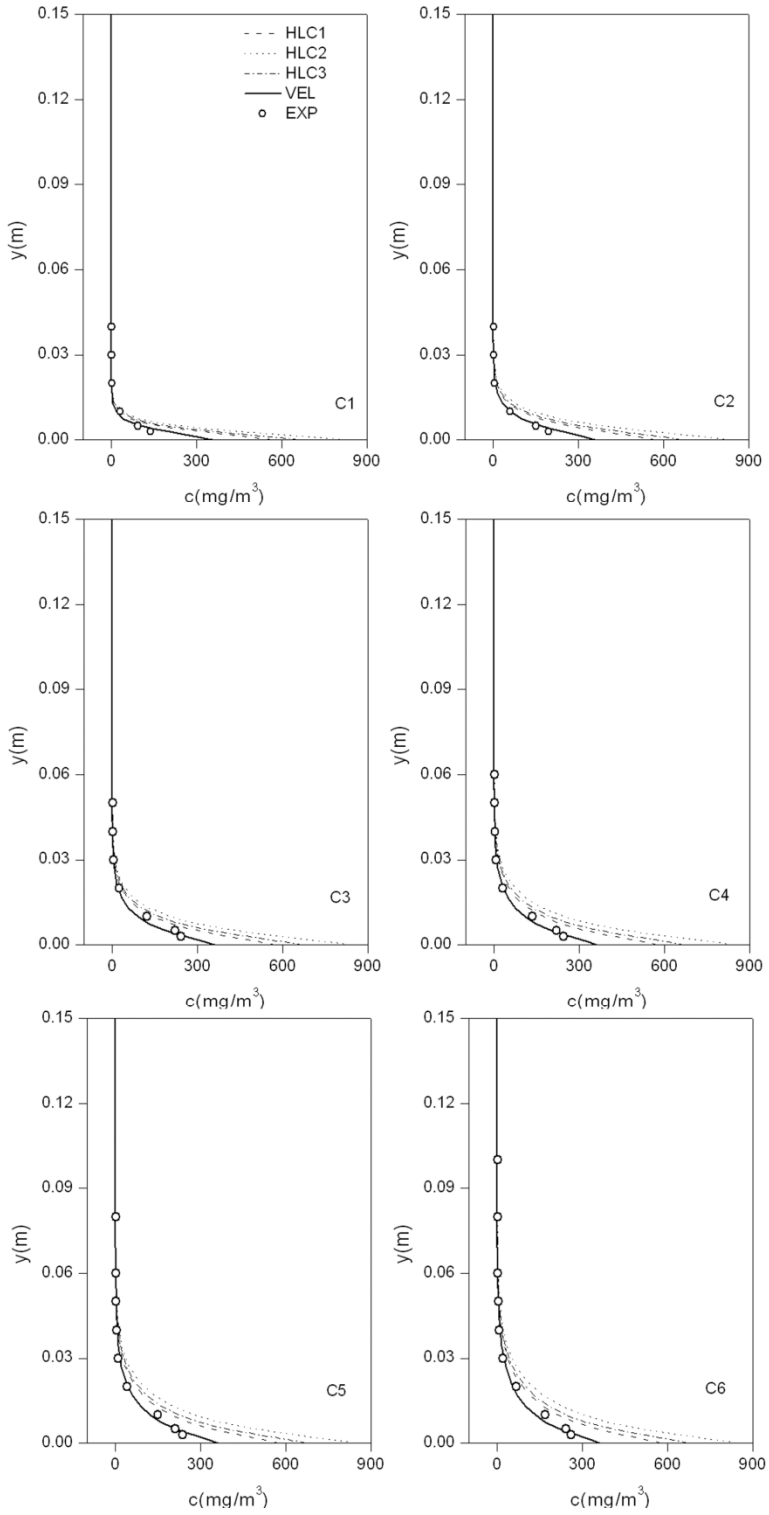

(a) Concentration profiles

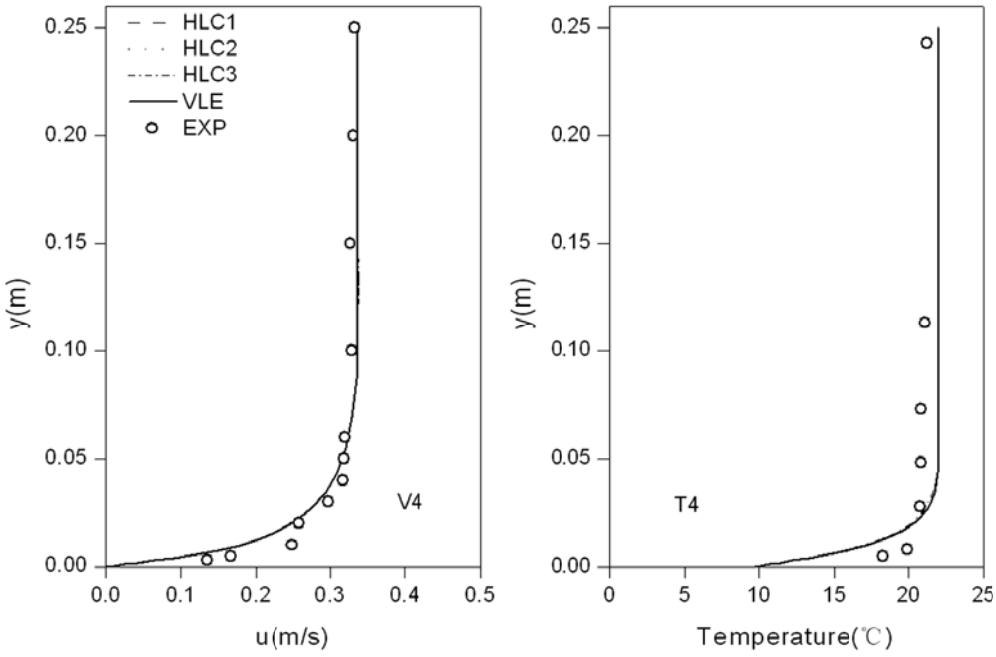

(b) Velocity and temperature profiles

Figure 3.9 Comparison of concentration, velocity and temperature profiles in the boundary layer between simulated and measured results for Tu10T10u3 using SST turbulence model

There was no difference of velocity and temperature profiles among these four models since ammonia emission hardly had effects on the air flow patterns, which was corresponding to the assumption that the ammonia was a passive gas in these simulations. It was noticed that there were also discrepancy of velocity and temperature in the boundary layer between numerical results and measurements. The velocity was measured by LDV and seeded by small liquid particles. It could be one of the reasons that the liquid particles bounced when they hit the liquid surface and gave errors to the measurements. The temperature was measured by thermocouples (T type). The sensor head was around 5mm~10mm and there could also be errors to measure the height of the points. From the overall comparison between numerical results and measurements, it was concluded that the VLE model was appropriate to define the concentration boundary conditions on the emission surface.

It should be kept in mind that Henry's law constant models in Table 3.1 are derived experimentally from a specific solution and only modeled as the function of solution temperature. It is well known that the HLC value has strong temperature dependence but some other parameters (such as pH, compound concentration, co-solutes, suspended solids etc.) are also identified to be significant (Staudinger and Roberts, 1996). The diverted forms of HLC models developed for different solutions (such as liquid solution, urine or manure) have been discussed by Ni (1999), which may compromise the possibility of other parameters' effect on HLC value. Therefore the HLC model developed by other researcher under different solution conditions to

define the boundary conditions of concentration on the emission surface could give a big difference of ammonia emission rate between simulated and measured results.

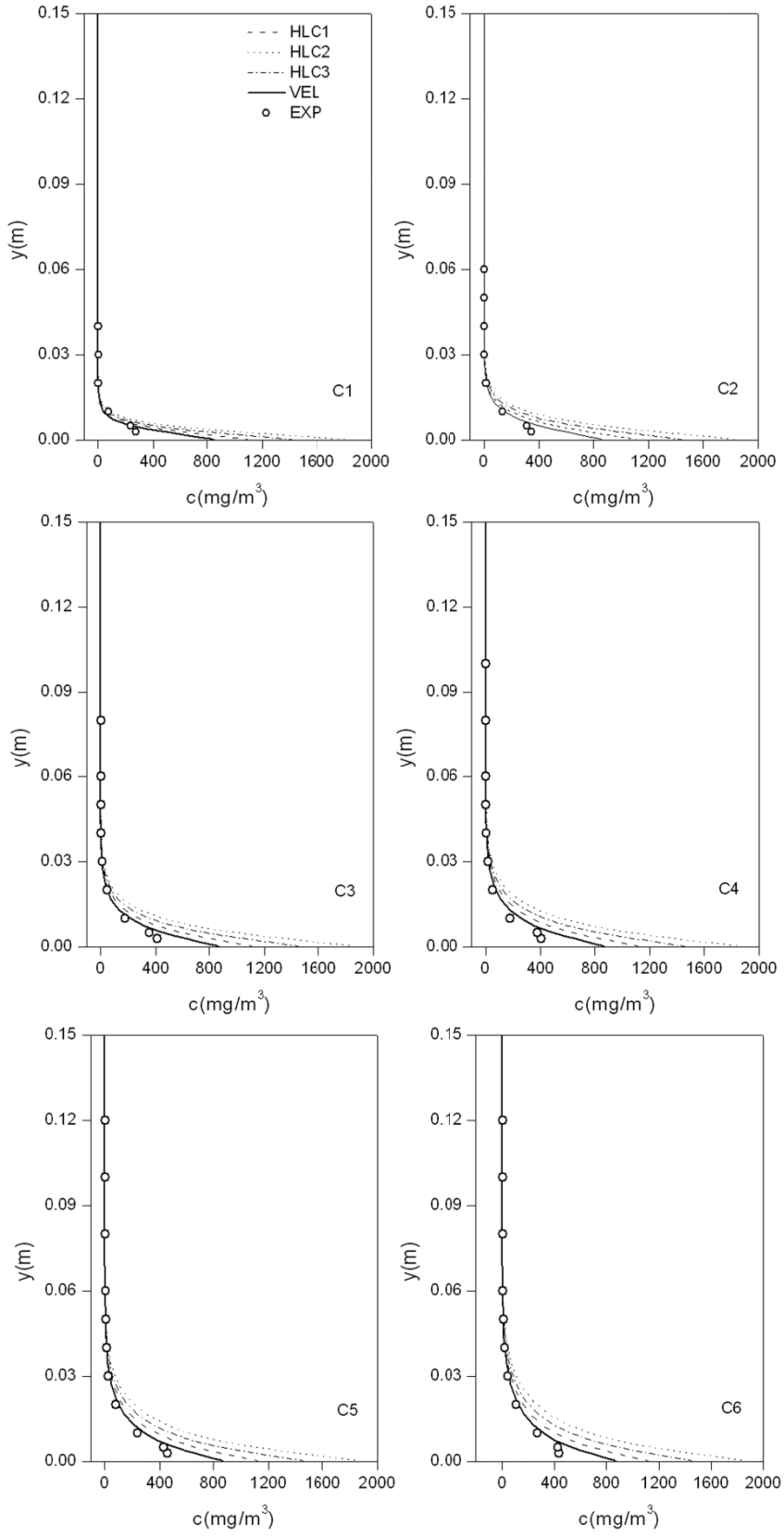

(a) Concentration profiles

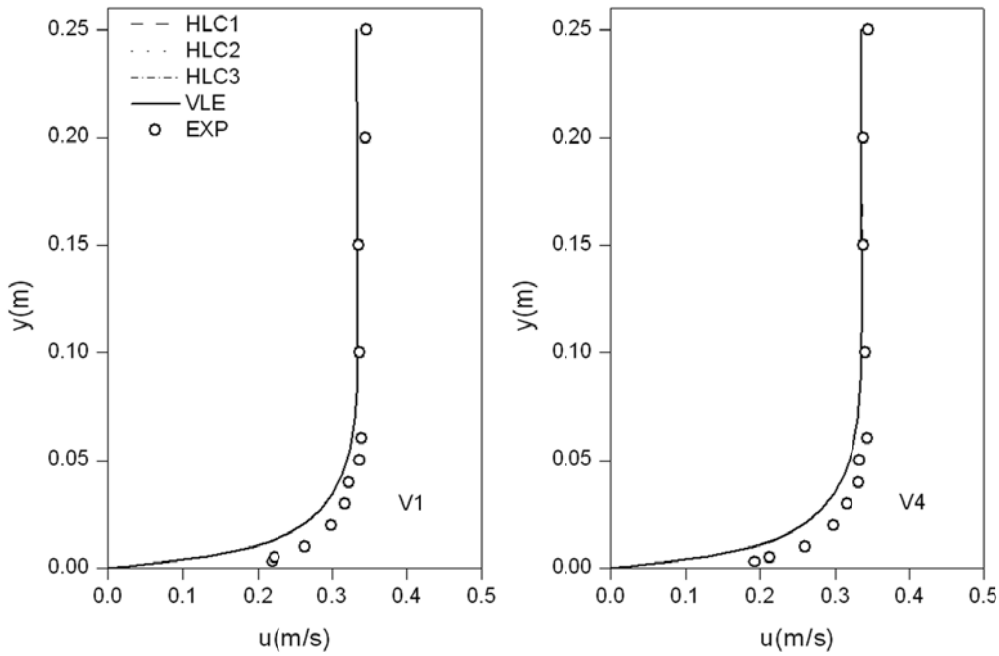

(b) Velocity profiles

Figure 3.10 Comparison of concentration and velocity profiles in the boundary layer between simulated and measured results for case Tu10T22u3 using SST turbulence model

3.3.5 Simplified form of partition coefficient using VLE model

Even though the simulated ammonia emissions were in better agreement with measurements when VLE model was used to determine the concentration boundary condition on the emission surface, it was not convenient to use it. Therefore, the ammonia concentration in the gas phase calculated from VLE equations was summarized and a model to relate the ammonia concentration in the air to the ammonia concentration in the liquid was developed. The form of this function is similar to the other HLC models introduced in this chapter. Figure 3.11 presents the relationship between the partition coefficient and liquid temperature obtained from VLE model. The simplified form of this partition coefficient model was typically presented as:

$$\log K_h = A + \frac{B}{T} \tag{3. 12}$$

Where A and B are constants and respectively are -3.337 and 1977.309; T is liquid temperature (K). This model will be applied in chapter 4 to simulate the ammonia emission in a full scale pig pen built at Air Physics Lab in Aarhus University.

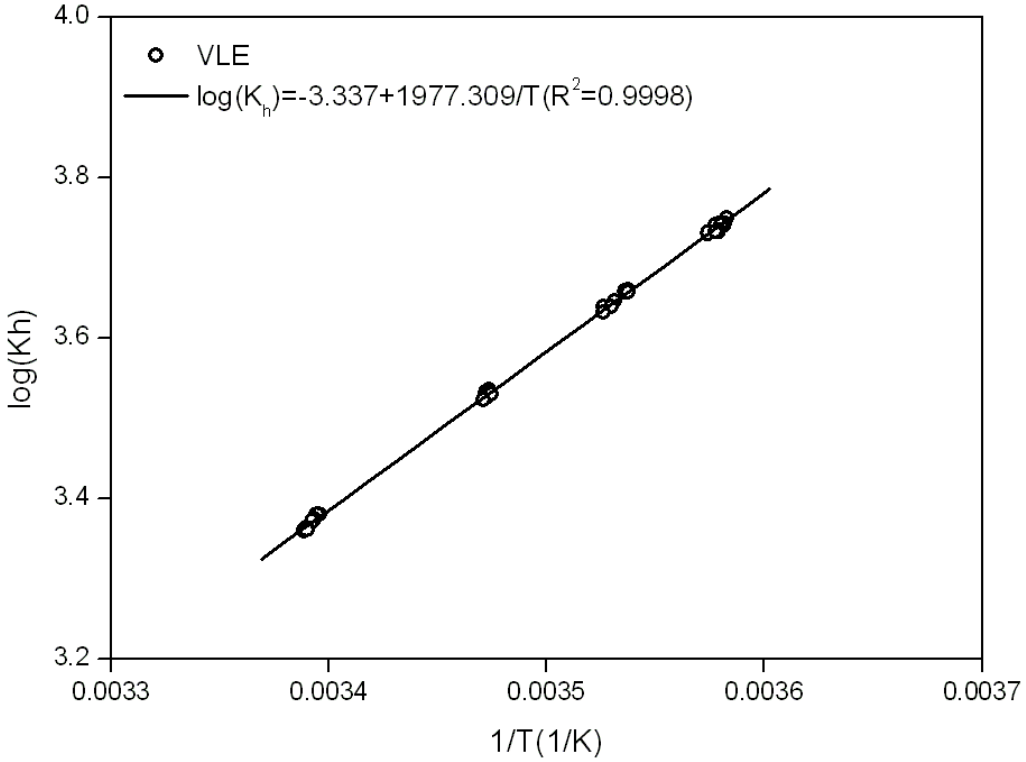

Figure 3.11 Relationship between partition coefficient and liquid temperature obtained from VLE model

3.3.6 Effects of airflow and liquid temperature on ammonia mass transfer coefficient

The effects of different HLC models and VLE model used to define the concentration boundary conditions on the ammonia emission rate have been discussed above. These models were established to define a constant concentration on the emission surface. However, sometimes it was difficult to determine the concentration on the emission surface, for instance, the concentration on the manure surface in actual pig houses. Under this condition, the constant flux is set as the concentration boundary condition in order to study the concentration distribution in the building. In this section, constant flux to define the concentration boundary condition was also used to perform the simulations comparing to the boundary condition of using constant concentration on the emission surface. The comparison of concentration, velocity and temperature profiles between simulated and measured results were presented for cases Tu10T10u3 and Tu10T22u3 using SST turbulence model as follows.

Figure 3.12 and Figure 3.13 presented the comparison of concentration, velocity and/or temperature profiles between simulated and measured results under constant flux concentration boundary conditions using SST model. The flux was calculated from the ammonia emission rate achieved from wind tunnel experiments in chapter 2. The velocity and temperature profiles were similar to the ones using constant concentration to determine the boundary conditions. The concentration profiles of

numerical results were in good agreement with the measurements, even better than the results presented in Figure 3.9 and Figure 3.10 for the point closest to the emission surface for case Tu10T22u3. It was noticed that the concentration on the emission surface increased downstream under constant flux concentration boundary conditions. This could be explained by the boundary layer theory. The concentration boundary layer thickness was becoming thicker along the emission surface and it required larger surface concentration to give the equal mass flux. Thus defining the constant concentration on the emission surface was actually contradictory to the constant flux boundary condition for specific cases. The results simulated by constant flux were presented only to see how big the difference of ammonia mass transfer coefficient was between those two methods and the effects of those boundary conditions on ammonia mass transfer coefficient.

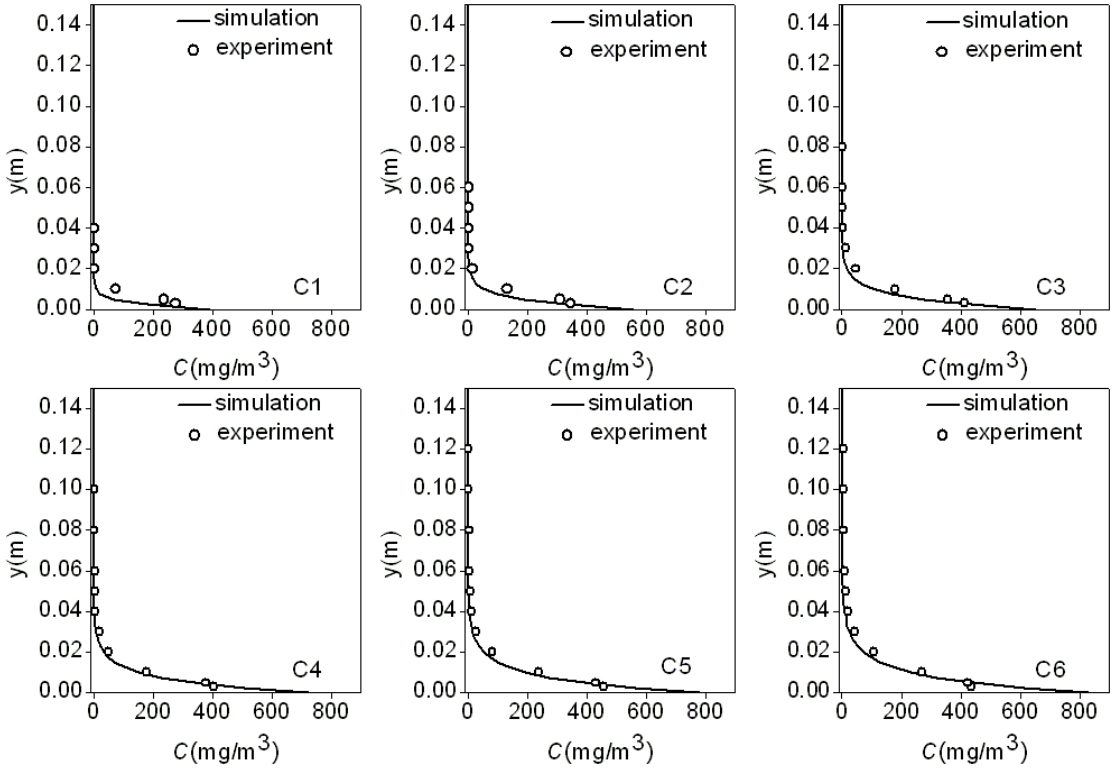

(a) Concentration profiles

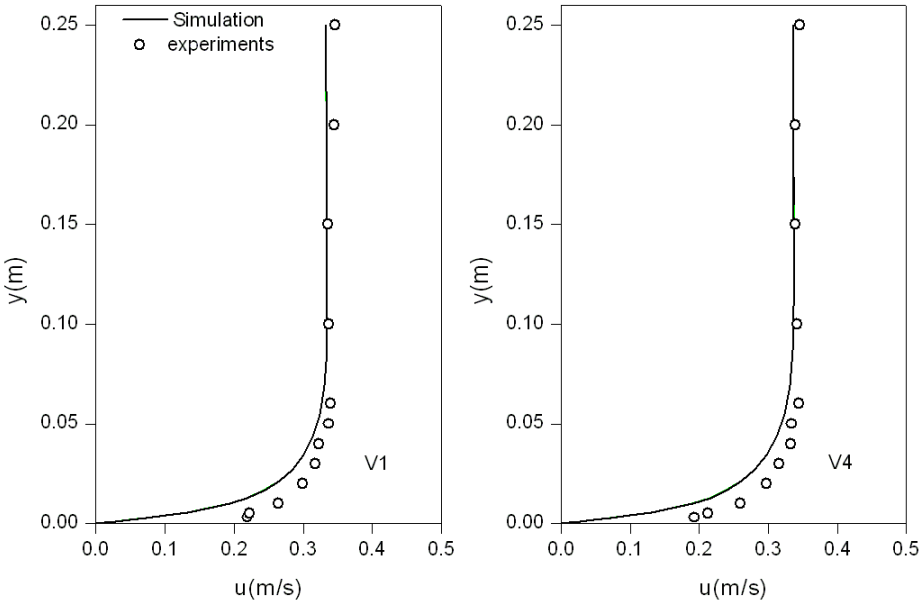

(b) Velocity profiles

Figure 3.12 Comparison of concentration and velocity profiles for case Tu10T22u3 using constant flux to define the concentration boundary conditions with SST model

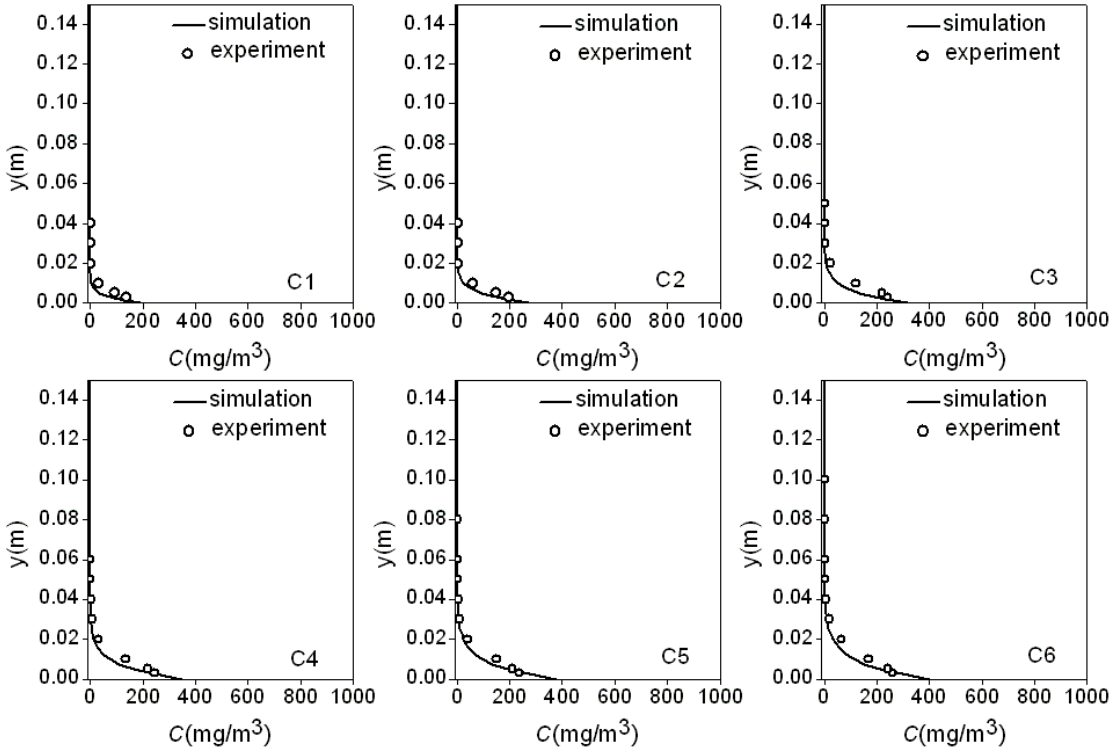

(a) Concentration profiles

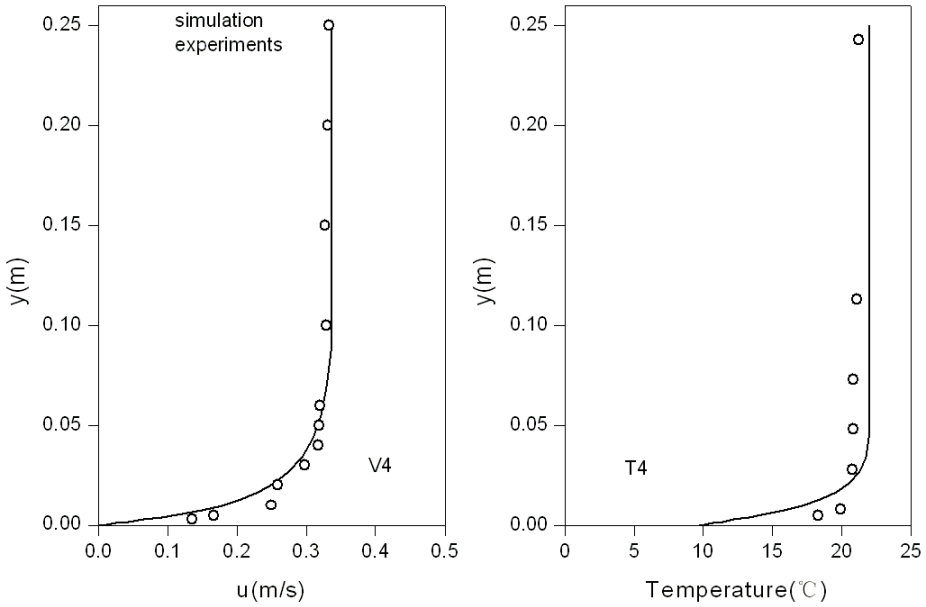

(b) Velocity and temperature profiles

Figure 3.13 Comparison of concentration, velocity and temperature profiles for case Tu10T10u3 using constant flux to define the concentration boundary conditions with SST model

The results in Figure 3.14 show the effects of airflow and liquid temperature on ammonia mass transfer coefficient under different concentration boundary conditions. The mass transfer coefficient generally increased with air velocity as expected by the theory of mass transfer. With velocity of 0.1m/s, the mass transfer coefficient increased slightly with the liquid temperature. With the velocity from 0.2m/s to 0.4m/s, the ammonia mass transfer coefficient changed little with liquid temperature except for HLC1 model, under which conditions the ammonia mass transfer coefficient increased slightly with the liquid temperature. Theoretically, the convective mass transfer coefficient in the air was a function of airflow parameters (air velocity, temperature, turbulence intensity etc). It should not be affected by the concentrations on the emission surface. Therefore, the accuracy of HLC1 model to relate the concentration at the gas-liquid interface should be further investigated.

The ammonia mass transfer coefficient was the biggest with constant flux boundary condition in Figure 3.14, varying from 1.1E-03 to 3.8E-03 m/s, which was followed by the VLE model with mass transfer coefficient varying from 1.05E-03 to 2.46E-03m/s when the turbulence intensity was 10%. The mass transfer coefficient was the smallest with constant concentration boundary condition decided by HLC2 model, varying from 5.42E-04 to 1.13E-03m/s. The ammonia mass transfer coefficient using VLE model was over twice as those using HLC2 model. The value of ammonia mass transfer coefficient presented in Figure 3.14 was in the order of the ammonia mass transfer coefficient found in other references. Ni (1998) estimated the convective mass transfer coefficient ranging from 1.0E-04 to 2.3E-03 m/s under the conditions

that manure temperature ranged from 8.0 to 21.5 ℃ and ventilation rate ranged from 200 to 5500 m^3/h in a pig house. Ye et al. (2008) found the ammonia mass transfer coefficient varied from 2.2E-03 to 4.1E-03 when the airflow rate ranged from 39.6 to 154.8 m^3/h in a scaled model (840mm×550mm) using an ammonia aqueous solution.

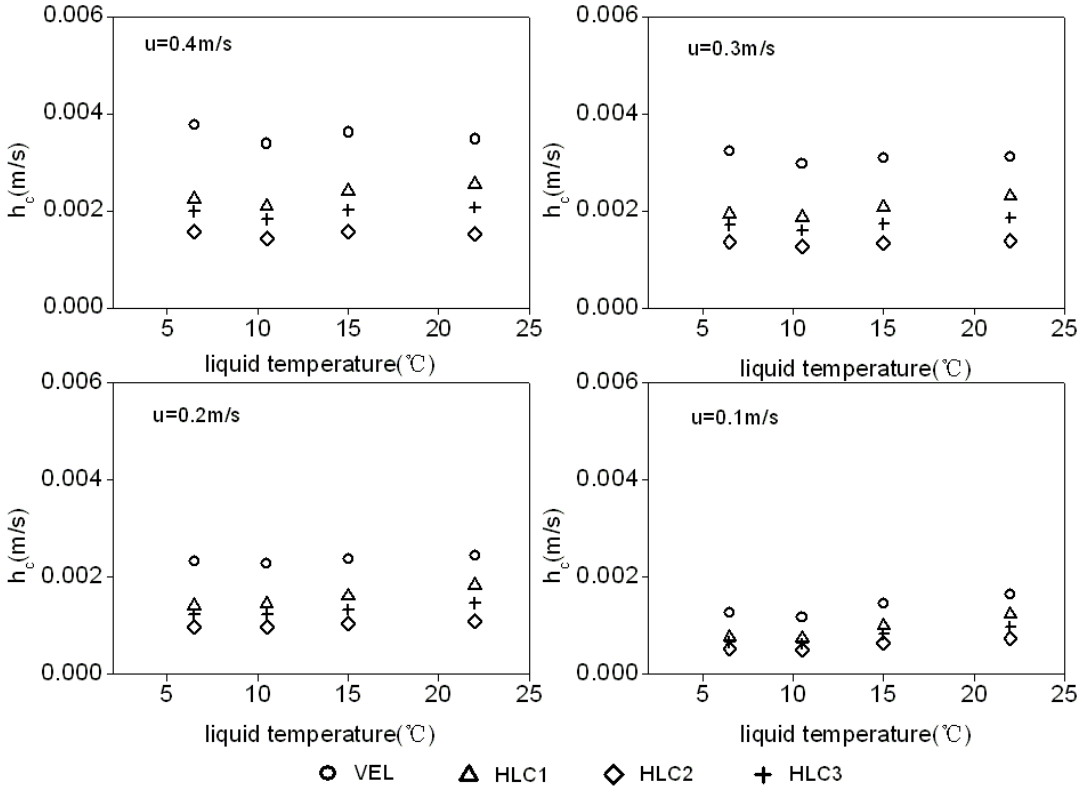

(a) Tu=35%

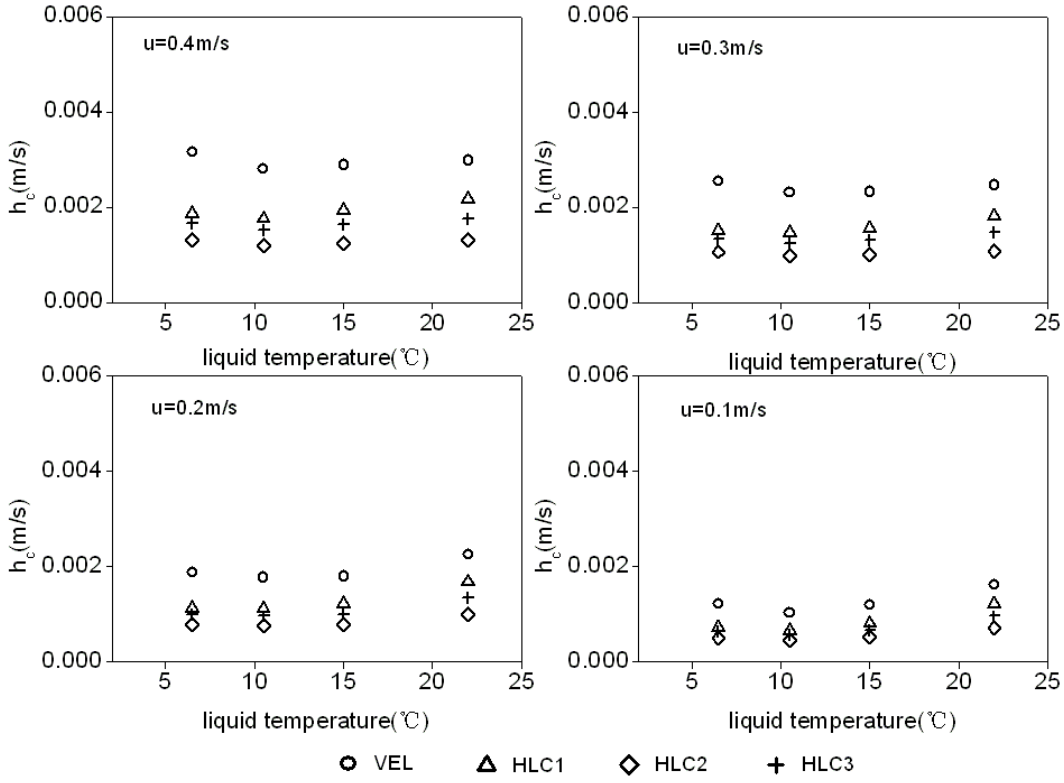

(b) Tu=16%

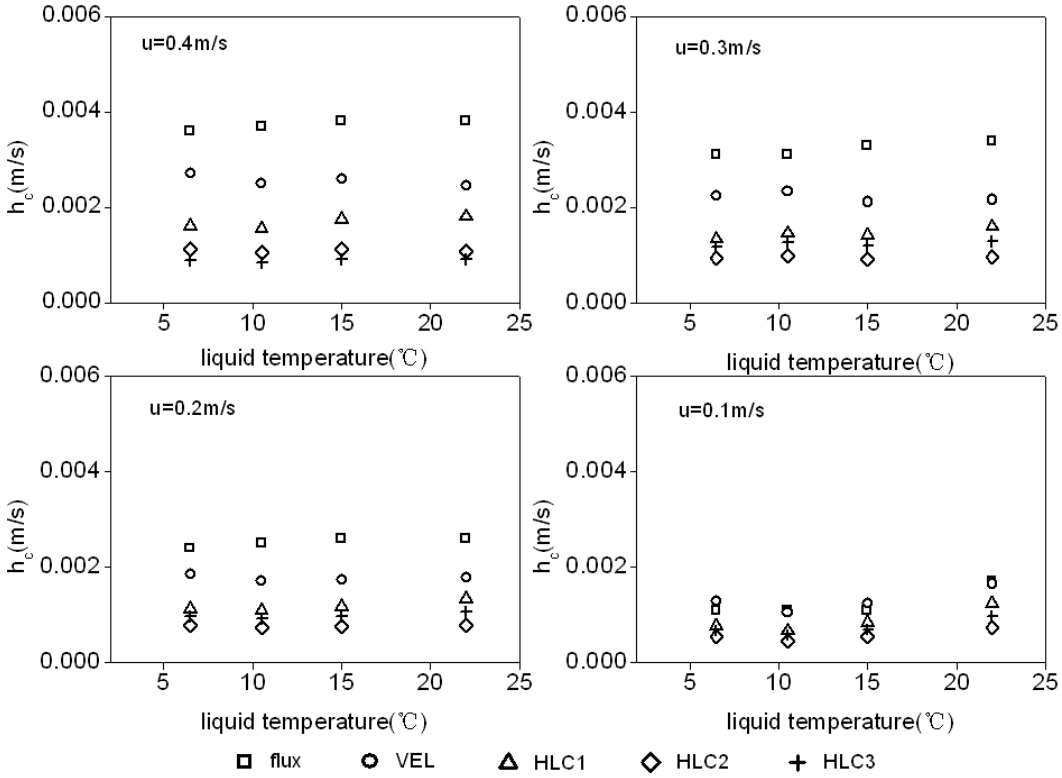

(c) Tu=10%

Figure 3.14 Effects of airflow and liquid temperature on ammonia mass transfer coefficient

The results in Figure 3.15 presented the relationship of ammonia mass transfer coefficient between using VLE model and HLC methods (HLC1, HLC2 and HLC3 model) to define the concentration on the emission surface. It indicated that there was a linear relationship between those mass transfer coefficients derived from different models.

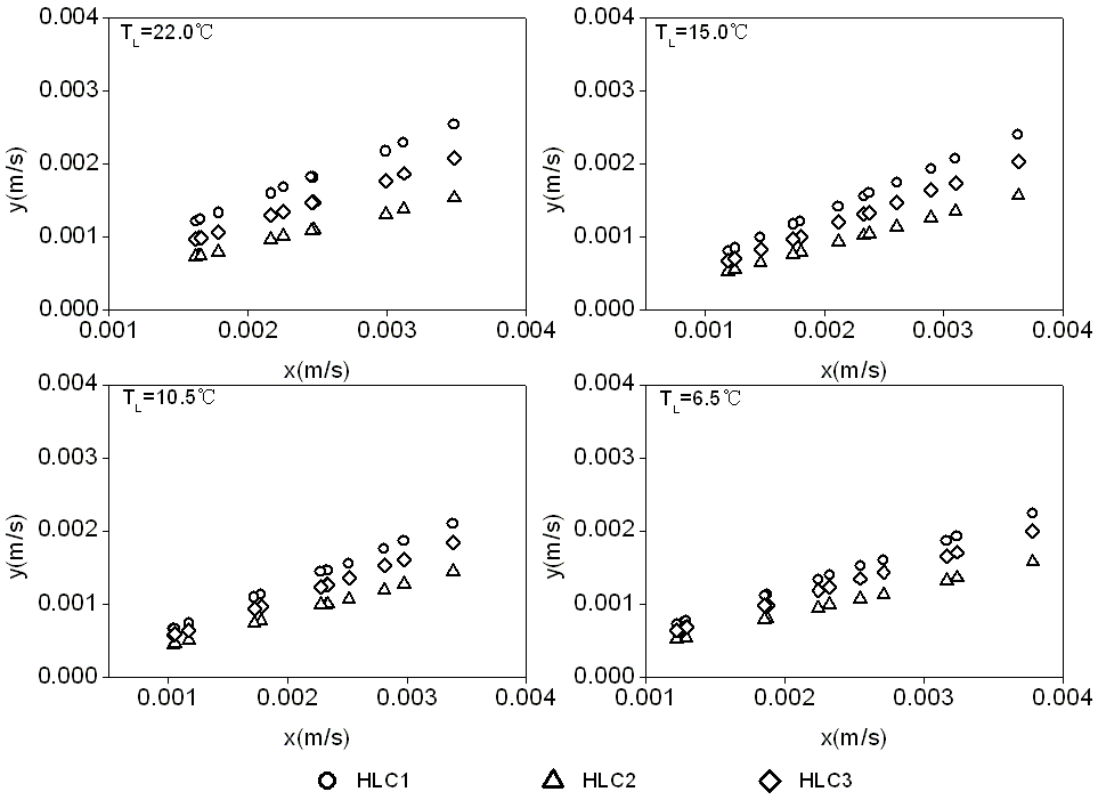

Figure 3.15 Relation of ammonia mass transfer coefficient between using VEL model and other methods to define the concentration on the emission surface. y—ammonia mass transfer coefficient using HLC1, HLC2 and HLC3 models, x—ammonia mass transfer coefficient using VLE model

In analogy to heat transfer, the mass transfer can be described by a dimensionless parameter, Sherwood number, Sh:

$$Sh = \frac{h_c L}{D_a} \tag{3.13}$$

Where L is the characteristic length (m) and D_a is the molecular diffusion coefficient of ammonia in the air (m^2/s).

Correlations are available to relate Sherwood number (Sh) with the Reynolds number (Re_L) and Schmidt number (Sc). Sissom and Pitts (1972) suggested the following correlations:

$$Sh = 0.664\,\mathrm{Re}_L^{1/2}\,Sc^{1/3} \quad \text{for } \mathrm{Re_L}<500{,}000 \tag{3.14}$$

$$Sh = 0.037\,\mathrm{Re}_L^{4/5}\,Sc^{1/3} \quad \text{for } \mathrm{Re_L}>500{,}000 \tag{3.15}$$

The Sh for ammonia calculated by Eq. (3.13) and those by numerical simulations were shown in Figure 3.16. The results indicated that the mass transfer coefficient obtained by numerical simulations with VLE model was closer to the Eq. (3.14), but the mass transfer coefficient obtained by numerical simulations with other methods was either over-predicted or under-predicted. One possible reason could be the methods used to define the concentration on the emission surface which deviated from the value provided by the solution in chapter 2.

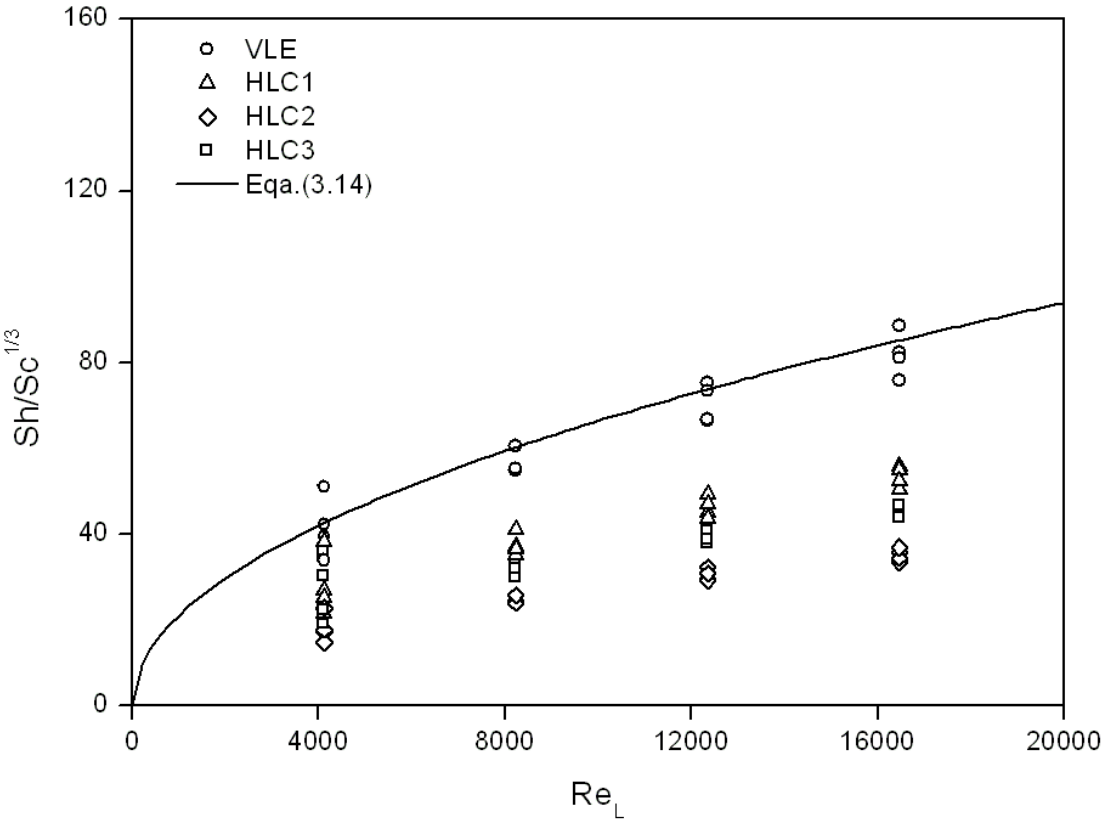

Figure 3.16 Predicted Sh in the wind tunnel under different Re

3.4 Conclusions

A mathematical model to connect the ammonia concentration in the air with the value in the liquid was developed using CFD simulations and VLE model to define the concentration boundary conditions. The form of this model was similar with the forms of other HLC models in order to make it be more convenient for applications. By comparing the numerical simulations and measurements using different methods to define the concentration boundary condition on the emission surface, the following conclusions were summarized:

(1) Since the HLC models were developed either by directing measurements for specific solutions or estimation from quantitative property-property relationships, the accuracy should be further validated when they were used to study the

ammonia emission rate and effects of different parameters on the mass transfer coefficient.

(2) The numerical simulations further confirmed the effects of airflow and liquid temperature on the ammonia mass transfer process in the air. The ammonia mass transfer coefficient increased with higher velocity and changed little with liquid temperature when velocity ranged from 0.2m/s to 0.4m/s. The effects of velocity were in accordance with the effects of velocity on ammonia emission rate while the effects of liquid temperature on the mass transfer coefficient were not corresponding to the effects of liquid temperature on the ammonia emission rate.

(3) There was a linear relationship between the mass transfer coefficient obtained from VLE model and those obtained from HLC models. It indicated that the difference of concentration determined by VLE model or HLC models can be connected by a linear factor no matter what conditions of ammonia solution is.

Chapter 4

Study on the Effects of Ventilation Systems on the Airflow and Ammonia Emissions

In this chapter, a numerical study is carried out to predict the airflow and ammonia emissions in a full scale pig pen. The study is for different solution temperature, slatted floor opening ratios and ventilation systems. A commercial CFD software is used to simulate the airflow patterns and ammonia concentration distribution. The effects of diffusive ceiling ventilation system on ammonia emissions and mass transfer coefficient have been investigated and compared with the other two mixing ventilation systems. The results show that the diffusive ceiling ventilation system can provide a relative low velocity environment and generate low ammonia emissions to the atmosphere but may not provide good air quality (low ammonia concentration) at the animal occupied zone in a pig pen. Further, the effects of solution temperature on ammonia emissions and mass transfer coefficient are also studied. The results show that the solution temperature affects not only the ammonia emissions greatly but also the mass transfer coefficient. This is different from the observation of the effect of solution temperature on ammonia mass transfer coefficient in chapter 3.

4.1 Introduction

In previous chapters, the effects of airflow and ammonium solution temperature on ammonia emission rate and the accuracy of Henry's law constant to determine the concentration on the emission surface have been studied in a wind tunnel. The ultimate goal of the study is to provide effective ventilation system for the pig houses and decrease the ammonia emission from livestock buildings. Due to the complexity of the phenomena involved in pig production systems, the amount of information required to fully quantify the effects of ventilation systems, pollutant sources and the structure designs (e.g. slatted floor opening ratio) on the ammonia emissions is dependant both on the physics involved and the level of precision associated with the analysis tools. As discussed in previous chapters, experiments performed in field studies lumped the effects of both internal factors and external factors on the ammonia emissions even though these field studies can provide a comprehensive estimate of ammonia emissions. Therefore numerical modeling techniques such as CFD can provide an effective way of appropriately quantifying the effects of the ventilation systems, slatted floor opening ratio and manure temperature on ammonia emissions within a virtual environment.

Norton et al. (2007) reviewed application of computational fluid dynamics in the modeling and design of ventilation systems in the agricultural industry. It indicated that CFD application is becoming more important to predict the effectiveness of ventilation systems in the agricultural industry, which is evidenced by the increase in peer reviewed papers of CFD applications in recent years. It is apparent that most of the studies are related to the greenhouse ventilation system design and there are a few

papers to compute the environment of animal buildings. Choi et al. (1988, 1990) used $k-\varepsilon$ model to predict air distribution in a slot ventilated enclosure and approximated the geometry of livestock buildings as a two-dimensional rectangle. Hoff et al. (1992) used CFD to simulate the buoyant flow in a three-dimensional scaled livestock confinement facility model and compared the simulated results with experiments. Harral and Boon (1997) used standard $k-\varepsilon$ model to simulate a mechanically ventilated livestock building without animals and compared the air flow patterns with the measurements. Bjerg et al. (1999, 2002) studied the three-dimensional effects in a livestock test room with two-dimensional boundary conditions. The results revealed that the flow was highly three dimensional when the room's width-height ratio was less than one. Bjerg et al. (2000) also investigated the effects of pen partitions and thermal pig simulations on airflow in a livestock test room. It indicated that both the measurements and CFD simulations showed that the introduction of pen partitions and thermal pig simulators reduced the air velocities in the occupied zone of the test room. Bjerg et al. (2008) studied the porous media as boundary condition for air inlet, slatted floor and animal occupied zone to simulate the airflow in a pig unit. The simulated velocities were in reasonable agreement with the measurements. The above mentioned literatures mainly studied the air flow patterns in livestock buildings and investigated the method to model the inlet, slatted floor and animal occupied zone appropriately. These studies have not concerned the contaminants distribution (e.g. ammonia, H_2S) at all.

The effects of ventilation rate on contaminant concentration were simulated in a 1:6 scaled ventilation chamber using tracer gas CO_2 (Hoff et al. 1995). The distribution of ammonia was studied in an isothermal, two-dimensional CFD model of an alternative pig housing systems, a high rise hog building (HRHB) by Sun et al. (2002). In a later study, Sun et al. (2004) simulated ammonia distribution in the same isothermal building in three dimensions without animals inside. Van Wagenberg et al. (2004) simulated airflow, temperature and CO_2 concentration distribution in a three-dimensional pig house. Rong et al. (2008) studied the effects of airflow patterns on the CO_2 distribution in a scaled livestock building. Although the above studies simulated the contaminant distribution in either scaled model or full scale pig houses, the CO_2 concentration distribution basically was only functioned as the tracer gas for the airflow patterns. The boundary condition of the ammonia defined on the manure surface was not physically reasonable in the reference of ammonia distribution studied by Sun et al. (2004) since they used the data of ammonia concentration measured just above the manure.

The above review indicates that there are few simulation studies of ammonia emissions from pig houses. Therefore, the effects of ventilation systems, slatted floor opening ratio and manure temperature on the ammonia emissions in a pig pen are studied in this chapter.

4.2 CFD modeling

CFD is a powerful tool to study the ventilation performance and contaminant dispersion and transfer in buildings. Chen (2009) presented an overview of the tools used to predict ventilation performance and concluded that the CFD models are most popular and contributed to 70% of the literature found in the review. However, there are only a few literatures found to study the contaminants distribution in livestock buildings using CFD modeling. It is probably related to the following difficulties: (1) the difficulty to determine the ammonia concentration boundary condition on the manure surface, slatted floor and from the animals; (2) the difficulty to determine the amount of ammonia absorbed in the building structures and equipments inside the building; (3) the difficulty to determine the transient ammonia release from the contaminant sources. These difficulties are also confronted in this study and the following assumptions or simplifications are made in the simulations of this chapter:

- Unsteady ammonia release from the manure is not considered and only the steady concentration boundary condition on the manure surface is simulated.
- Animals and animals' movements are not modeled.
- The slatted floor is modeled as porous media instead of actual sizes to decrease the grid number in three-dimensional model.
- The slatted floor is modeled as the slats in two-dimensional model after the simulated results of porous media modeling and slats modeling are compared.

4.2.1 Study cases

The study cases are about ammonia emissions from the manure below the slatted floor. The effectiveness of a slot supplying ventilation and diffusive ceiling ventilation system on ammonia emissions is evaluated by comparing the ammonia emissions and ammonia concentrations in the room. The effects of slatted floor opening ratios on ammonia emissions are also studied as well as the effects of solution temperature on ammonia emissions.

The full scale pig pen built at Air Physics Lab in Aarhus University will be used to model the room, as shown in Figure 4.1. The size of the room is 6.0m×4.8m×2.5m and the slatted floor is 0.1m thick. The below sketch was an experiment setup for studying the effectiveness of diffusive ceiling ventilation system and odor emissions from the slurry without pigs inside. Unlike the traditional mixing ventilation system, the diffusive ceiling ventilation system supplies fresh air with low velocity and large volume to improve the comfort at both the animal occupied zone and human occupied zone. Bjerg et al. (2008) studied the method to model the diffusive ceiling inlet, the slatted floor and the animals' occupied zone as porous media with appropriate resistance properties. However, the effect of ventilation rate on the ammonia emissions was not included because of the limitation of the experiment data. It is important to evaluate the effectiveness of such a ventilation system since this ventilation system has been applied widely in animal houses in Denmark now. On the

other hand, different types of mixing ventilation systems are still popular. It is necessary to compare the performance of diffusive ceiling ventilation system with mixing ventilation systems in terms of decreasing ammonia emissions from animal houses.

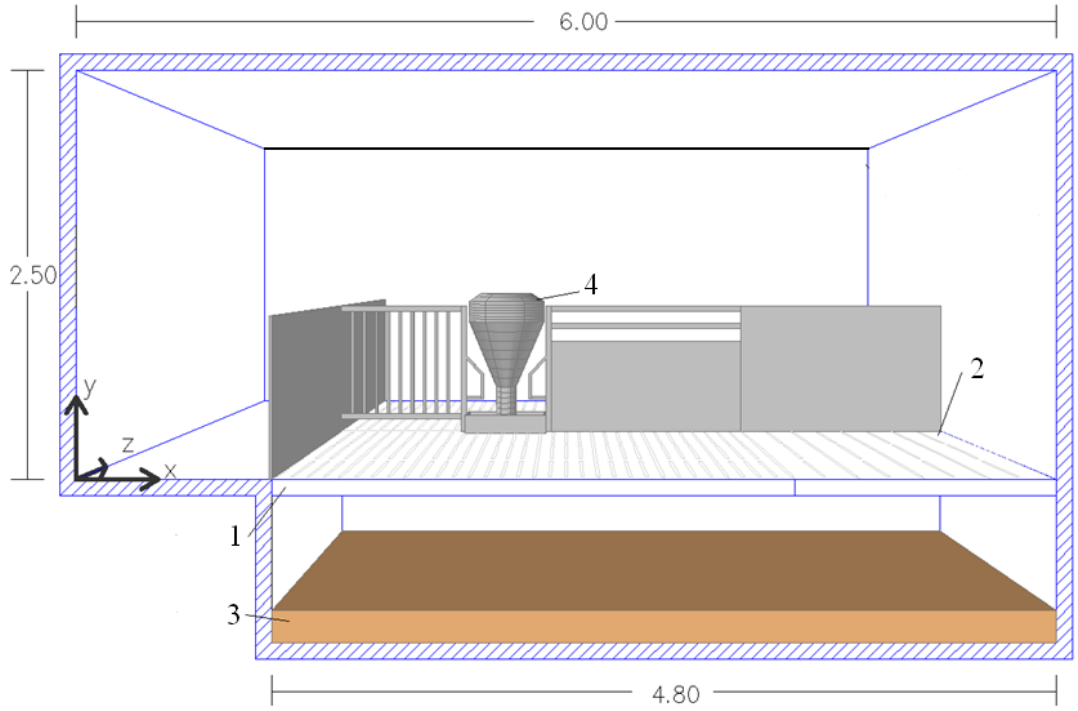

Figure 4.1 Sketch of the model pig pen. 1=slatted floor; 2=drained floor; 3=slurry; 4=feeding operation (revised from Bjerg et al. (2008)).

Many modern pig houses have concrete floors including fully or partially slatted surface with manure storage under the slats. The studies on the effects of slatted floor types or designs on ammonia emissions have been reported by some researchers (Aarnink et al. 1996; Aarnink et al. 1997; Morsing et al. 2008) in full scale pig houses or a scale model experiments. These studies indicated that decreasing the slatted floor area (or we can say decreasing the slatted floor opening ratio) resulted in the decrease of ammonia emissions in mixing ventilation system. In this chapter, the effects of slatted floor opening ratio on ammonia emissions will also be studied in diffusive ceiling ventilation system.

Besides the effects of ventilation systems and slatted floor opening ratios on ammonia emissions in pig pens, another very important factor is the manure temperature. The temperature not only affects the air flow patterns above the manure but also has an important influence on the ammonia concentration in the manure because the dissociation constant and Henry's law constant are the function of temperature (Staudinger and Roberts 1996). In chapter 2, it is also indicated that the temperature is the most important factor to affect the ammonia emission rates. Hence, the objectives of the case study are:

(1) To evaluate the effectiveness of diffusive ceiling ventilation system on ammonia emission and mass transfer coefficient, and compare with the mixing ventilation systems
(2) To investigate the effects of airflow rate and slatted floor opening ratios on ammonia emissions in both diffusive ceiling ventilation system and mixing ventilation systems.
(3) To study the impacts of the ammonium solution temperature on ammonia emissions and mass transfer coefficient under one mixing ventilation system.

To achieve the objectives mentioned above, a series of simulation cases were designed for ammonia emission study. The cases use different slatted floor opening ratios and ventilation systems as specified below.

Slatted floor:

- Type A: the opening ratio of the slatted floor is 0.165 and shown in Figure 4.2(a).
- Type B: the opening ratio of the slatted floor is 0.085 and shown in Figure 4.2(b).
- Type C: the slatted floor consists of two-third of Type A and one-third of Type B, and the opening ratio is 13.83%, as presented in Figure 4.1.

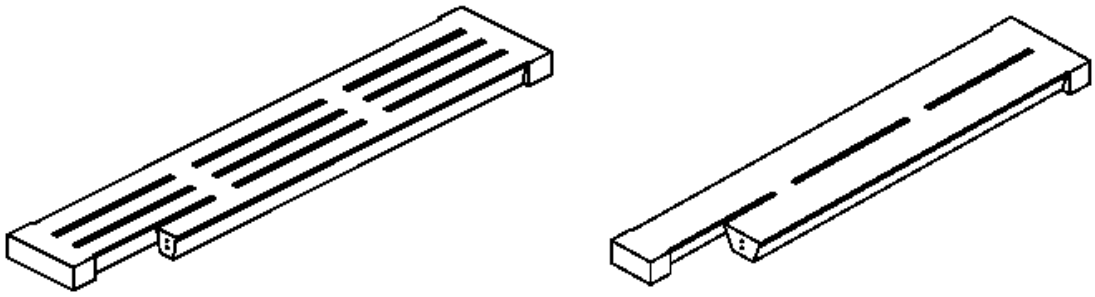

(a) Type A (b) Type B

Figure 4.2 Type of slatted floor

Ventilation systems:

- Diffusive ceiling ventilation system: the air supplied from a diffusive ceiling and exhausted from a grille on the left near the floor (Figure 4.3a).
- Mixing type I: the air supplied from a slot on the left near the ceiling and exhausted from a grille on the left near the floor (Figure 4.3b).
- Mixing type II: the air supplied from a slot on the right near the ceiling and exhausted from a grille on the left near the floor (Figure 4.3c).

Ammonium solution temperature:

- Four temperatures are studied including 15, 22, 25, 30℃.

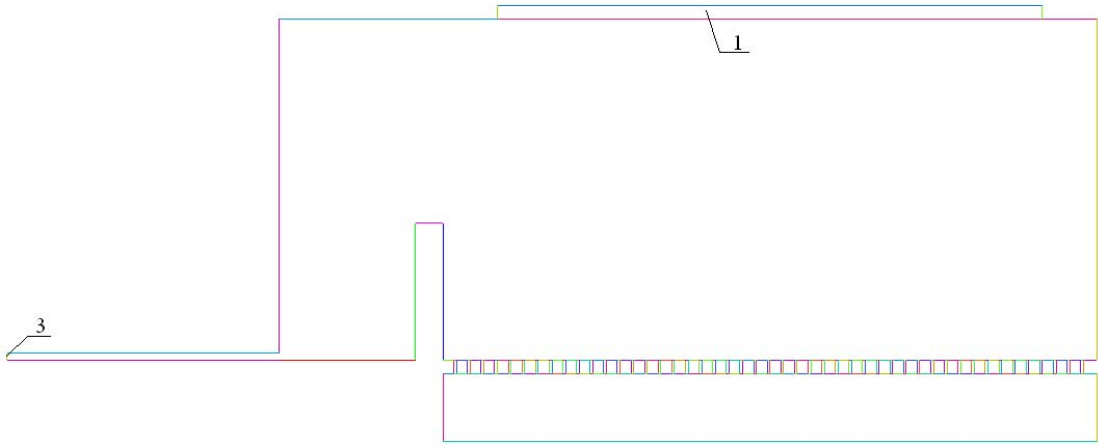

(a) Schematic of the model pig pen with diffusive ceiling ventilation (slatted floor Type A, 2D model)

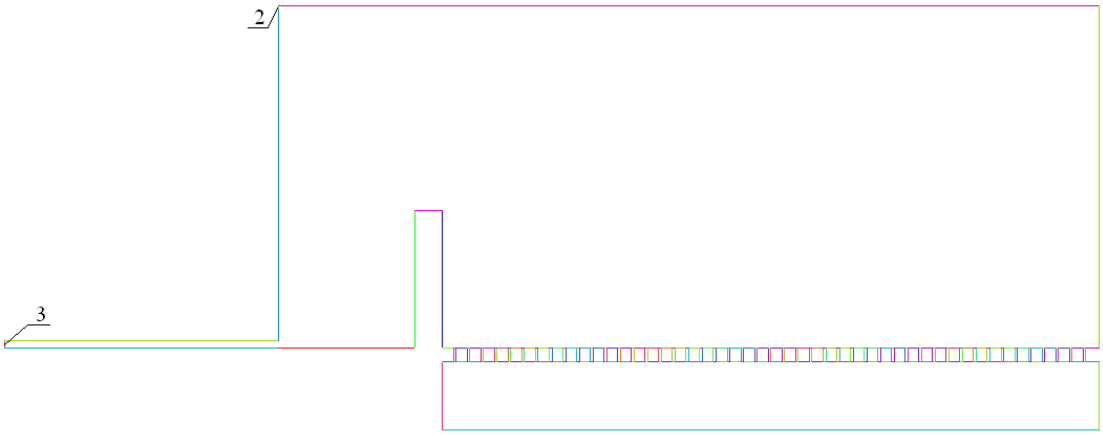

(b) Schematic of the model pig pen with mixing type I ventilation system (slatted floor Type A, 2D model)

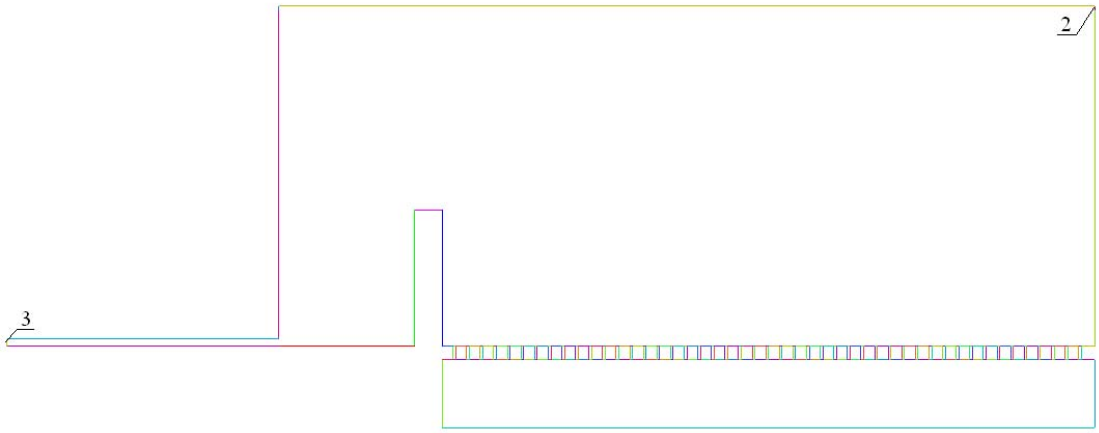

(c) Schematic of the model pig pen with mixing type II ventilation system (slatted floor Type A, 2D model)

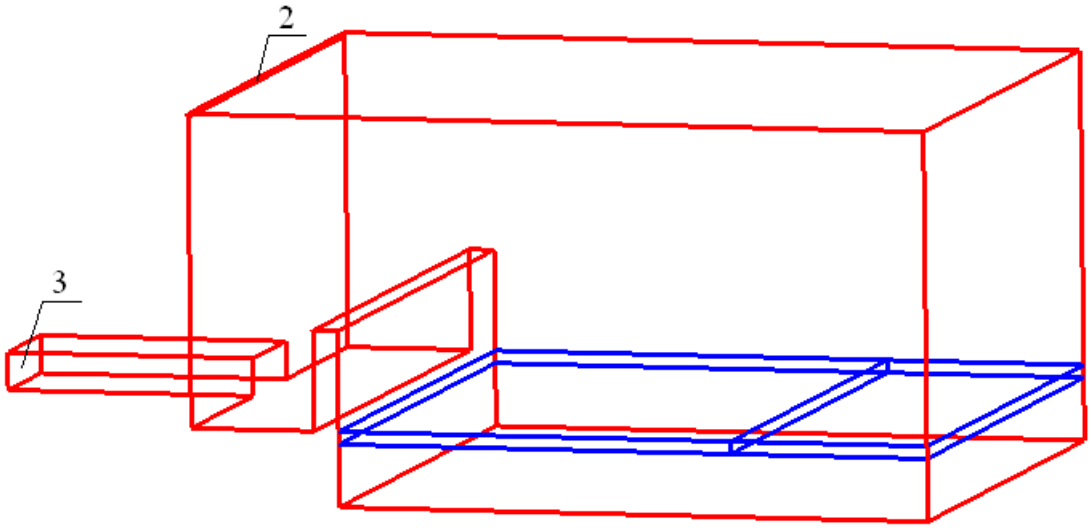

(d) Schematic of the model pig pen with mixing type I ventilation system (porous media modeling for the slatted floor, 3D model)

Figure 4.3 Schematics of the model pig pen with different ventilation systems. 1=Diffusive ceiling, 2=slot inlet, 3=exhaust

The study is arranged for the selected combinations of above slatted floor opening ratios, ventilation systems and ammonium solution temperature. Table 4.1 lists a total of 26 isothermal cases for each type of slatted floor and 4 non-isothermal cases. The simulated results between 3D porous media modeling for slatted floor, 2D porous media modeling for slatted floor and 2D slats modeling are compared in order to study the probability of simplify the 3D model to 2D model and the influence of modeling the slatted floor as a porous media and slats.

Table 4.1 Cases for ammonia emissions studies in a pig pen

Model	Slatted floor	Ventilation system	Air exchange rate (ACH)	Air supply temperature (℃)	Solution temperature (℃)
3D	Type A	Mixing type I	9, 12, 15, 18, 21	22.0	22.0
2D	Type A	Diffusive ceiling	9, 12, 15, 18, 21	22.0	22.0
		Mixing type I	9, 12, 15, 18, 21	22.0	22.0
		Mixing type II	9, 12, 15, 18, 21	22.0	22.0
	Type B	Diffusive ceiling	15	22.0	22.0
		Mixing type I	15	22.0	22.0
		Mixing type II	15	22.0	22.0
	Type C	Diffusive ceiling	15	22.0	22.0
		Mixing type I	15	22.0	22.0
		Mixing type II	15	22.0	22.0
	Type A	Mixing type I	15	22.0	15.0, 22.0, 25.0, 30.0

4.2.2 Turbulence Model, Numerical Schemes and Boundary Conditions

The RNG model was used with enhanced wall treatment in the simulations of mixing ventilation systems, which has already been introduced in chapter 3 and Appendix A. A Cartesian coordinate system with a structured mesh was applied to the geometry. The flow was steady state and the SIMPLE algorithm was applied. Second-order accurate upwind schemes were employed for momentum equations, energy equation and species equation. A body weighted scheme was used for the pressure interpolation. The convergence criteria was set as 10^{-5} of residual for all solved equations and the convergence was not assumed to be reached until the velocity magnitude at a specific point above the slatted floor and the concentration at outlet have stabilized.

The supply air exchange rate and temperature are listed in Table 4.1 as well as the ammonium solution temperature. The ammonia concentration is calculated by the Eq. (3.9), Eq. (3.10) and Eq. (3.12) with TAN 6.8g/l. The other walls are treated as adiabatic.

4.2.3 Porous media modeling

The animal houses usually have a complex geometry such as slatted floor, feeding devices and animals. It would be ideal that the geometry can be modeled specifically but it would be very time consuming. An alternative way of overcoming this disadvantage is to assume that the animal occupied zone and the slatted floor consists of porous media with a certain flow resistance. A similar method has been used to model the slatted floor (Sun et al. 2004), the partly open pen partitions (Wagenberg et al. 2004) and the animal occupied zones (Bjerg et al. 2008).

The pressure drop through a porous media is generally calculated using the following equation:

$$\Delta p = 0.5 \cdot R_1 \cdot \rho \cdot v^2 + \mu \cdot R_2 \cdot v \tag{4.1}$$

where Δp is the pressure drop over the porous media (Pa); R_1 is the internal resistance coefficient; R_2 is the viscous resistance coefficient; ρ is the air density (kg/m^3); v is the air velocity through the porous media (m/s); μ is the air viscosity (kg/m•s).

In this study, the same type of diffusive ceiling and slatted floor are used as Bjerg et al. (2008) applied in the simulations. They investigated the potential of using the porous media approach as boundary for diffusive ceiling inlet, slatted floor and animal occupied zone in a pig pen. The appropriate flow resistance properties for each element (e.g. slatted floor, diffusive ceiling, and animal occupied zone) were studied and established. The internal resistance coefficient and viscous resistance coefficient for the diffusive ceiling was determined from the measurement of pressure drop. The internal resistance coefficient and viscous resistance coefficient for the slatted floor was determined by using CFD simulation of airflow through a segment of the slatted

floor in actual size modeling. The resistance coefficients for CFD simulation are summarized in Table 4.2.

Table 4.2 Summarization of resistance coefficients for porous media

Item	x-direction		y-direction		z-direction	
	R_1	R_2	R_1	R_2	R_1	R_2
Diffusive ceiling	4000	5.4E06	4000	5.4E06	4000	5.4E06
Slatted floor Type A	-	-	40	11000	40	11000

4.2.4 Emission rate and Mass transfer coefficient

The fundamental equation in mass transfer is Fick's law diffusion. Assuming diffusion only in one direction, the mass flux of ammonia transferring to the air is proportional to the gradient of concentration described by Fick's first law (Cussler 1985):

$$J = -D_a \frac{\partial c}{\partial y} \tag{4.2}$$

where J is the mass flux (kg/m^2.s); c is the concentration (kg/m^3) and y is the distance of the concentration gradient (m). D_a is the molar diffusion coefficient of ammonia into air (m^2/s). It is a function of temperature, pressure and component composition and can be described as (Bird et al. 1960):

$$D_a = 10^{-7} \frac{T^{1.75}\left(1/M_{air} + 1/M_{NH_3}\right)^{0.5}}{P\left[\left(\sum v\right)_{air}^{1/3} + \left(\sum v\right)_{NH_3}^{1/3}\right]^2} \tag{4.3}$$

where T is temperature in degrees Kelvin, P is pressure in atmospheres and $\sum v$ are the molecular volumes.

The emission in turbulent flow can be calculated by mass transfer coefficient and concentration difference between the emission surface and the bulk air (see Eq. 2.2). The concentration profile in turbulent flow through a flat is shown in Figure 4.1.

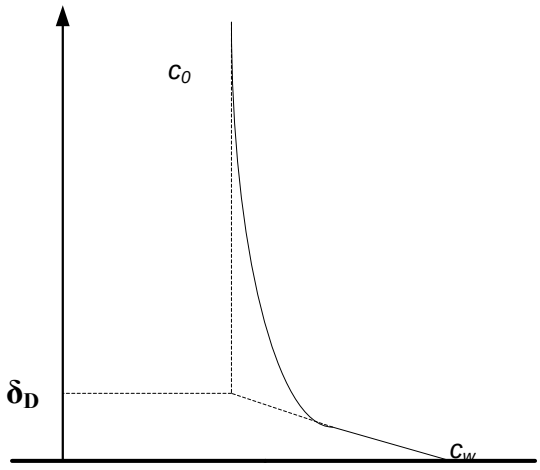

Figure 4.1 Concentration profile of turbulent flow

The thickness of diffusion boundary layer, δ_D, is defined so that the layer offers the same resistance to diffusion as encountered in the combined process of molar and turbulent diffusion (Sissom and Pitts, 1972). Evaluating Fick's first law at $y = \delta_D$ yields:

$$E = \frac{D}{\delta_D}(c_w - c_0) \tag{4.4}$$

Comparing the Eq. 2.2, then the mass transfer coefficient can be expressed by the diffusion coefficient and diffusion boundary layer thickness:

$$h_c = \frac{D}{\delta_D} \tag{4.5}$$

In the following section, the local mass transfer coefficient is calculated by Eq. (4.5). On the other hand, the global emission rate can also be calculated by ventilation rate and concentration difference between outlet and inlet. In this chapter, the emission rate is calculated in this method which was introduced in Chapter 2 (Eq. 2.1).

4.3 Results and discussion

4.3.1 Comparison of simulation results between 3D and 2D modeling

The results shown in Figures from 4.4 to 4.6 indicate that the difference in concentration distribution, velocity vector distribution and ammonia emissions is within a reasonable range between 3D porous media modeling and 2D porous media modeling for slatted floor. However, the results between 2D porous media modeling and 2D slats modeling are very different from each other. The higher velocity below

the slatted floor is found in slats modeling, which can explain why higher ammonia emission is seen in slats modeling in Figure 4.6. The ammonia emissions per one air exchange rate in slats modeling are around 1.5 times as those in porous media modeling. Since the 3D model can be simplified as 2D model and there is big difference in the results between porous media modeling and slats modeling, the following simulations are performed in 2D slats modeling.

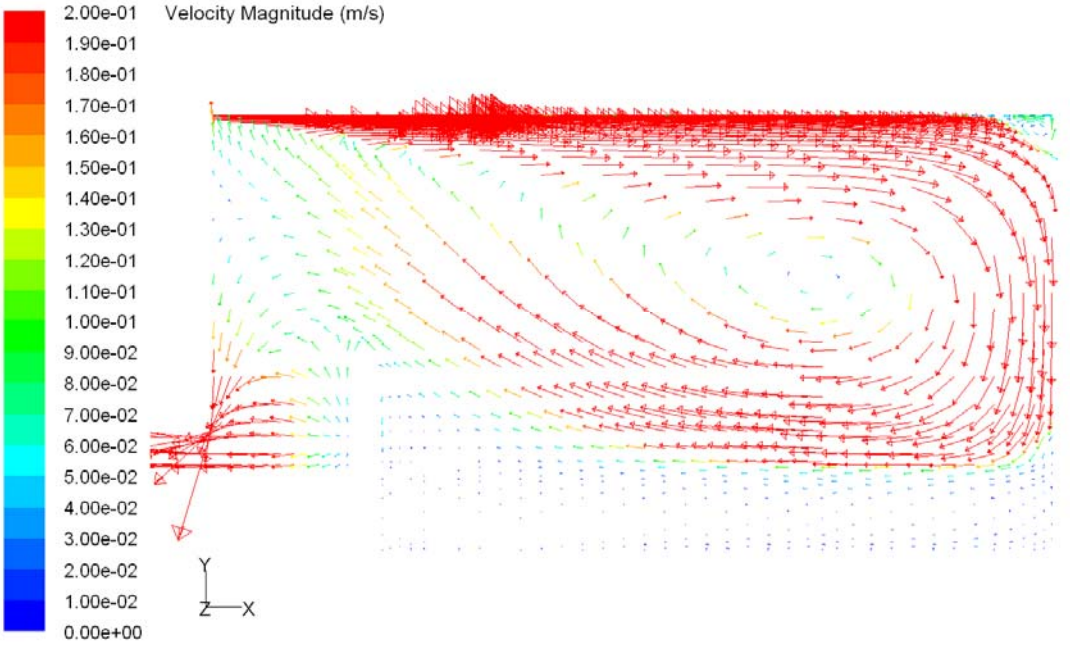

(a) Vector distribution of porous media modeling for slatted floor in 3D model

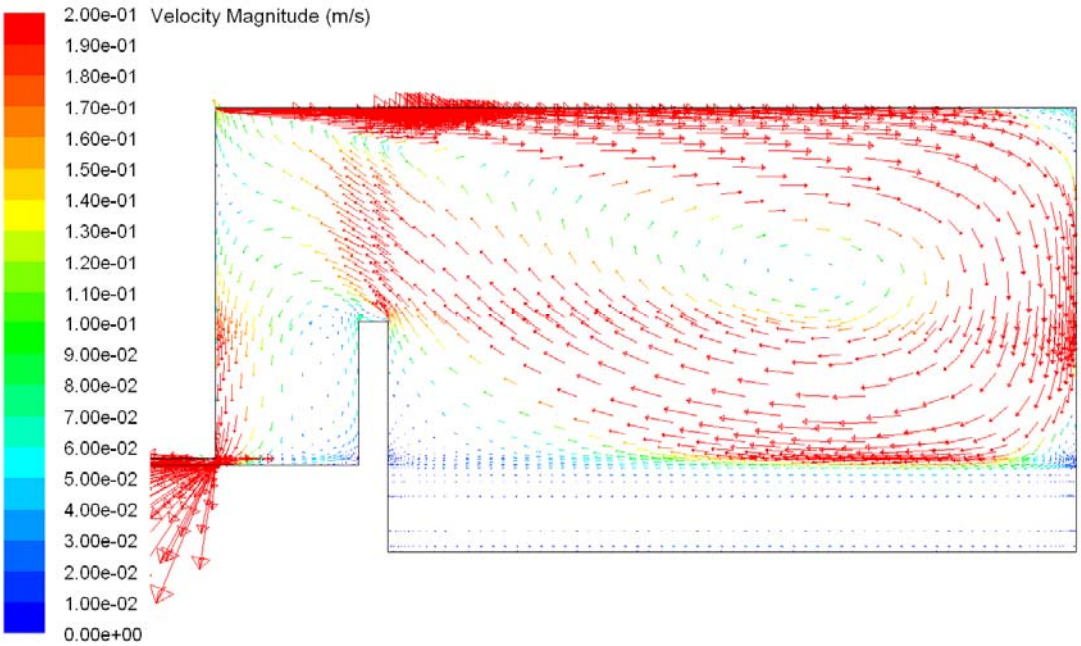

(b) Vector distribution of porous media modeling for slatted floor in 2D model

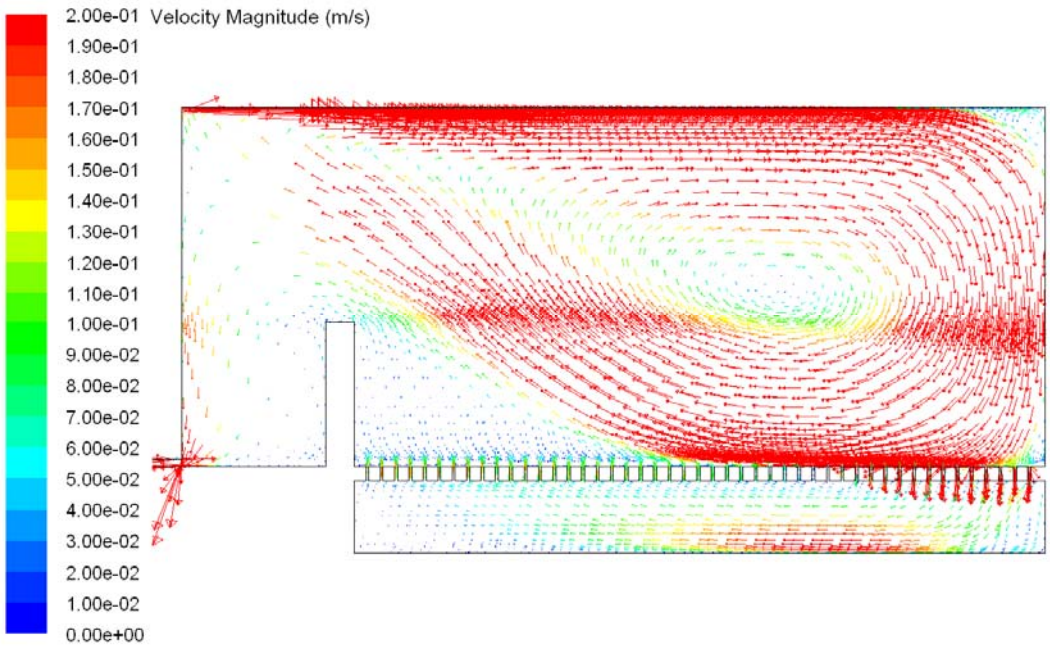

(c) Vector distribution of slats modeling in 2D model

Figure 4.4 Vector distributions for 15ACH ventilation rate

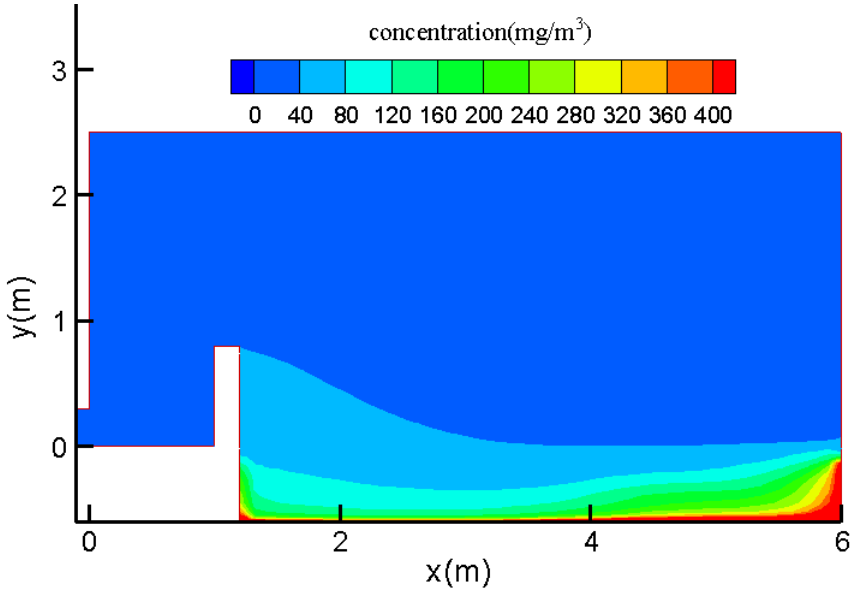

(a) Ammonia concentration distribution of porous media modeling for slatted floor of 3D model

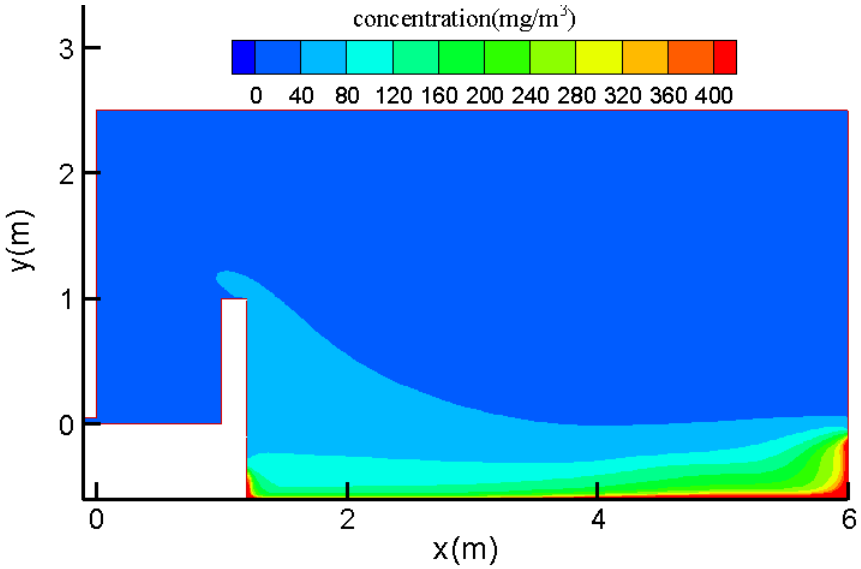

(b) Ammonia concentration distribution of porous media modeling for slatted floor in 2D model

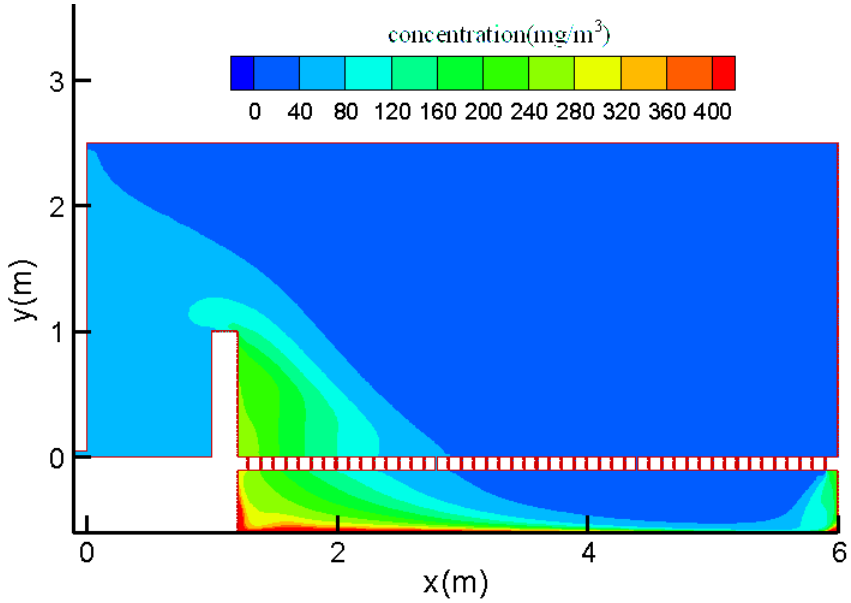

(c) Ammonia concentration distribution (mg/m^3) of slats modeling in 2D model

Figure 4.5 Ammonia concentration distributions for 15ACH ventilation rate

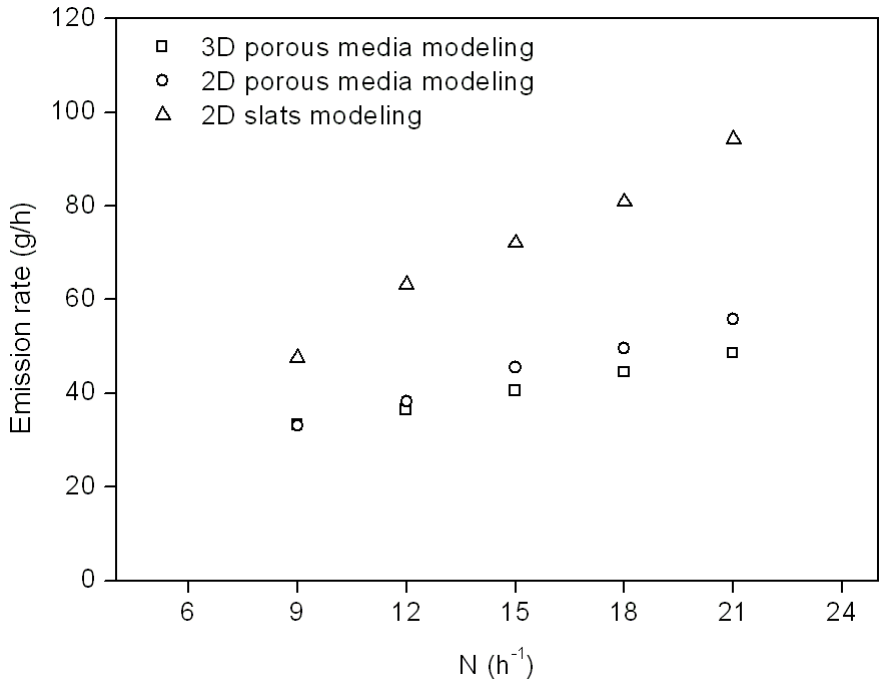

Figure 4.6 Comparison of ammonia emissions among 3D porous media modeling, 2D porous media modeling and 2D slats modeling for 15 ACH ventilation rate

4.3.2 Effects of ventilation systems and ventilation rate on ammonia emissions

Predicted velocity vectors are displayed in Figure 4.7 (The velocity vector distribution of mixing ventilation type I system is shown in Figure 4.4c) for 15ACH ventilation rate in 2D model. For diffusive ceiling ventilation system, the air from the diffusive ceiling spreads to the room at low velocity and induces a reverse flow on the right of the room. The air goes through the middle of the slatted floor to slurry container and two eddy recirculations are found there. The maximum velocity is found to be around 0.02m/s below the slatted floor. For mixing ventilation systems, a jet flow with high velocity is found near the ceiling. The jet flow generates recirculation in the room. The air goes through the slatted floor on the right to the slurry container and the maximum velocity is found to be 0.2m/s for mixing ventilation type I and 0.07m/s for mixing ventilation type II respectively.

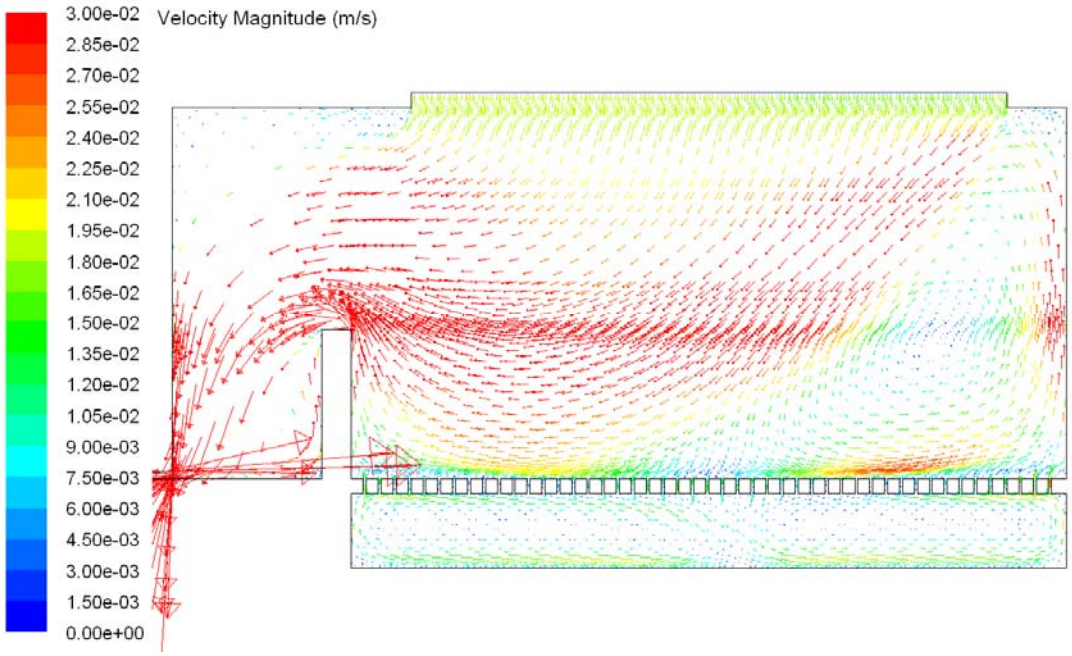

(a) Vector distribution of diffusive ceiling ventilation system

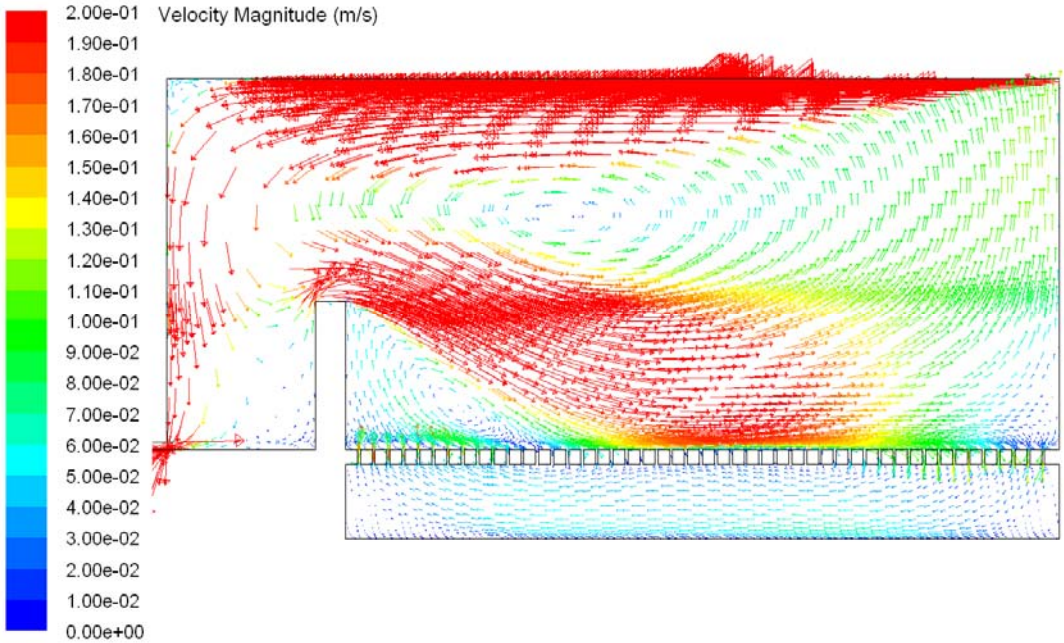

(b) Vector distribution of mixing ventilation type II system

Figure 4.7 Vector distribution of 15 ACH ventilation rate in 2D model

The predicted concentration distribution is shown in Figure 4.8 (The concentration distribution of mixing ventilation type I system is shown in Figure 4.5c) and Figure 4.9 for 15ACH ventilation rate in 2D model. For mixing ventilation systems, higher ammonia concentration is found at human occupied zone for mixing ventilation type I system and at animal occupied zone for mixing ventilation type II system. For

diffusive ceiling ventilation system, very high ammonia concentrations are found both below the slatted floor and close to the slatted floor in the room. As to the effectiveness of ventilation systems, the diffusive ceiling ventilation system can provide a relatively low velocity environment but also provide a higher contaminant concentration for the animal occupied zone. According to the continuous observation of the pig's activities, it was found that pigs prefer to stay at the area close to the wall where the ammonia concentration is high (around 110ppm ~ 570ppm) in Figure 4.8a (personal discussion with Professor Bjerg). This is not good for the pigs' well-being.

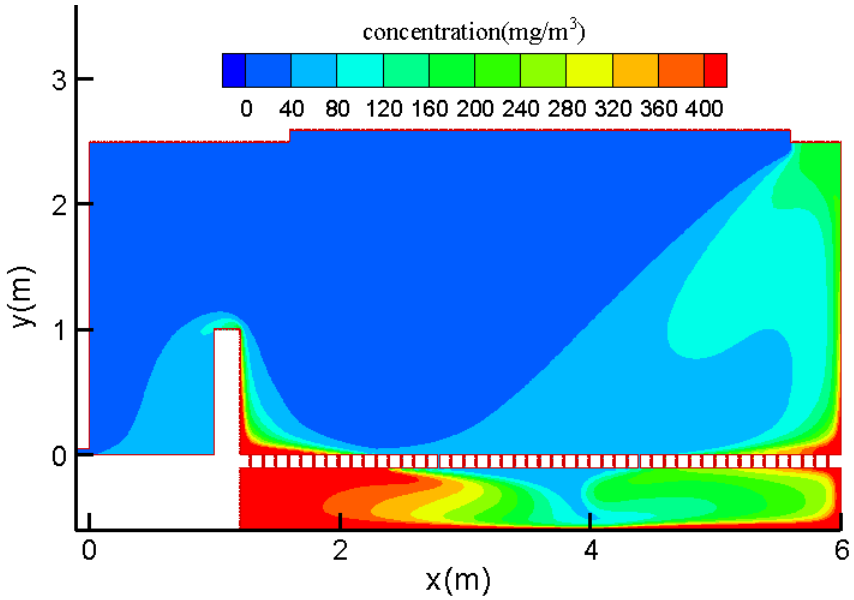

(a) Concentration distribution of diffusive ceiling ventilation system

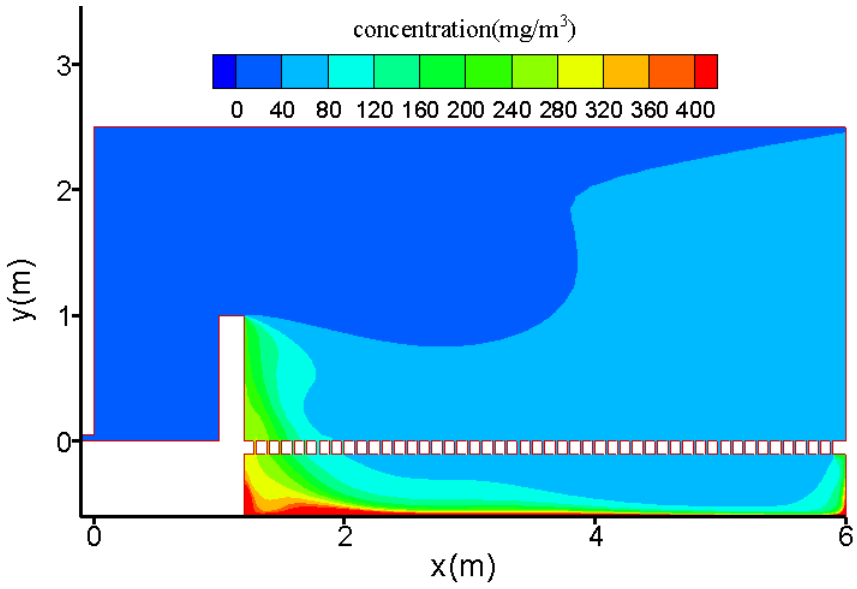

(b) Concentration distribution (mg/m^3) of mixing ventilation type II system

Figure 4.8 Ammonia concentration distribution of 15ACH ventilation rate

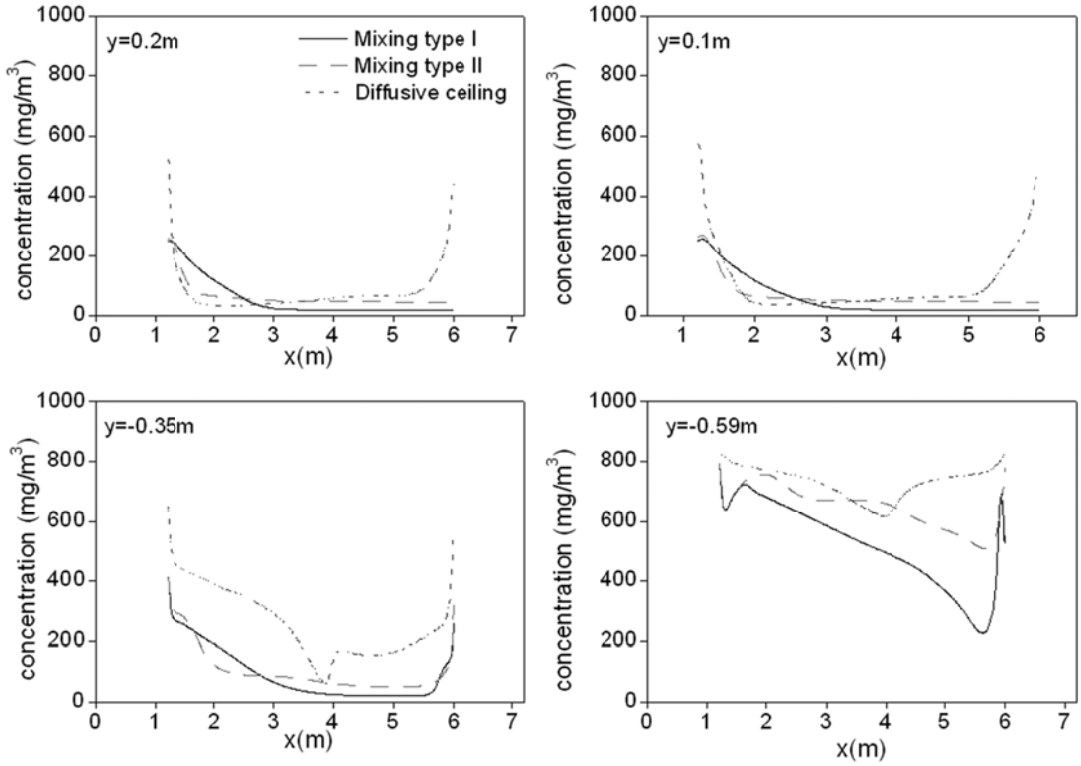

Figure 4.9 Ammonia concentration distributions along four horizontal lines under different ventilation systems for 15ACH ventilation rate

The effects of the ventilation rate on ammonia emissions under different ventilation systems with slatted floor Type A are illustrated in Figure 4.10. The ammonia emissions of diffusive ceiling ventilation system are generally lower than the mixing ventilation system and vary slightly when one increases the ventilation rate. The ammonia emission changes from 20.32g/h to 23.38g/h when the ventilation rate increases from 9ACH to 21ACH in diffusive ceiling ventilation system. For mixing ventilation type I system, the ammonia emissions increases sharply when the ventilation rate increases. The emission at 21ACH is almost double as that at 9ACH. For mixing ventilation type II system, the ammonia emissions are also generally lower than those of mixing ventilation type I and they increase with higher ventilation rate. Nevertheless, they do not increase with ventilation rate as fast as the emission of mixing ventilation type I system does.

These results indicate that increasing ventilation rate in mixing ventilation systems could improve the indoor air quality but will increase the ammonia emissions to the atmosphere. However, this effect of ventilation rate on ammonia emissions in diffusive ceiling ventilation system is not obvious. In order to improve the effectiveness of diffusive ceiling ventilation system (It means to decrease the ammonia concentration close to the slatted floor in the room), increasing the ventilation rate can realize it and would not increase the ammonia emissions significantly. Certainly, it will increase the energy exhaust of fans.

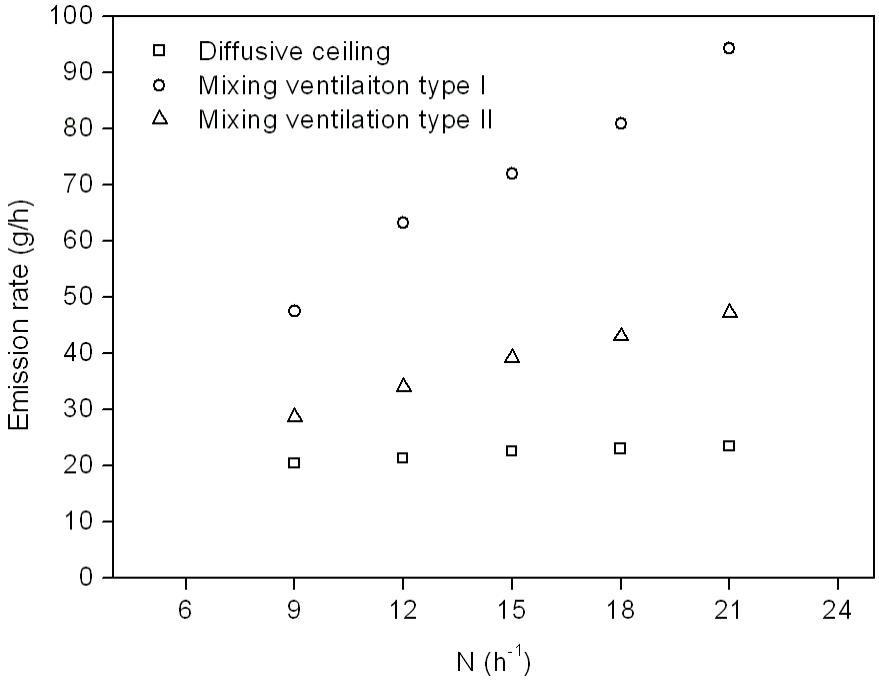

Figure 4.10 Effects of ventilation rate on ammonia emissions under different ventilation systems with slatted floor Type A

4.3.3 Effects of slatted floor opening ratio on ammonia emissions

The effects of slatted floor opening ratio (the opening ratio of slatted floor Type A, Type B and Type C is 16.5%, 8.5% and 13.83% respectively) on ammonia emissions are shown in Figure 4.11 and the velocity and concentration distribution under different slatted floor types are shown in Appendix D. The ammonia emission decreases 21.17% when the slatted floor opening ratio changes from 16.5% to 13.83%, and 10.42% when the slatted floor opening ratio changes from 13.83% to 8.5% respectively for mixing ventilation type I system. The ammonia emission decreases 10.37% when the slatted floor opening ratio changes from 13.83% to 16.5%, and 15.52% when the slatted floor opening ratio changes from 8.5% to 13.83% respectively for mixing ventilation type II system. The ammonia emission increases 0.94% when the slatted floor opening ratio changes from 16.5% to 13.83%, and decreases 20.34% when the slatted floor opening ratio changes from 8.5% to 13.83% for diffusive ceiling ventilation system. These results indicate that the change of slatted floor opening ratio has different effects on ammonia emissions under these three ventilation systems. For mixing type I, the ammonia emissions decreasing is more sensitive to the change of slatted floor opening ratio at a high value compared to the change of slatted floor opening ratio at a lower value. For diffusive ventilation systems, the ammonia emissions decreasing is more sensitive to the change of slatted floor opening ratio at a low value compared to the change of slatted floor opening ratio at a higher value.

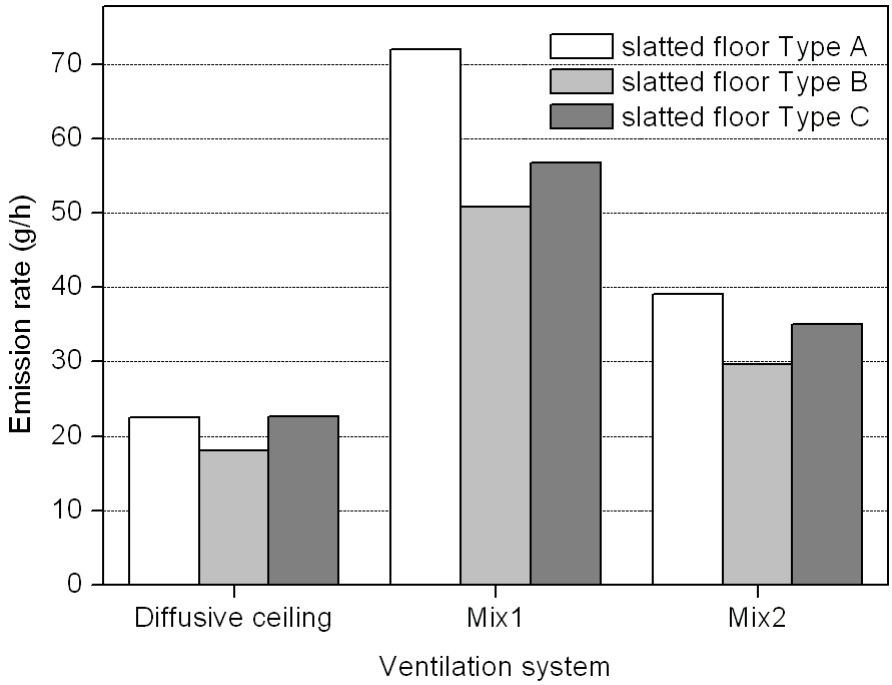

Figure 4.11 Effects of slatted floor opening ratio on ammonia emissions with 15ACH ventilation rate under three ventilation systems

4.3.4 Effects of ammonium solution temperature on ammonia emissions

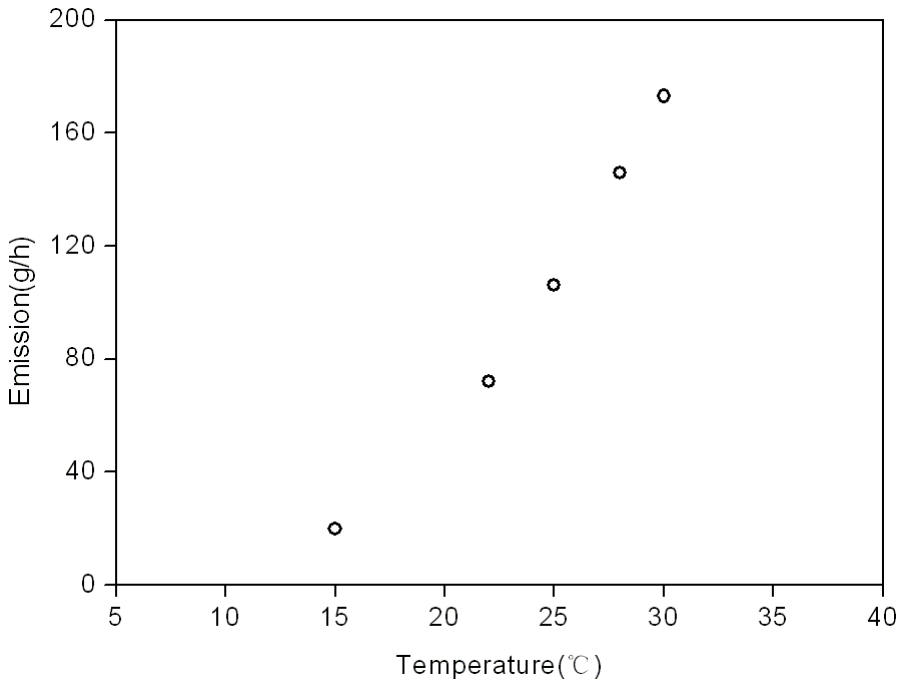

Figure 4.12 Effects of solution temperature on ammonia emissions

The effects of ammonium solution temperature on ammonia emissions are shown in Figure 4.12. The emission rate increases quickly at higher solution temperatures. This

is also expectable because higher temperatures cause higher ammonia concentration on the emission surface. Besides, the air velocity will increase because of the buoyancy effect when the solution temperature is higher than the air temperature. The influence of buoyancy (or temperature) on the velocity and mass transfer coefficient will be analyzed in the next section.

4.3.5 Mass transfer coefficient

In section 4.3.2, the velocity vector distribution of three ventilation systems show that the emissions are higher in mixing ventilation systems that the local velocity close to the emission surface is bigger. The emissions are also increasing with higher ventilation rate. In this section, the local mass transfer coefficient is shown under different ventilation systems and different ventilation rate.

The velocity distributions under different ventilation systems with slatted floor type A and different ventilation rate for mixing ventilation system type I are shown in Appendix D. The maximum velocity close to the emission surface under these conditions is summarized in Table 4.3. The maximum velocity close to the emission surface increases with higher ventilation rate. Under different ventilation systems, mixing ventilation system type I has the largest velocity close to the emission surface and the diffusive ceiling ventilation system has the lowest. When the ventilation rate is the same, higher solution temperature causes bigger velocity close to the emission surface. This indicates that the temperature not only affects the ammonia concentration on the emission surface but also affects the airflow so that the mass transfer coefficient will be influenced.

Table 4.3 Maximum velocity magnitude (m/s) close to the emission surface under different ventilation systems, ventilation rates and solution temperature

Item	Ventilation rate				
	9ACH	12ACH	15ACH	18ACH	21ACH
Mixing type I &slatted floor Type A	0.113	0.16	0.205	0.252	0.303
Mixing type II &slatted floor Type A	0.037	0.051	0.068	0.081	0.096
Diffusive ceiling &slatted floor Type A	0.018	0.018	0.0195	0.0195	0.021
	Temperature(℃)				
	15	22	25	28	30
Mixing type I & slatted floor Type A & 15ACH	0.12	0.205	0.223	0.245	0.252

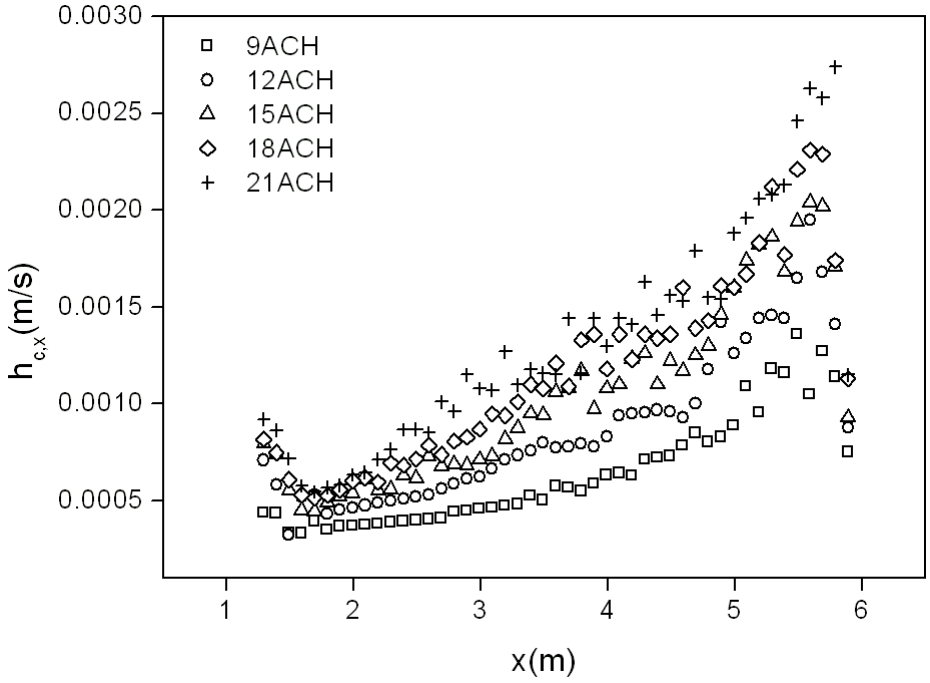

(a) Mixing ventilation system type I

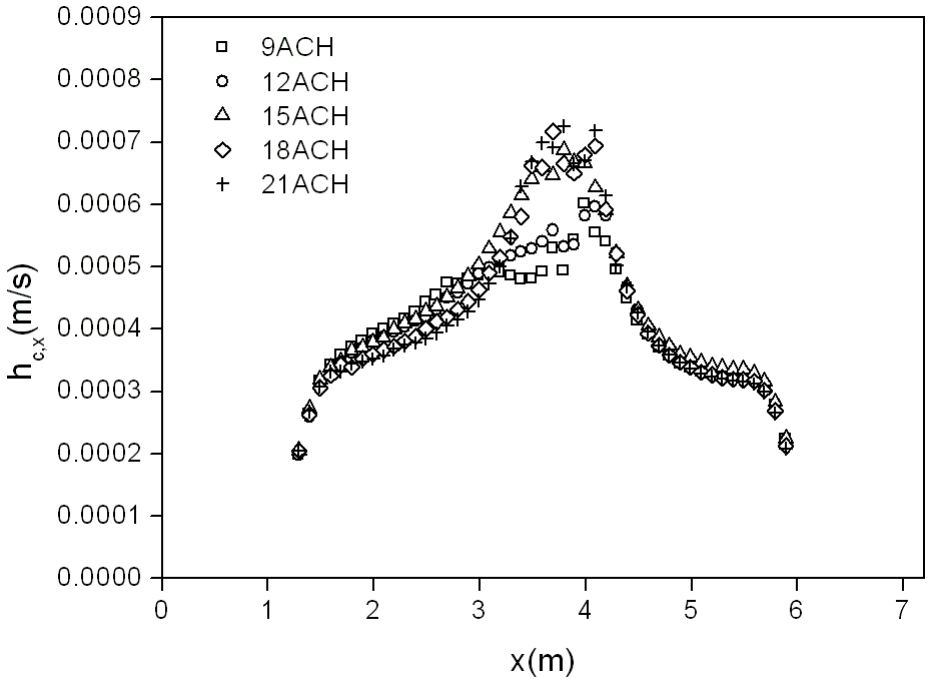

(b) Diffusive ceiling ventilation system

Figure 4.13 local mass transfer coefficient along the emission surface at different ventilation rates with slatted floor type A

The local mass transfer coefficient shown in Figure 4.13 increases with higher ventilation rate for mixing ventilation system type I which is caused by higher

velocity distribution below the slatted floor. For mixing ventilation system type I, the local mass transfer coefficients are bigger on the right than those on the left. This is because the air flows into the slurry container from the right of the slatted floor so that the concentration boundary layer thickness on the right is smaller. For diffusive ceiling ventilation system, the local mass transfer coefficients are similar to each other at different ventilation rate except from 3.4m to 4.1m. This somehow explains why ammonia emissions vary slightly with different ventilation rates.

Figure 4.14 shows the relationship of local mass transfer coefficient and ventilation systems with slatted floor type A under 15 ACH ventilation rate. The results show that the local mass transfer coefficients are generally bigger for mixing ventilation system type I, which is expected because of the larger velocity distribution. For mixing ventilation system type II, the local mass transfer coefficients at some places on the emission surface are higher than those of diffusive ceiling ventilation system and vise verse. This indicates that the local mass transfer coefficient is not only affected by local velocity distribution but also affected by the concentration boundary layer thickness.

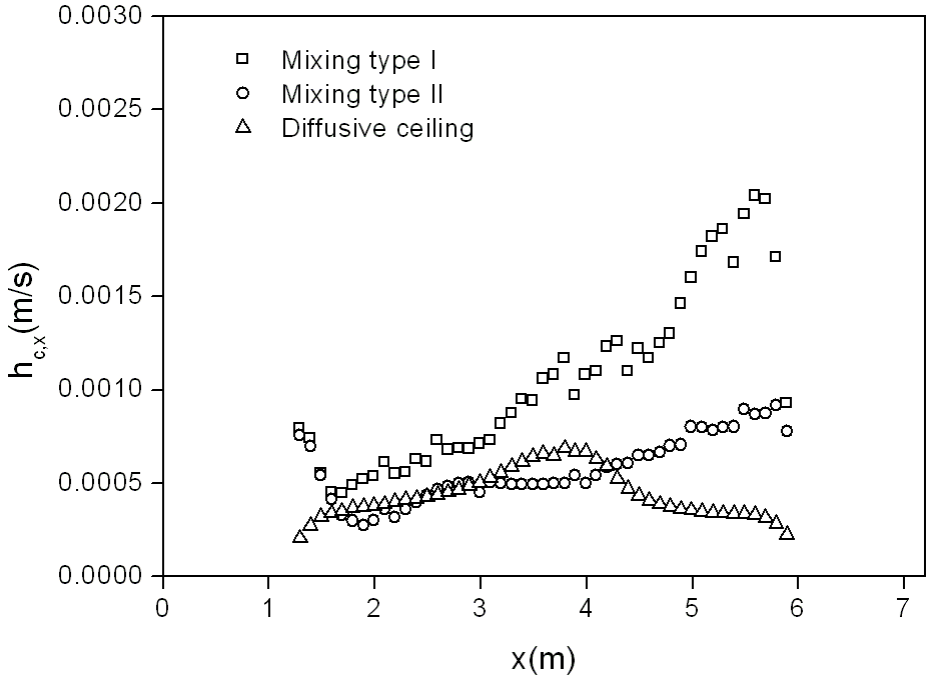

Figure 4.14 local mass transfer coefficient along the emission surface of slatted floor type A and 15ACH under different ventilation systems

Figure 4.15 shows the relationship of mass transfer coefficient and velocity. The velocity magnitude in Figure 4.15 is the maximum velocity magnitude close to the emission surface. The mass transfer coefficient is calculated by Eq. 2.2, in which the ammonia concentration in the bulk air is the average concentration of the line 0.1m below the slatted floor for mixing ventilation system. The mass transfer coefficient is linear with the velocity under isothermal conditions. For the diffusive ceiling

ventilation system, the mass transfer coefficient varies little because the velocity under the slatted floor changes little (from 0.018 to 0.021m/s) at different ventilation rates. Therefore, the mass transfer process below the slatted floor is controlled by diffusion under diffusive ceiling ventilation system.

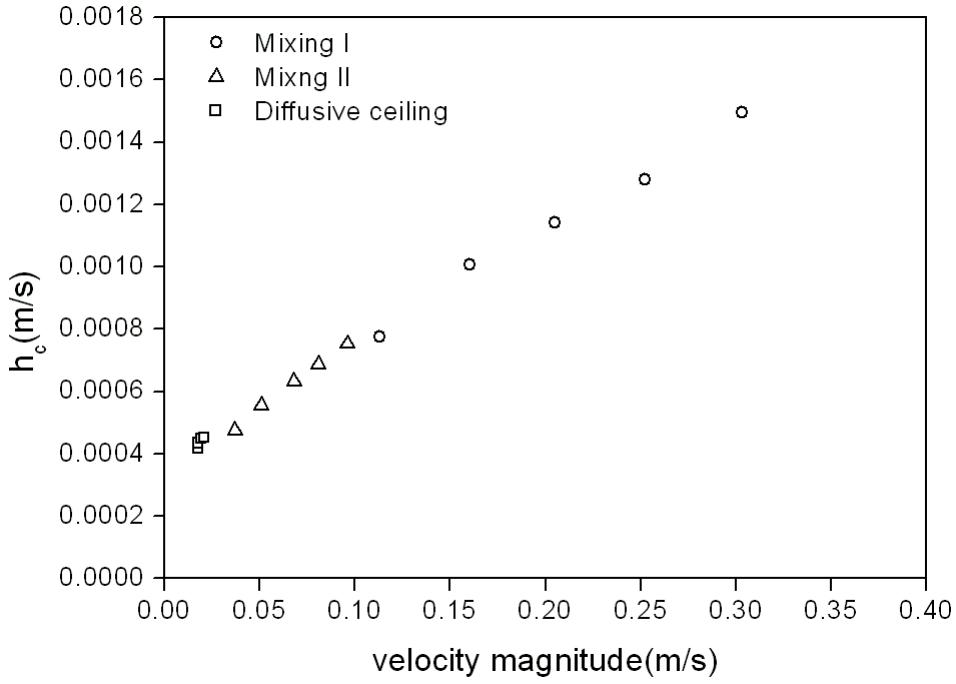

Figure 4.15 Relationship of mass transfer coefficient and velocity

Figure 4.16 shows the effect of solution temperature on ammonia mass transfer coefficient. The mass transfer coefficient increases with higher solution temperature. As summarized in Table 4.3, higher solution temperature generates bigger velocity close to the emission surface. Therefore, the mass transfer coefficient is affected not only by the temperature but also by the velocity. For example, the mass transfer coefficient is 1.278E-03 when the maximum velocity is 0.252m/s with 18ACH ventilation rate under isothermal conditions for mixing ventilation type I but the mass transfer coefficient is 1.703E-03 when the maximum velocity is also 0.252m/s with 15ACH ventilation rate and 30℃ solution temperature for mixing ventilation type I. Even though the velocity close to the emission surface is the same for these two cases, higher solution temperature gives larger mass transfer coefficient. This effect was not found in chapter 3. The mass transfer coefficient in chapter 3 varies little with solution temperature in the wind tunnel. In the wind tunnel, the velocity boundary layer developed for 2.05m before the temperature boundary layer was formed and the length of the emission surface in the wind tunnel was only 0.62m. Under this condition, the temperature may hardly affect the velocity boundary layer development. However, the velocity and temperature boundary layer develop along the same distance (the length of the emission surface is 4.8m) and the temperature can affect the air velocity.

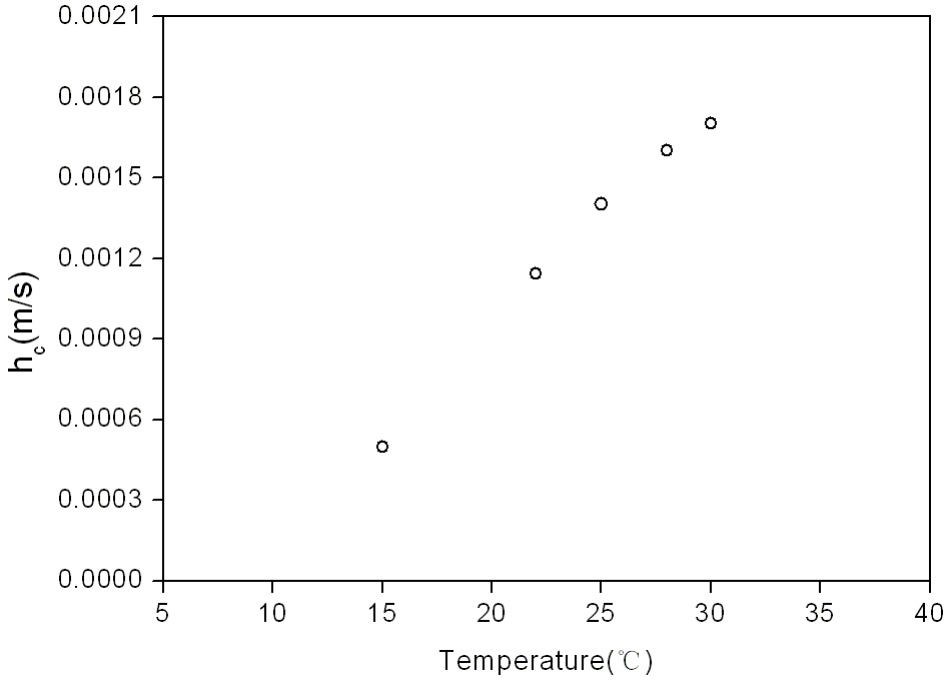

Figure 4.16 Effects of solution temperature on mass transfer coefficient

4.4 Conclusions

Using the relationship between partition coefficient and solution temperature summarized from vapor-liquid equilibrium properties in chapter 3 to determine the concentration boundary condition on the emission surface, this chapter has studied the effects of ventilation systems, ventilation rates, slatted floor opening ratios and solution temperature on ammonia emissions and mass transfer coefficient in a full-scale pig pen. The following conclusions can be drawn from the full-scale two-dimensional pig pen studies under previous assumptions:

(1) The big difference of velocity vector distribution and ammonia concentration distribution is found between porous media modeling and slats modeling for slatted floor. The ammonia emissions of slats modeling is around 1.5 times per air exchange rate as those of porous media modeling under different ventilation rates.
(2) For mixing ventilation systems, the ammonia emissions increase with higher ventilation rates, bigger slatted floor opening ratios and higher solution temperature. For diffusive ceiling ventilation system, the ammonia emissions increase slightly with higher ventilation rates.
(3) The ammonia emissions of diffusive ceiling ventilation system are much lower than those of mixing ventilation systems. This can decrease the ammonia emissions to the atmosphere. However, the diffusive ceiling ventilation system has considerably higher concentration at the animal occupied zone than mixing ventilation systems.
(4) The maximum velocity of diffusive ceiling ventilation system (0.018~0.021m/s) is much lower than the mixing ventilation systems (0.037~0.096m/s for mixing

ventilation type II and 0.113~0.303 for mixing ventilation system type I) under different ventilation rates and isothermal condition. This explains why the ammonia emissions of diffusive ceiling ventilation system vary slightly with the ventilation rates. It also indicates that the ammonia mass transfer process of diffusive ventilation system is likely a diffusion-controlled process below the slatted floor. The maximum velocity of mixing ventilation system type I increases with higher solution temperature (from 0.12 to 0.252m/s).

(5) The mass transfer coefficient of diffusive ventilation system is lower than the mixing ventilation systems and increases with higher local velocity under isothermal condition. The mass transfer coefficient also increases with higher solution temperature in the pig pen.

Chapter 5

Conclusions and Recommendations

This chapter summarizes the results and conclusions obtained from this study. Some limitations of the current work and future perspectives for ammonia emission studies from animal houses are also discussed.

The objective of this thesis was to study the ammonia emission characteristics under different environmental conditions and ammonium solution temperature and validate the accuracy of Henry's law constant to determine the boundary condition of concentration on the emission surface. This objective has been achieved by using both experimental and numerical modeling approaches. The major conclusions from this study are summarized as follows.

5.1 Experimental studies

The effects of environmental conditions (velocity, velocity fluctuations) and ammonium solution temperature on ammonia emissions have been measured. It was found that:

(1) Airflow (velocity and velocity fluctuations) has an important effect on ammonia emissions. The results show that the ammonia emission rate increases with the air velocity, which is expected since larger amount of ammonia is removed from the boundary layer when the air velocity increases. The results also confirm that the emission is more sensitive to the change of velocity at a low value compared to the change of velocity at a higher value. Besides, velocity fluctuations have slight effects on ammonia emission.
(2) Ammonium solution temperature has a very significant effect on ammonia emissions. The results show that the ammonia emission rate increases with higher ammonium solution temperature. The ammonia emission is more sensitive to the change of temperature at a high value compared to the change of temperature at a lower value.
(3) The ammonia emissions are reversed linear with the boundary layer thickness of velocity under a specific solution temperature. The results also demonstrate that the boundary layer thickness of velocity decreases with higher velocity but changes little with ammonium solution temperature.
(4) The emission data measured in a wind tunnel cannot be applied directly to a building due to the different flow and thermal conditions between the wind tunnel and a building. Therefore, the emission data measured in this chapter will be used for further CFD simulation validation and study the accuracy of the Henry's law constant to determine the boundary condition of concentration.

5.2 Numerical modeling

A series of CFD simulations has been performed using the cases measured in the wind tunnel. The validation of CFD turbulence models and the study on accuracy of current Henry's law constant models to determine the boundary condition of concentration are studied. It was found that:

(1) The turbulence model (LRN model, SST model and RNG model with enhanced wall treatment) is capable of predicting the velocity profiles appropriately but cannot predict the velocity fluctuations well.
(2) The boundary condition of concentration determined by the current Henry's law constant models used in manure or ammonium solutions is not very accurate to predict the ammonia emissions. The comparison of ammonia emissions and concentration profiles between the simulated results and data measured in the wind tunnel shows big differences. All these HLC models over predict the ammonia emissions (around 1.5 ~ 2.0 times). The VLE (vapor-liquid equilibrium) properties produce a better consistency between simulated and measured results (e.g. ammonia emissions, and concentration profiles). Therefore, a simplified function between partition coefficient and solution temperature is achieved from VLE properties and will be used for case studies in chapter 4.
(3) The mass transfer coefficient of ammonia increases with higher velocity and velocity fluctuations while it varies little with solution temperature. The mass transfer coefficient using VLE model to determine the concentration boundary condition is bigger than those using the current HLC models to determine the concentration boundary conditions.
(4) The mass transfer coefficient using VLE model and HLC models is linear to each other. It is known that the temperature is the most important parameter to affect the Henry's law constant and there are also other factors that may influence the Henry's law constant. However, it seems those effects may be included by multiplying a linear coefficient no matter what kind of the effects that these factors may have on the Henry's law constant.

5.3 Case studies

The simplified function between partition coefficient and solution temperature to determine the concentration boundary condition is used to study the ammonia emissions under different environmental conditions and solution temperatures. The following conclusions are based on the ammonia emission study of a pig pen without animals and feeding equipments inside, that is, under previous assumptions.

(1) The comparison among 3D porous media modeling and 2D porous media modeling shows that the 3D geometry model can be simplified as a 2D model in this case. Large differences of ammonia emissions are found between porous media modeling and slats modeling for slatted floor under different ventilation rates in a 2D geometry model. The flow patterns and concentration distribution

below the slatted floor are quite different between porous media modeling and slats modeling. Thus, the study of effects of environmental conditions and solution temperature on ammonia emissions is performed in 2D geometry model and slats modeling for slatted floor.

(2) The ammonia emissions increase with higher ventilation rate for mixing ventilation systems, but they change little with ventilation rates for diffusive ceiling ventilation system. The ammonia emissions of diffusive ceiling ventilation system are much lower than those of mixing ventilation system, which is good for the atmosphere in order to decrease the ammonia emission from animal houses. However, the ammonia concentration close to the slatted floor (the animal occupied zone) in the room is much higher than that of mixing ventilation systems, which is not good for the animal well-being and workers' health in animal houses. One way to solve this problem is to increase the ventilation rate in the diffusive ceiling ventilation system.

(3) Generally, the ammonia emissions increase with larger slatted floor opening ratios for both mixing ventilation systems and diffusive ceiling ventilation system. The ammonia emissions also increase with higher solution temperatures.

(4) Local velocity close to the emission surface is found to be much higher in mixing ventilation systems and increases with bigger ventilation rates. However, the local velocity below the slatted floor is quite low (0.018~0.021m/s) for diffusive ventilation system. The velocity close to the emission surface also increases with higher solution temperature for mixing ventilation system type I at the same ventilation rate.

(5) The mass transfer coefficient increases with higher velocity and solution temperature. This indicates that both the local air velocity and solution temperature affects the mass transfer coefficient under the slatted floor in the pig pen.

5.4 Limitations of the Current Work

Apart from the limitations that have already been mentioned, the current work is still subject to further improvements in several areas:

(1) The work in this thesis is focused on ammonia emission from an ammonium solution. The ammonium solution is quite different from the manure, in which there exist more chemical reactions and other odor gases. These gases may affect the ammonia emissions with more complicated boundary conditions.

(2) The study on ammonia emissions results directly from the current level of understanding regarding the fundamental processes that control the transport of ammonia under the steady state conditions. The author's knowledge on complicated ammonia emission is limited under unsteady state conditions.

(3) The case study conducted is based on a simplified pig pen without considering animals inside and ammonia emissions from walls or feeding equipment in the room. The study needs to be extended to more complicated scenarios. Meanwhile,

validation of the simulation results using measurements is also limited in this study.

5.5 Future perspectives

Ammonia emission (widely speaking odor emissions) affecting the air quality indoor or outdoor is a high priority environmental problem that affects the atmosphere eco-system and humans' health as well as the animals' well-being. In the future, the public interest and investment in controlling odor emission will be continued. Several areas need further investigation:

(1) A deeper understanding of mass transfer processes of important odors inside the manure should be studied.
(2) More detailed conditions for Henry's law constant application should be investigated for manure under different situations.
(3) Development of active odor emission control strategies should be conducted other than the use of ventilation system alone.
(4) The effects of particles on odor emission can also be further studied.

Appendix A

Turbulent models

A.1 Introduction

Solving CFD problem usually consists of four main components: geometry and grid generation, setting-up a physical model, solving it and post-processing the computed data. The way that geometry and grid are generated, the set problem is computed and the acquired data is presented is well known. However, it is difficult for setting-up a physical model for turbulence flows because people always try to model complex phenomena with a model as simple as possible. The complexity of different turbulence models may strongly depend on the details that people want to observe and study. Currently turbulent flows can be computed using several different approaches. The main approaches are summarized below:

- Reynolds-Averaged Navier-Stokes (RANS) models
- Large-Eddy simulation (LES)
- Direct numerical simulation (DNS)

The modeling of certain CFD approach is illustrated in Figure A.1. It is clearly seen that LES and DNS resolve shorter length scales so that they have the ability to provide better results. However, they require much greater computer power than the models applying RANS method. Hence, the RANS method is applied in this study.

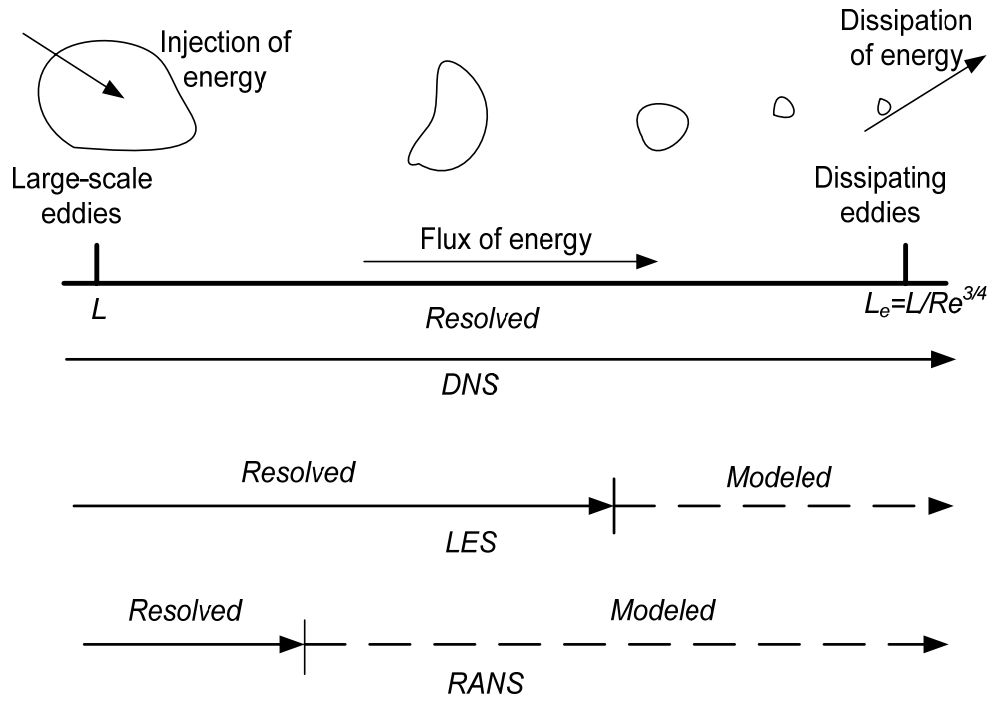

Figure A.1 Modeling for certain types of turbulent models

A.2 RNG $k-\varepsilon$ Model

RNG $k-\varepsilon$ model was derived using a rigorous statistical technique (called renormalization group theory). Comparing to standard $k-\varepsilon$ model, the RNG $k-\varepsilon$ model has the following refinements:

- The RNG $k-\varepsilon$ model has an additional term in its ε equation that significantly improves the accuracy for rapidly strained flows.
- The effect of swirl on turbulence is included in the RNG model, enhancing accuracy for swirling flows.
- The RNG theory provides an analytical formula for turbulent Prandtl numbers, while the standard $k-\varepsilon$ model uses user-specified, constant values.
- While the standard $k-\varepsilon$ model is a high-Reynolds-number model, the RNG theory provides an analytically-derived differential formula for effective viscosity that accounts for low-Reynolds-number effects. Effective use of this feature does, however, depend on an appropriate treatment of the near-wall region.

It has a similar form to the standard $k-\varepsilon$ model:

$$\frac{\partial}{\partial x_i}(\rho k u_i) = \frac{\partial}{\partial x_j}\left(\alpha_k \mu_{eff} \frac{\partial k}{\partial x_j}\right) + G_k + G_b - \rho\varepsilon + S_k \tag{A.1}$$

and

$$\frac{\partial}{\partial x_i}(\rho \varepsilon u_i) = \frac{\partial}{\partial x_j}\left(\alpha_\varepsilon \mu_{eff} \frac{\partial \varepsilon}{\partial x_j}\right) + C_{1\varepsilon}\frac{\varepsilon}{k}(G_k + C_{3\varepsilon}G_b) - C_{2\varepsilon}\rho\frac{\varepsilon^2}{k} - R_\varepsilon + S_\varepsilon \tag{A.2}$$

In these equations, G_k represents the generation of turbulence kinetic energy due to the mean velocity gradients. G_b is the generation of turbulence kinetic energy due to buoyancy. R_ε is an additional term that significantly improves the accuracy for rapidly strained flows. The quantities α_k and α_ε are the inverse effective Prandtl numbers for k and ε respectively. S_k and S_ε are user-defined source term.

The main difference between the RNG and standard $k-\varepsilon$ models lies in the additional term in the ε equation given by:

$$R_\varepsilon = \frac{C_\mu \rho \eta^3 (1-\eta/\eta_0)}{1+\beta\eta^3}\frac{\varepsilon^2}{k} \tag{A.3}$$

where $\eta = Sk/\varepsilon$, $\eta_0 = 4.38$, $\beta = 0.012$.

The inverse effective Parndtl numbers, α_k and α_ε, are computed using the following formula derived analytically by the RNG theory:

$$\left|\frac{\alpha-1.3929}{\alpha_0-1.3929}\right|^{0.6321}\left|\frac{\alpha+2.3929}{\alpha_0+2.3929}\right|^{0.3679}=\frac{\mu_{mol}}{\mu_{eff}} \tag{A.4}$$

where $\alpha_0=1.0$. In the high-Reynolds-number limit ($\mu_{mol}/\mu_{eff}<<1$), $\alpha_k=\alpha_\varepsilon\approx 1.393$.

The scale elimination procedure in RNG theory results in a differential equation for turbulent viscosity:

$$d\left(\frac{\rho^2 k}{\sqrt{\varepsilon\mu}}\right)=1.72\tilde{\nu}\Big/\sqrt{\tilde{\nu}^3-1+C_\nu}\,d\tilde{\nu} \tag{A.5}$$

where

$$\tilde{\nu}=\mu_{eff}/\mu \tag{A.6}$$

$$C_\nu\approx 100 \tag{A.7}$$

In the high-Reynolds-number limit, Eq. (A.5) gives:

$$\mu_t=\rho C_\mu\frac{k^2}{\varepsilon} \tag{A.8}$$

The generation of turbulence kinetic energy due to the mean velocity gradients G_k and the generation of turbulence kinetic energy due to the buyoncy G_b are computed by the following equations:

$$G_k=\mu_t S^2 \tag{A.9}$$

$$G_b=\beta g_i\frac{\mu_t}{\mathrm{Pr}_t}\frac{\partial T}{\partial x_i} \tag{A.10}$$

The model constants $C_{1\varepsilon}$, $C_{2\varepsilon}$ and C_μ have the following default values:

$C_{1\varepsilon}=1.42$, $C_{2\varepsilon}=1.68$, $C_\mu=0.09$

A.3 SST (Shear Stress Transport) $k-\omega$ Model

The shear stress transport $k-\omega$ model was developed by Menter to effectively blend the robust and accurate formulation of the $k-\omega$ model in the near-wall region with the free-stream independence of the $k-\varepsilon$ model in the far field. To achieve this, the

$k-\varepsilon$ model is converted into a $k-\omega$ formulation. The SST $k-\omega$ model is similar to the standard $k-\omega$ model, but include the following refinements:

- The standard $k-\omega$ model and the transformed $k-\varepsilon$ model are both multiplied by a blending function and both models are added together. The blending function is designed to be one in the near-wall region, which activates the standard $k-\omega$ model, and zero away from the surface, which activates the transformed $k-\varepsilon$ model.
- The SST model incorporates a damped cross-diffusion derivative term in the ω equation.
- The definition of the turbulent viscosity is modified to account for the transport of the turbulent shear stress.
- The modeling constants are different.

The SST $k-\omega$ model has a similar form to the standard $k-\omega$ model:

$$\frac{\partial}{\partial x_i}(\rho k u_i) = \frac{\partial}{\partial x_j}\left(\Gamma_k \frac{\partial k}{\partial x_j}\right) + \tilde{G}_k - Y_k + S_k \tag{A.11}$$

and

$$\frac{\partial}{\partial x_i}(\rho \omega u_i) = \frac{\partial}{\partial x_j}\left(\Gamma_\omega \frac{\partial w}{\partial x_j}\right) + G_\omega - Y_\omega + D_\omega + S_\omega \tag{A.12}$$

In these equations, $\tilde{G}_k$ represents the generation of turbulence kinetic energy due to mean velocity gradients. G_ω represents the generation of ω. Γ_k and Γ_ω represent the effective diffusivity of k and ω due to turbulence. Y_k and Y_ω represent the dissipation of k and ω. D_ω represents the cross-diffusion term. S_k and S_ω are user-defined source terms.

The effective diffusivities for the SST $k-\omega$ model are given by:

$$\Gamma_k = \mu + \mu_t/\sigma_k \tag{A.13}$$

$$\Gamma_\omega = \mu + \mu_t/\sigma_\omega \tag{A.14}$$

where σ_k and σ_ω are the turbulent Prandtl numbers for k and ω, respectively. The turbulent viscosity, μ_t, is computed as follows:

$$\mu_t = \frac{\rho k}{\omega} \frac{1}{\max\left[\frac{1}{\alpha^*}, \frac{SF_2}{a_1 \omega}\right]} \tag{A.15}$$

where S is the strain rate magnitude and

$$\sigma_k = \frac{1}{F_1/\sigma_{k,1} + (1-F_1)/\sigma_{k,2}} \tag{A.16}$$

$$\sigma_\omega = \frac{1}{F_1/\sigma_{\omega,1} + (1-F_1)/\sigma_{\omega,2}} \tag{A.17}$$

α^* is defined as:

$$\alpha^* = \alpha^*_\infty \left(\frac{\alpha^*_0 + \mathrm{Re}_t/R_k}{1 + \mathrm{Re}_t/R_k} \right) \tag{A.18}$$

$\mathrm{Re}_t = \rho k/\mu\omega$, $R_k = 6$, $\alpha^*_0 = \beta_i/3$, $\beta_i = 0.072$, $\alpha^*_\infty = 1$

The blending functions, F_1 and F_2, are given by:

$F_1 = \tanh(\Phi_1^4)$

$$\Phi_1 = \min\left[\max\left(\frac{\sqrt{k}}{0.09\omega y}, \frac{500\mu}{\rho y^2 \omega} \right), \frac{4\rho k}{\sigma_{\omega,2} D^+_\omega y^2} \right] \tag{A.19}$$

$$D^+_\omega = \max\left[2\rho \frac{1}{\sigma_{\omega,2}} \frac{1}{\omega} \frac{\partial k}{\partial x_j} \frac{\partial \omega}{\partial x_j}, 10^{-10} \right] \tag{A.20}$$

$$F_2 = \tanh\left(\Phi_2^2\right) \tag{A.21}$$

$$\Phi_2 = \max\left[2\frac{\sqrt{k}}{0.09\omega y}, \frac{500\mu}{\rho y^2 \omega} \right] \tag{A.22}$$

The turbulence production of k, $\tilde{G}_k$, and the production of ω, G_ω, are defined as:

$$\tilde{G}_k = \min\left(G_k, 10\rho\beta^* k\omega\right) \tag{A.23}$$

$$G_w = \frac{\alpha_\infty}{v_t} G_k \quad \text{(A.24)}$$

$$\alpha_\infty = F_1 \alpha_{\infty,1} + (1-F_1)\alpha_{\infty,2} \tag{A.25}$$

where

$$\alpha_{\infty,1} = \frac{\beta_{i,1}}{\beta^*_\infty} - \frac{\kappa^2}{\sigma_{\omega,1}\sqrt{\beta^*_\infty}} \tag{A.26}$$

$$\alpha_{\infty,2} = \frac{\beta_{i,2}}{\beta_\infty^*} - \frac{\kappa^2}{\sigma_{\omega,2}\sqrt{\beta_\infty^*}} \tag{A.27}$$

and $\kappa = 0.41$.

The dissipation of k, Y_k, and the dissipation of ω, Y_ω, are computed by:

$$Y_k = \rho\beta^* k\omega \tag{A.28}$$

$$Y_w = \rho\beta\omega^2 \tag{A.29}$$

$$\beta = \beta_i\left[1 - \frac{\beta_i^*}{\beta_i}\zeta^* F(M_t)\right] \tag{A.30}$$

$$\beta_i = F_1\beta_{i,1} + (1 - F_1)\beta_{i,2} \tag{A.31}$$

$$\beta_i^* = \beta_\infty^*\left(\frac{4/15 + (\mathrm{Re}_t/R_\beta)^4}{1 + (\mathrm{Re}_t/R_\beta)^4}\right) \tag{A.32}$$

The SST $k-\omega$ model is based on both the standard $k-\omega$ model and the standard $k-\varepsilon$ model. To blend these two models together, the standard $k-\varepsilon$ model has been transformed into equations based on k and ω, which leads to the introduction of a cross-diffusion term D_ω, which is defined as:

$$D_\omega = 2(1 - F_1)\rho\sigma_{\omega,2}\frac{1}{\omega}\frac{\partial k}{\partial x_j}\frac{\partial \omega}{\partial x_j} \tag{A.33}$$

The model constants are given the values as:

$\sigma_{k,1} = 1.176$, $\sigma_{\omega,1} = 2.0$, $\sigma_{k,1} = 2.0$, $\sigma_{\omega,2} = 1.168$, $a_1 = 0.31$, $\beta_{i,1} = 0.075$, $\beta_{i,2} = 0.0828$, $\beta_\infty^* = 0.09$, $\zeta^* = 1.5$, $R_\beta = 8$

A.4 LRN (Low Reynolds Number) $k-\varepsilon$ model

The LRN model is given by:

$$\frac{\partial}{\partial x_i}(\rho k u_i) = \frac{\partial}{\partial x_i}\left[\left(\mu + \frac{\mu_t}{\sigma_k}\right)\frac{\partial k}{\partial x_i}\right] + G_k - \rho\varepsilon - D \tag{A.34}$$

$$\frac{\partial}{\partial x_i}(\rho\varepsilon u_i) = \frac{\partial}{\partial x_i}\left[\left(\mu + \frac{\mu_t}{\sigma_\varepsilon}\right)\frac{\partial \varepsilon}{\partial x_i}\right] + C_{1\varepsilon}\frac{\varepsilon}{k}G_k - f_2 C_{2\varepsilon}\rho\frac{\varepsilon^2}{k} + E \tag{A.35}$$

where

$$\mu_t = f_\mu C_\mu \rho \frac{k^2}{\varepsilon} \tag{A.36}$$

$$f_\mu = \exp\left(\frac{-3.4}{\left(1+R_t/50\right)^2}\right) \tag{A.37}$$

$$f_2 = 1 - 0.2\exp\left(-R_t^2\right) \tag{A.38}$$

$$D = 2\mu\left(\frac{\partial k^{0.5}}{\partial x_i}\right) \tag{A.39}$$

$$E = 2\frac{\mu\mu_t}{\rho}\left(\frac{\partial u_i}{\partial x_i}\right)^2 \tag{A.40}$$

$$R_t = \frac{\rho k^2}{\mu\varepsilon} \tag{A.41}$$

And empirical constants are:

$C_\mu = 0.09$, $C_{1\varepsilon} = 1.44$, $C_{2\varepsilon} = 1.92$, $\sigma_k = 1.0$, $\sigma_\varepsilon = 1.3$

Appendix B

Boundary conditions for numerical simulation in chapter 3

Case	inlet			Emission surface					
					ammonia mass fraction or flux				T
	u	Tu	T	flux	VLE	HLC1	HLC2	HLC3	
	(m/s)	(%)	(℃)	(mg/m^2.s)					(℃)
Tu10T22u4	0.4	9.7	23.6	2.041	7.49E-04	9.58E-04	1.59E-03	2.01E-03	21.7
Tu10T22u3	0.3	14.5	23.2	1.845	7.53E-04	9.63E-04	1.61E-03	2.02E-03	21.8
Tu10T22u2	0.2	17.1	22.5	1.564	7.71E-04	9.79E-04	1.64E-03	2.06E-03	22.1
Tu10T22u1	0.1	8.5	22.1	1.452	7.65E-04	9.74E-04	1.63E-03	2.05E-03	22.0
Tu10T15u4	0.4	9.7	21.6	1.365	4.53E-04	6.54E-04	1.01E-03	1.29E-03	15.0
Tu10T15u3	0.3	14.5	21.6	1.118	4.53E-04	6.54E-04	1.01E-03	1.29E-03	15.0
Tu10T15u2	0.2	17.1	21.5	0.930	4.56E-04	6.58E-04	1.01E-03	1.30E-03	15.1
Tu10T10u4	0.4	9.7	22.1	0.881	2.97E-04	4.71E-04	6.89E-04	8.87E-04	9.7

Tu10T10u3	0.3	14.5	22	0.825	2.97E-04	4.71E-04	6.89E-04	8.87E-04	9.7
Tu10T10u2	0.2	17.1	21.5	0.656	3.19E-04	4.99E-04	7.36E-04	9.48E-04	10.6
Tu10T6.5u4	0.4	9.7	22.3	0.735	2.27E-04	3.82E-04	5.44E-04	6.97E-04	6.5
Tu10T6.5u3	0.3	14.5	21.5	0.604	2.24E-04	3.77E-04	5.36E-04	6.86E-04	6.3
Tu10T6.5u2	0.2	17.1	21.5	0.514	2.27E-04	3.82E-04	5.44E-04	6.97E-04	6.5

Appendix C

CFD results in chapter 3

C.1 RNG model with enhanced wall treatment

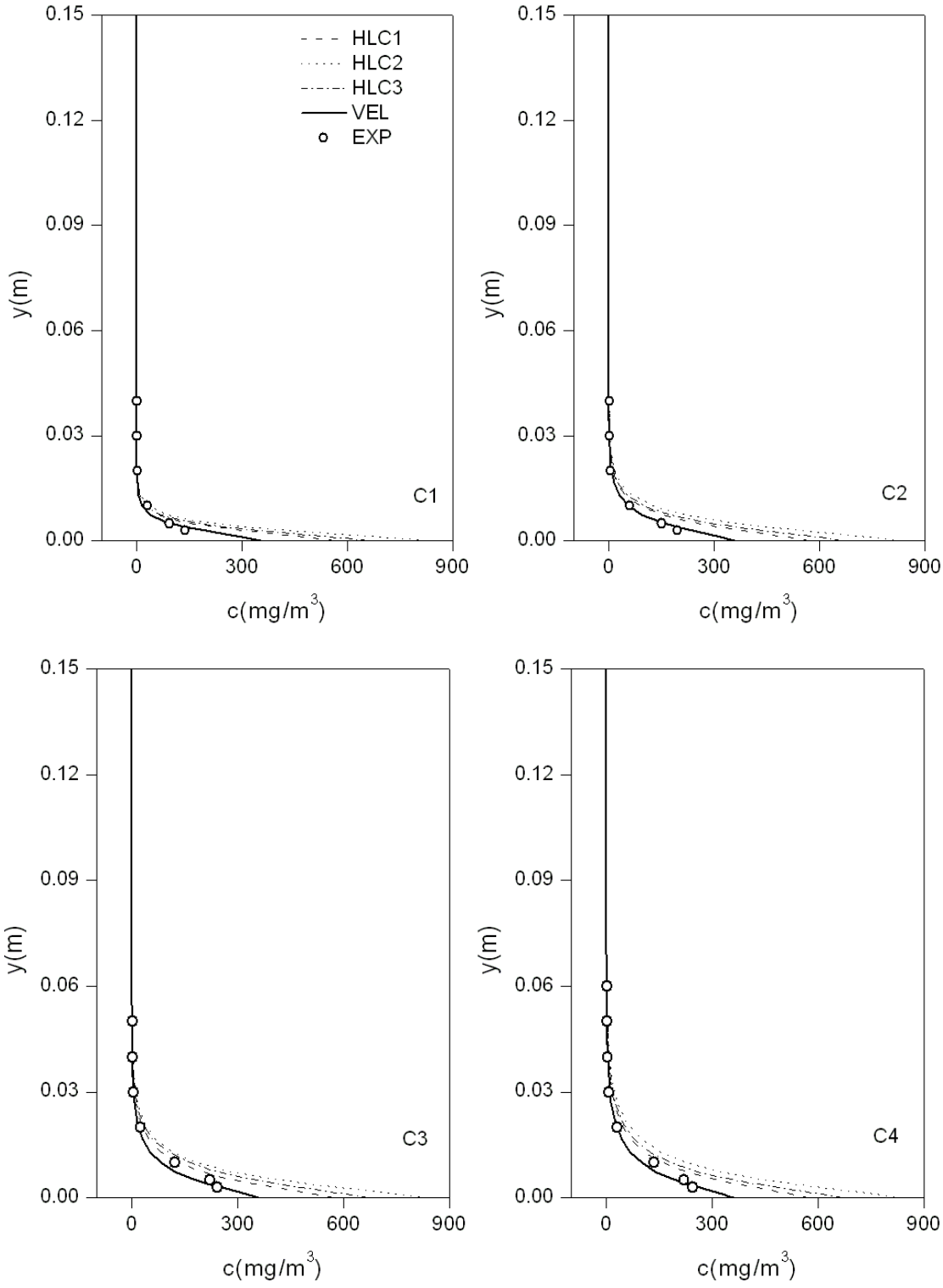

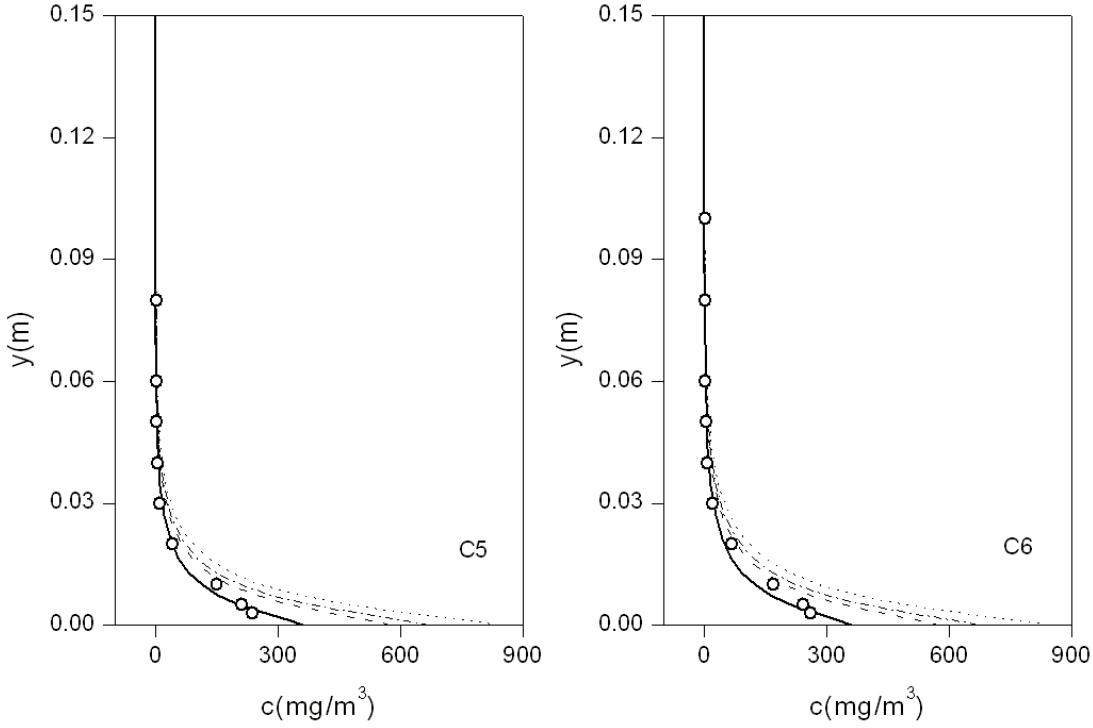

(a) Concentration profiles

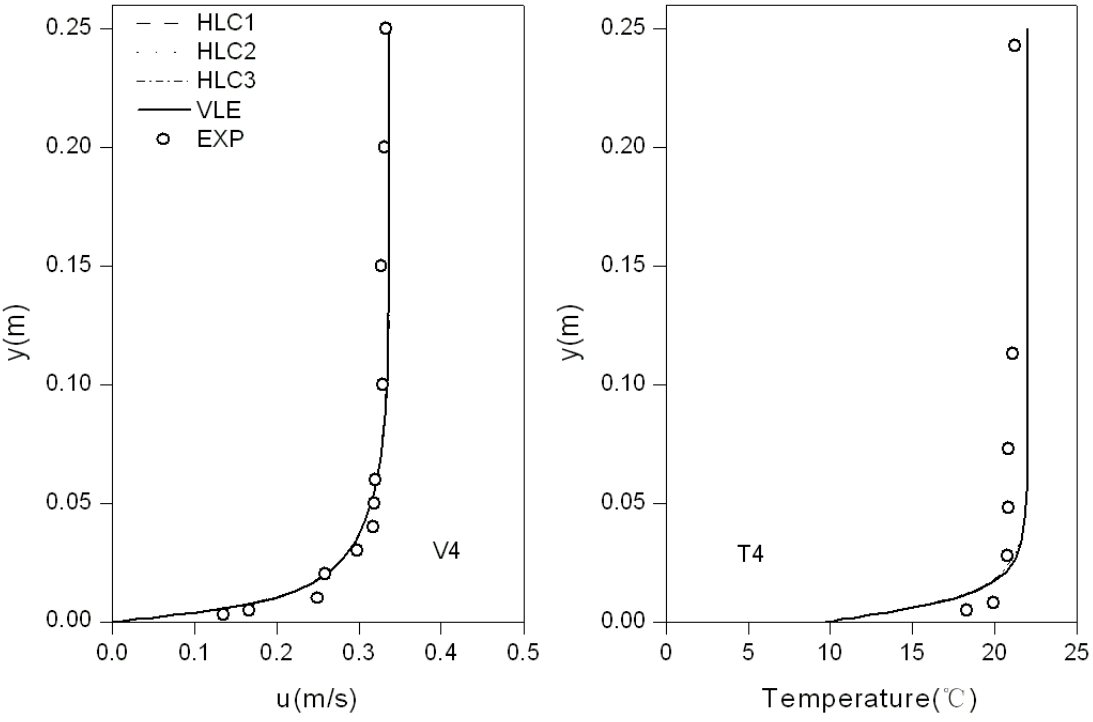

(b) Velocity and temperature profiles

Figure C.1 Comparison of concentration, velocity and temperature profiles between numerical simulations and measurements for case Tu10T10u3 using RNG model

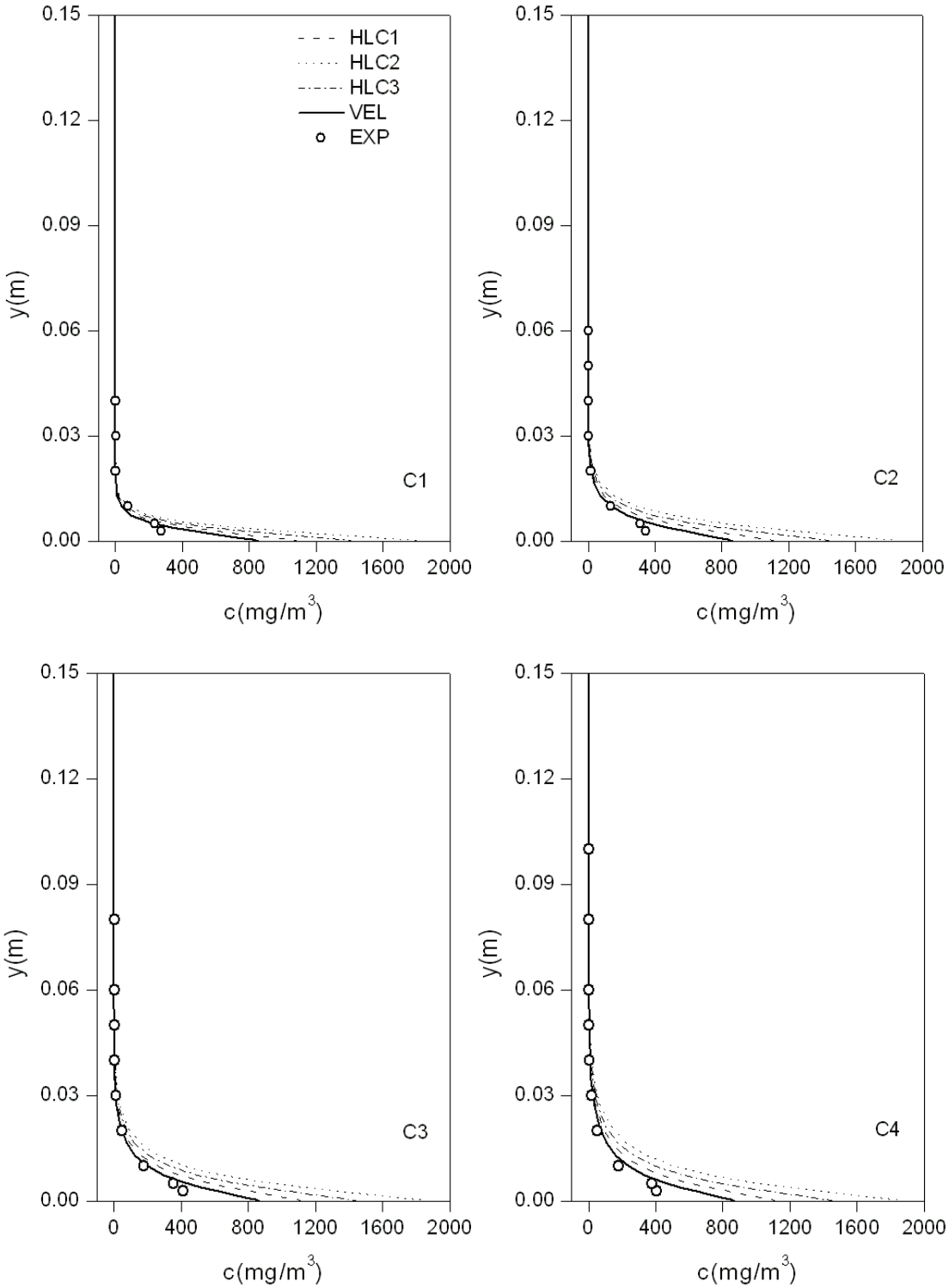
HLC1
HLC2
HLC3
VEL
EXP
C1
C2
C3
C4
y(m)
c(mg/m3)
0.15
0.12
0.09
0.06
0.03
0.00
0
400
800
1200
1600
2000

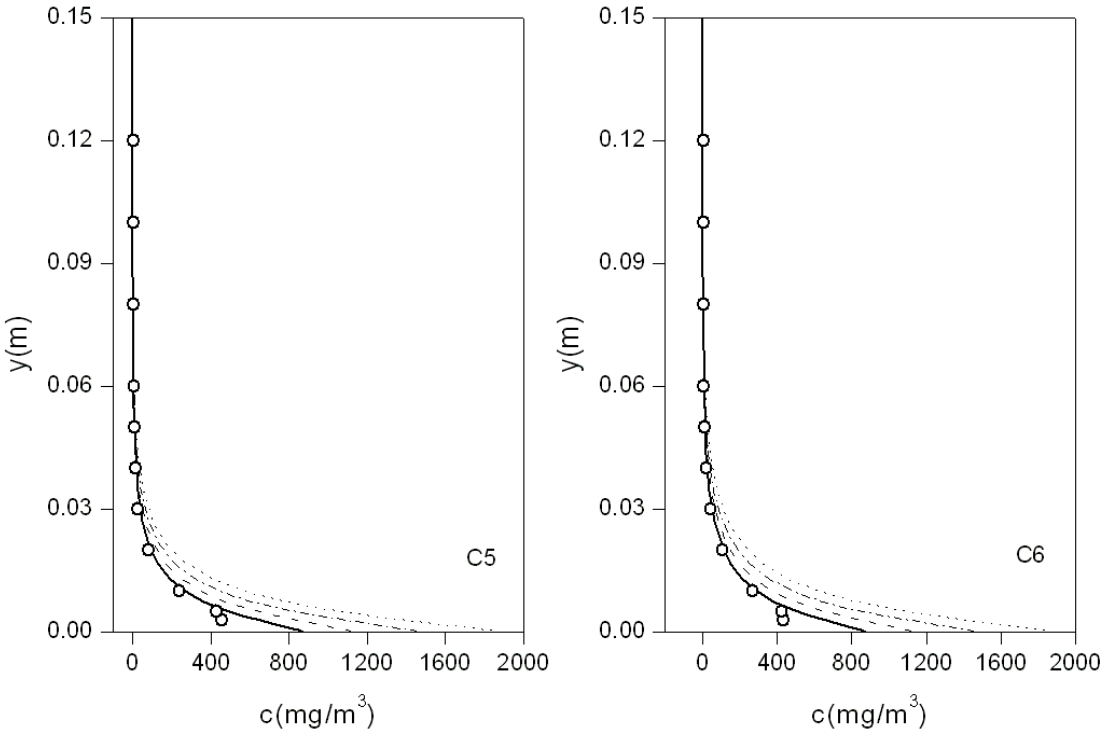

(a) Concentration profiles

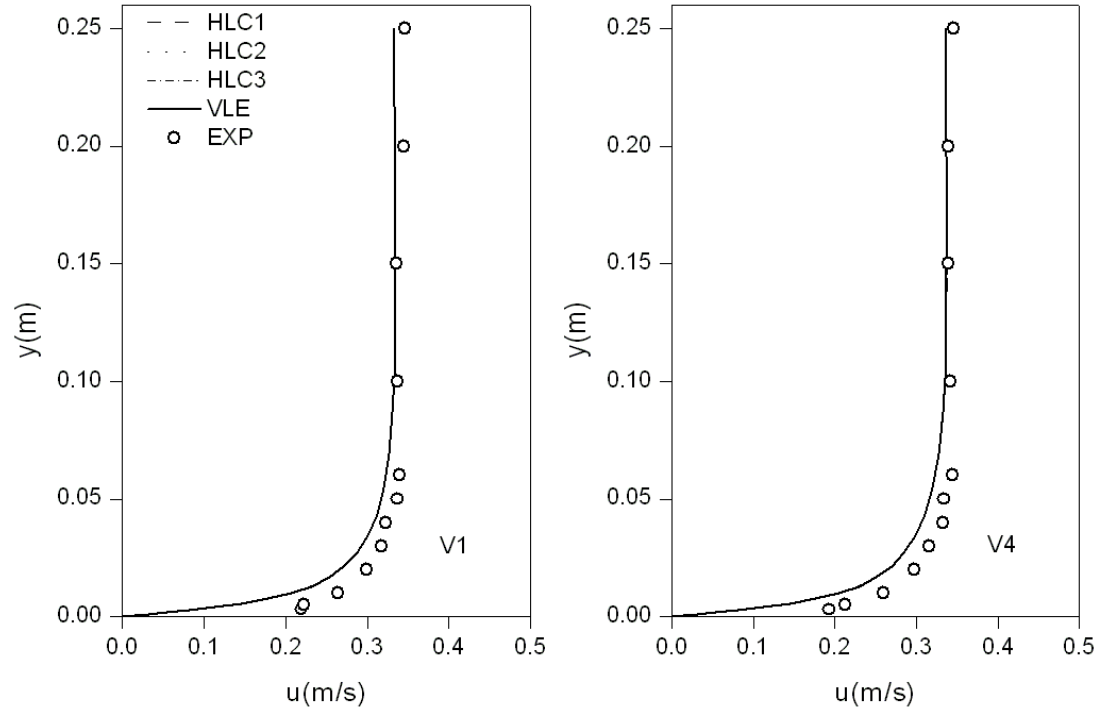

(b) Velocity profiles

Figure C.2 Comparison of concentration and velocity profiles between numerical simulations and measurements for case Tu10T22u3 using RNG model

C.2 LRN model

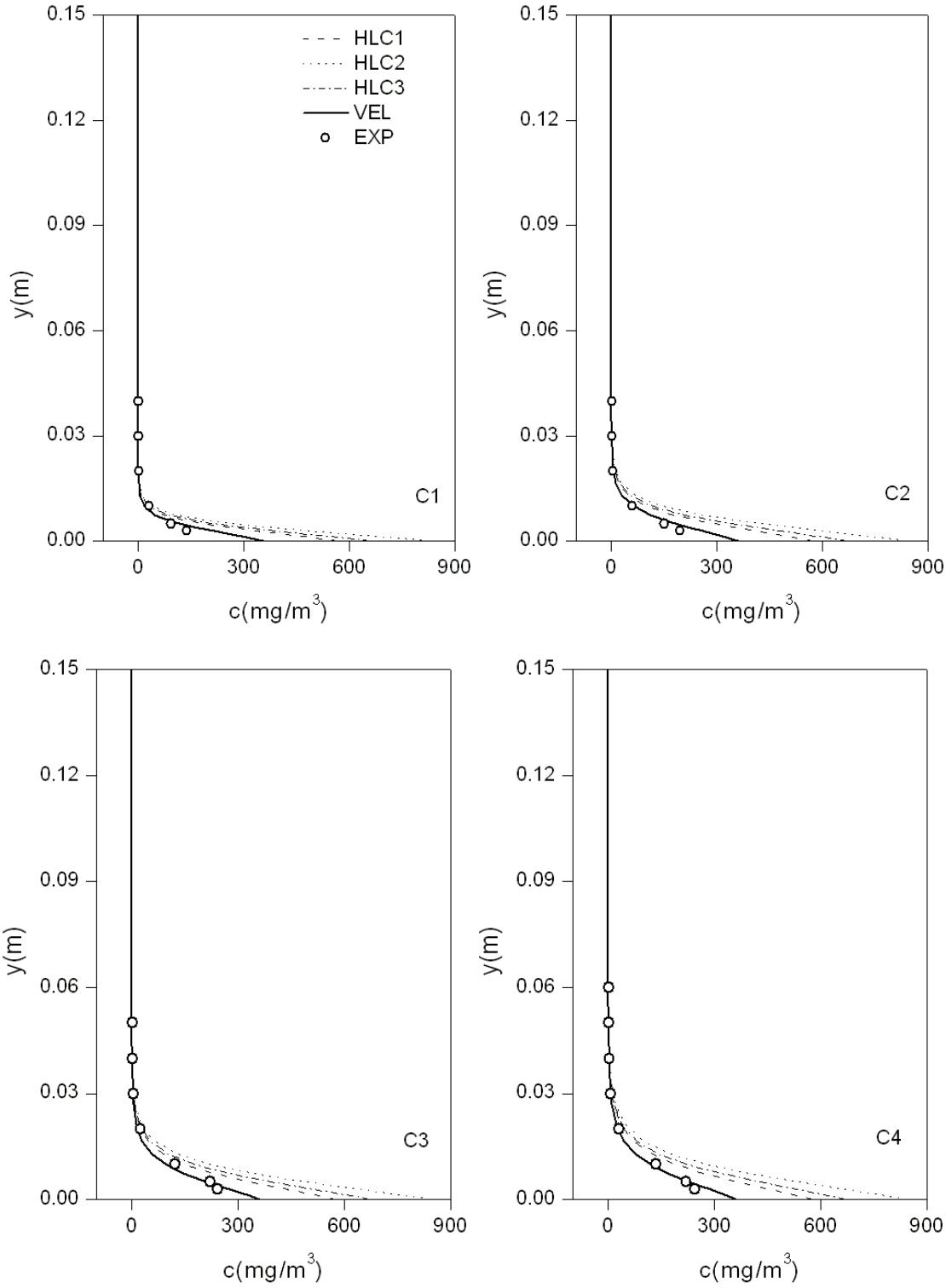
HLC1
HLC2
HLC3
VEL
EXP
C1
C2
C3
C4
y(m)
c(mg/m3)
0.15
0.12
0.09
0.06
0.03
0.00
0
300
600
900

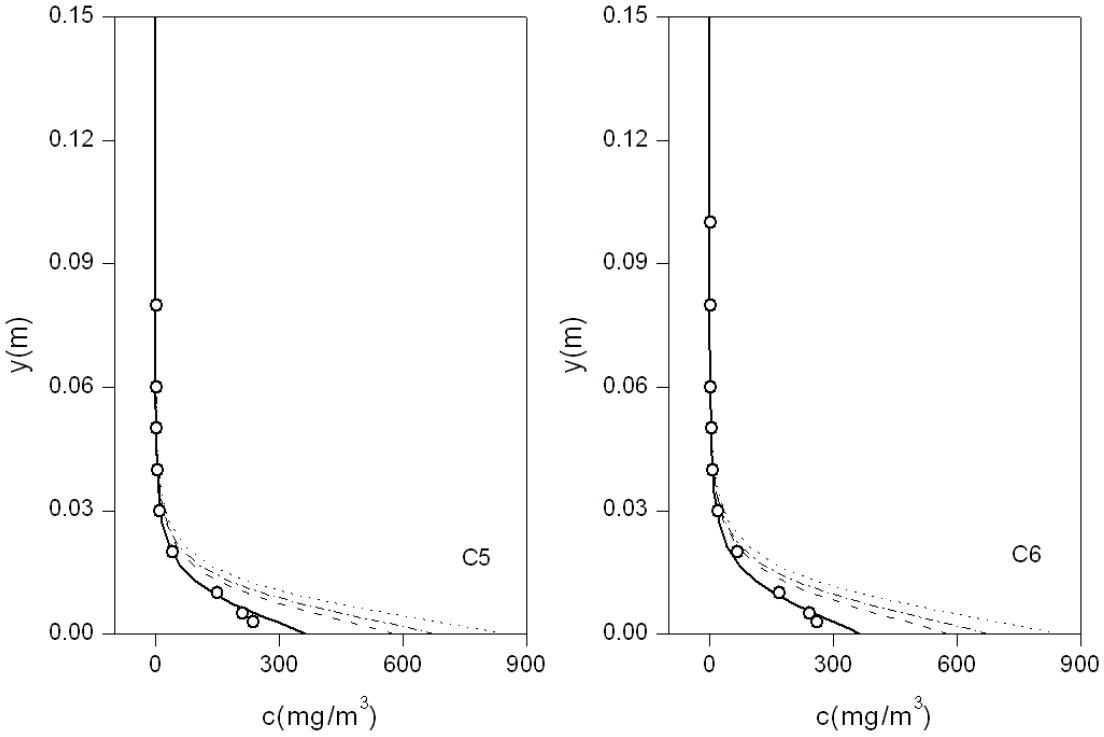

(a) Concentration profiles

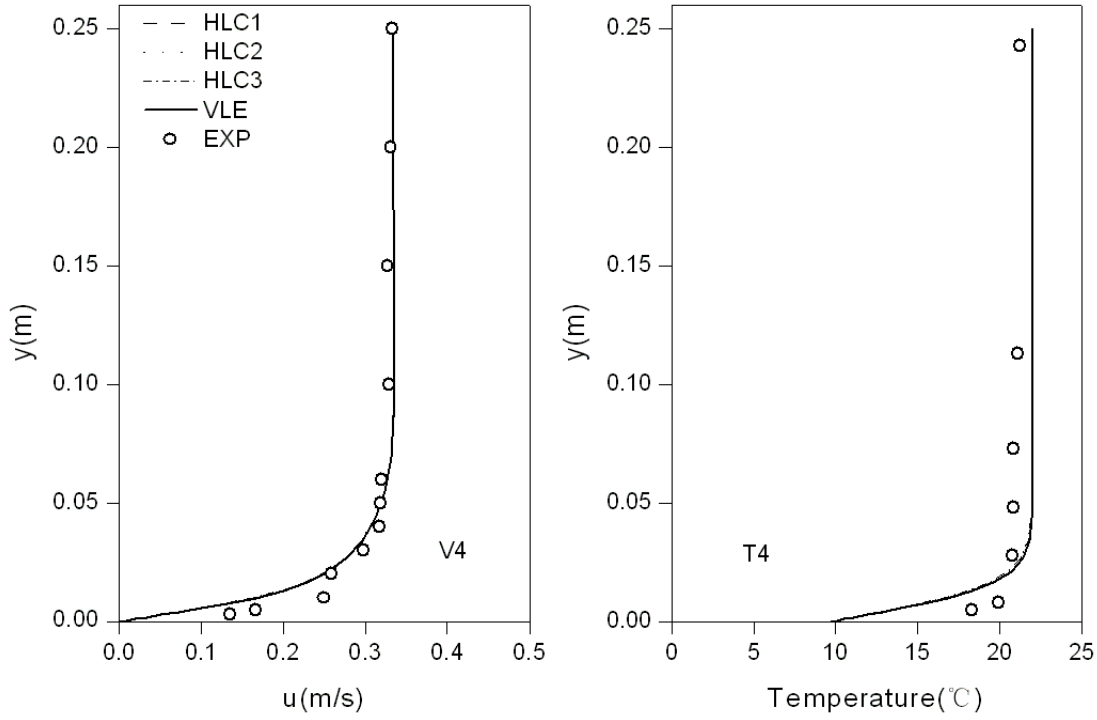

(b) Velocity and temperature profiles

Figure C.3 Comparison of concentration, velocity and temperature profiles between numerical simulations and measurements for case Tu10T10u3 using LRN model

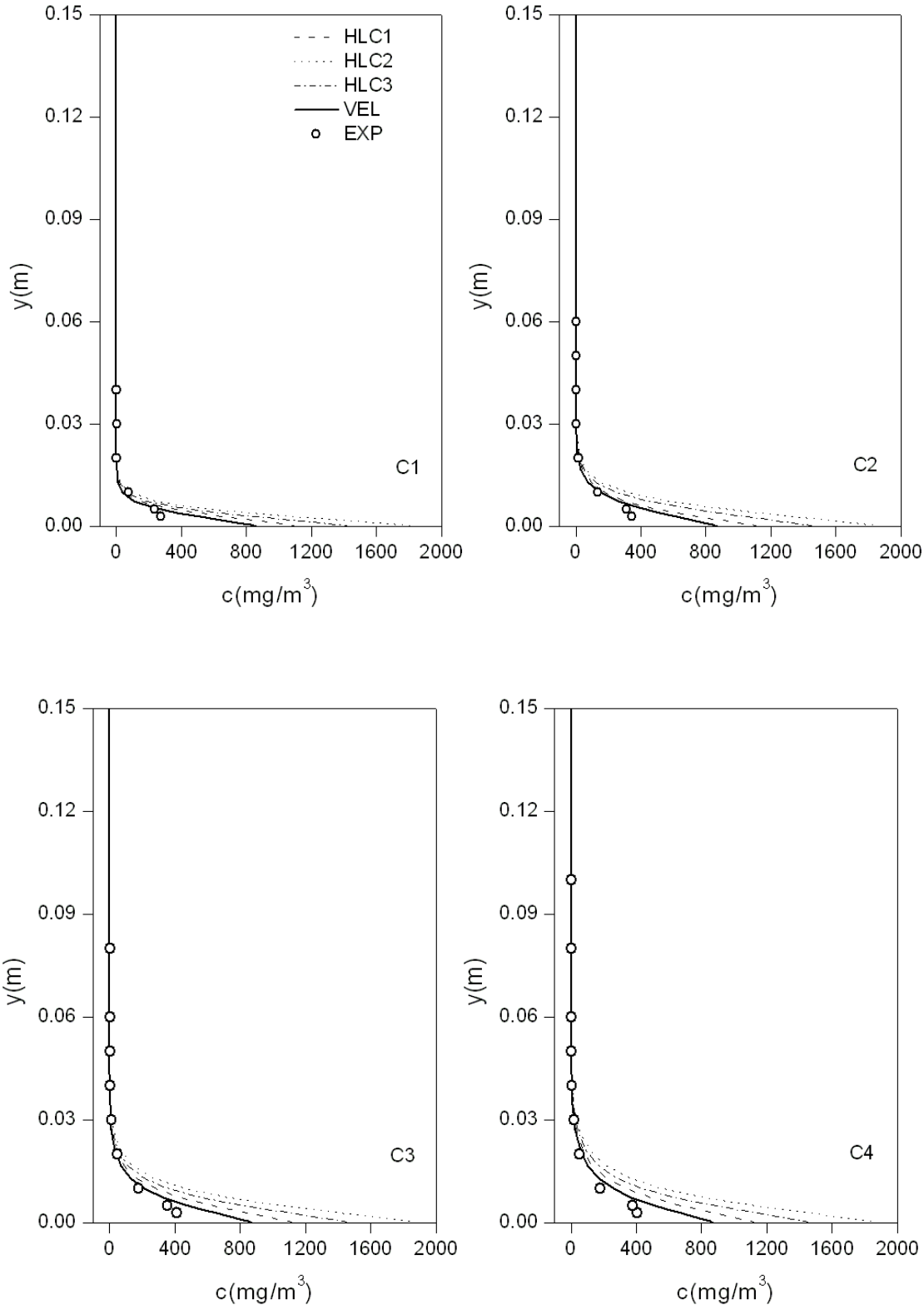
HLC1
HLC2
HLC3
VEL
EXP
C1
C2
C3
C4
y(m)
c(mg/m3)
0.15
0.12
0.09
0.06
0.03
0.00
0
400
800
1200
1600
2000

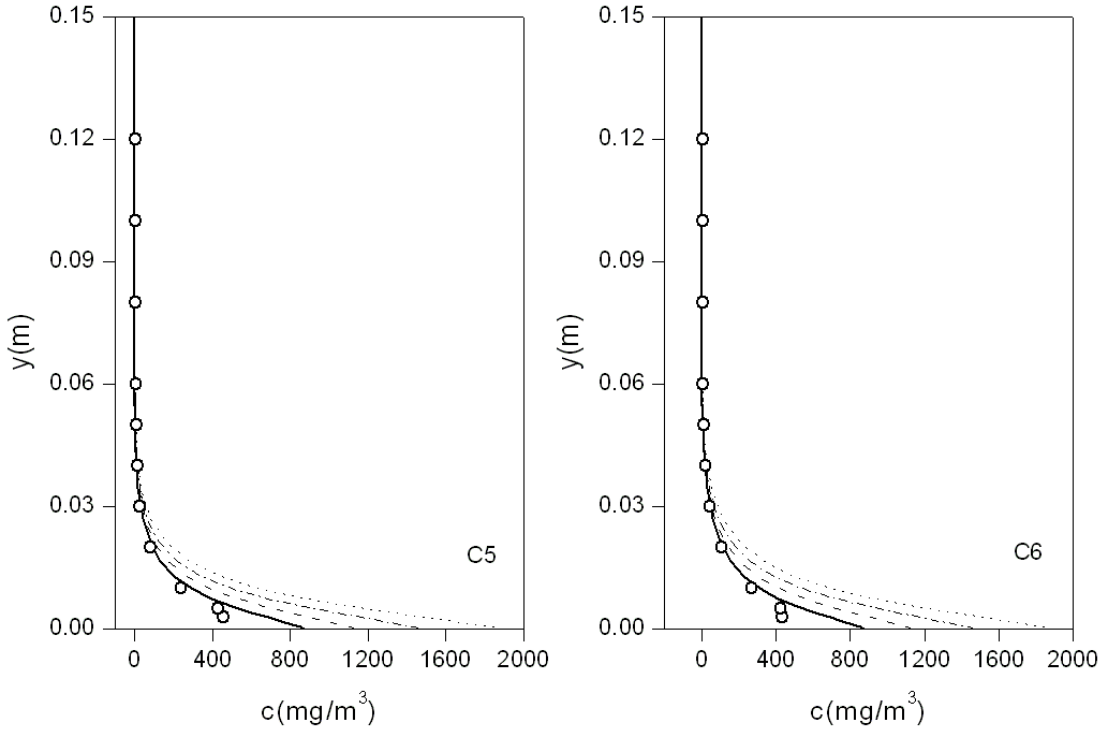

(a) Concentration profiles

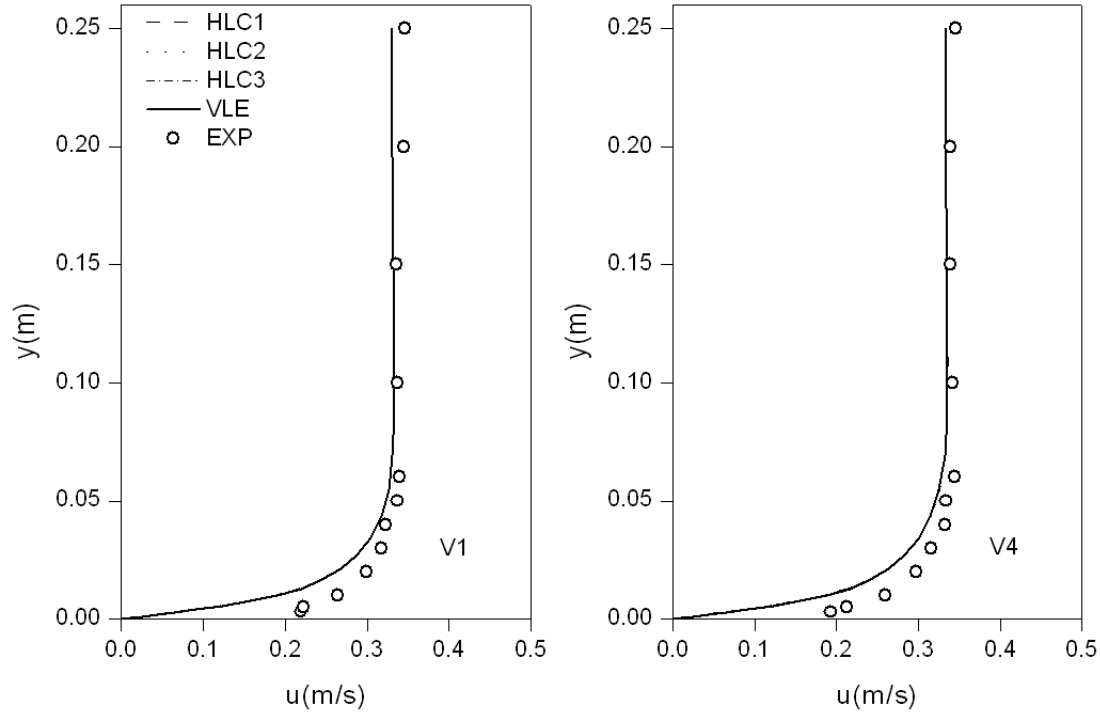

(b) Velocity profiles

Figure C.4 Comparison of concentration and velocity profiles between numerical simulations and measurements for case Tu10T22u3 using LRN model

Appendix D CFD results in a 2D full scale pig pen

D.1 Velocity and ammonia concentration distribution at different slatted floor opening ratios for mixing ventilation system type I and diffusive ceiling ventilation system

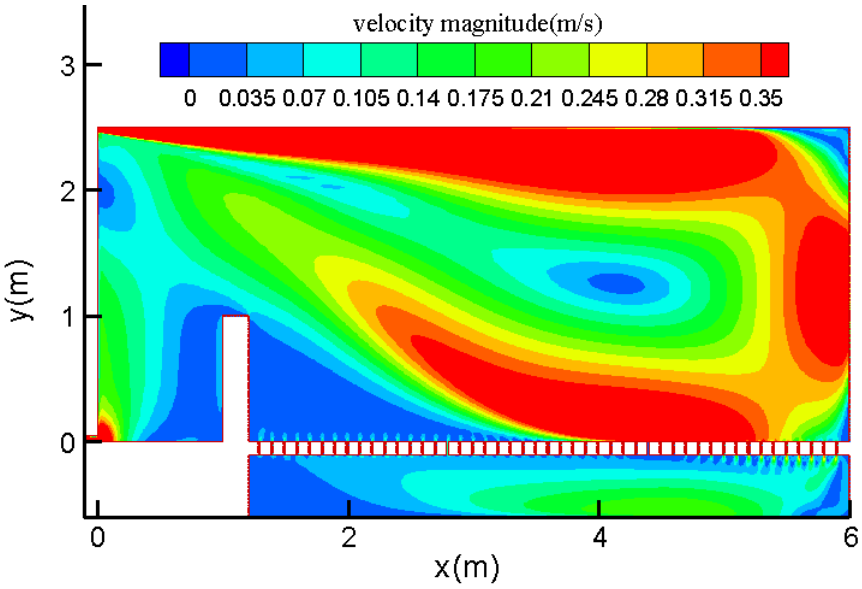

(a) Slatted floor Type A

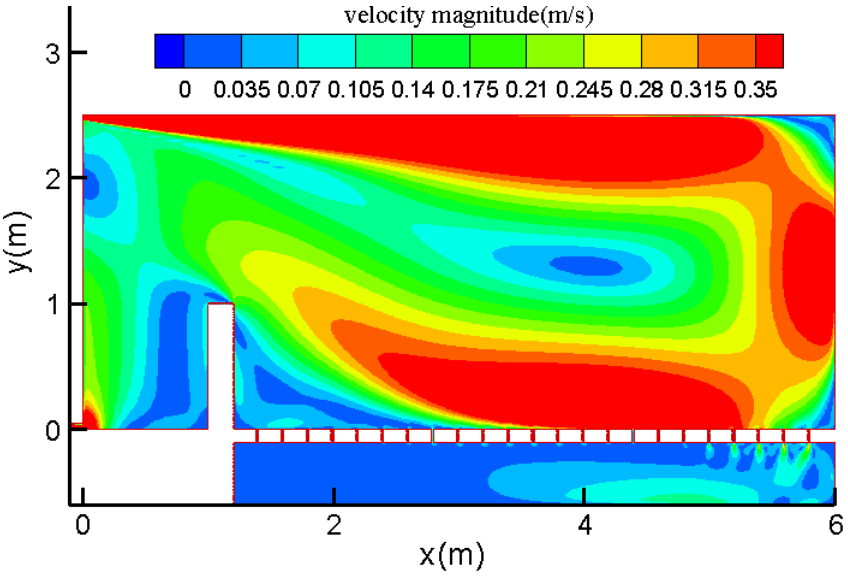

(b) Slatted floor Type B

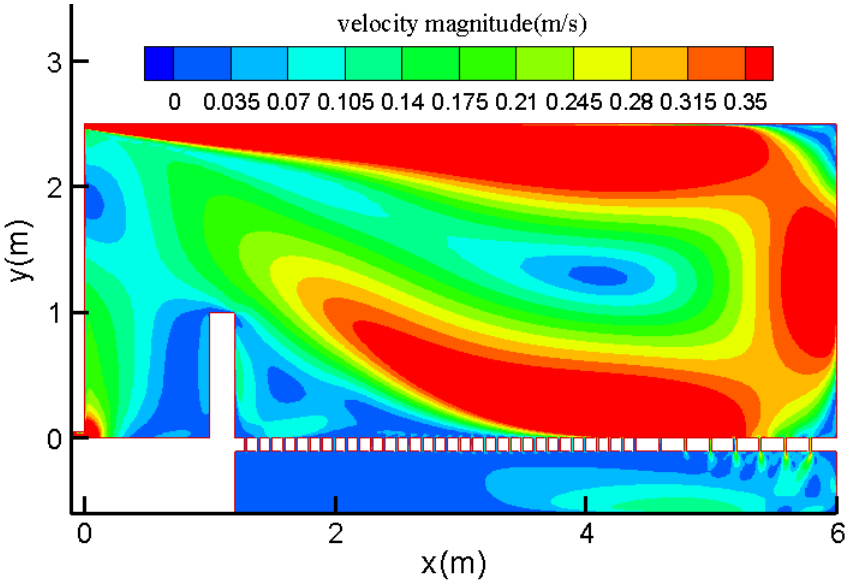

(c) Slatted floor Type C

Figure D.1 Velocity distribution of different slatted floor types for mixing ventilation system type I at 15ACH

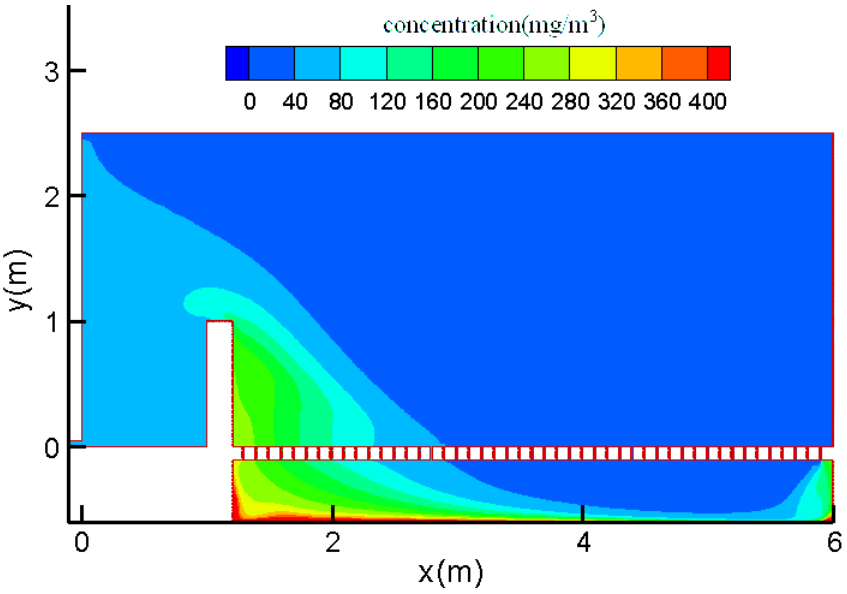

(a) Slatted floor Type A

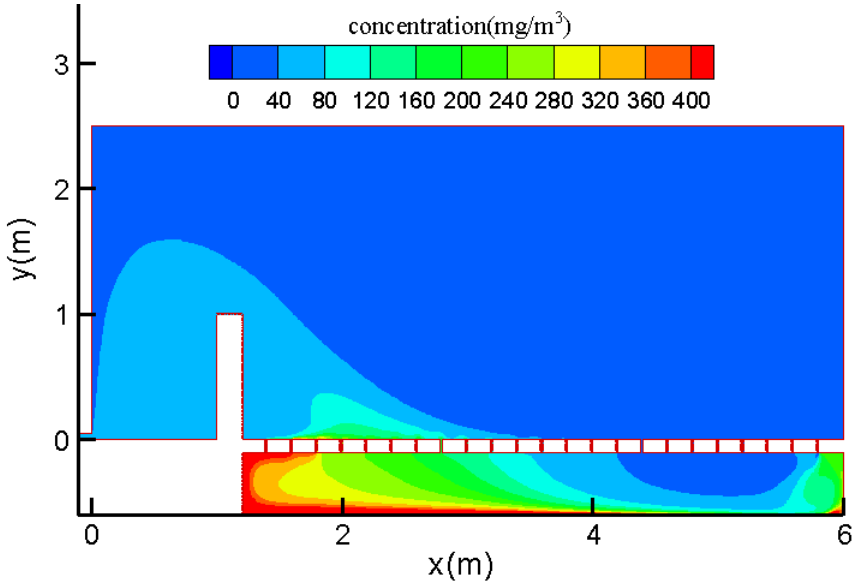

(b) Slatted floor Type B

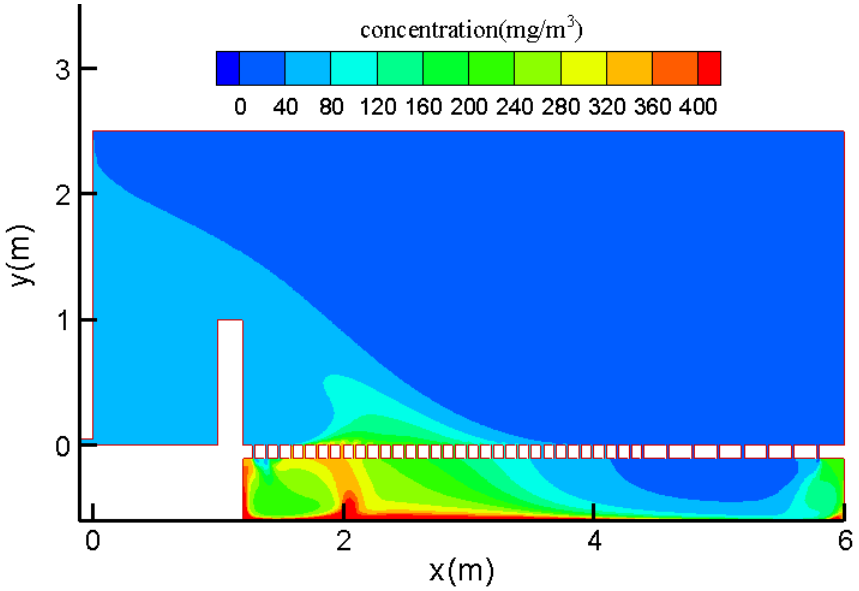

(c) Slatted floor Type C

Figure D.2 Concentration distribution of different slatted floor types for mixing ventilation system type I at 15ACH

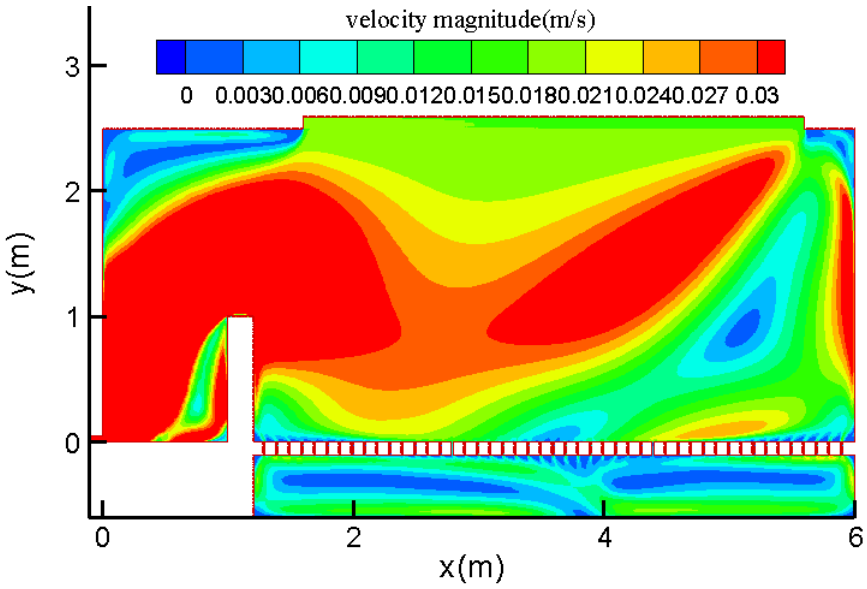

(a) Slatted floor Type A

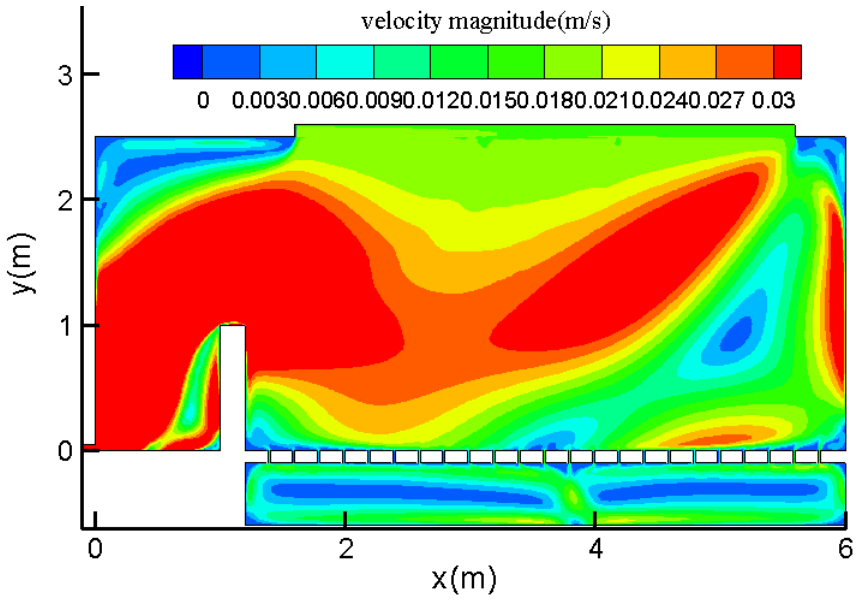

(b) Slatted floor Type B

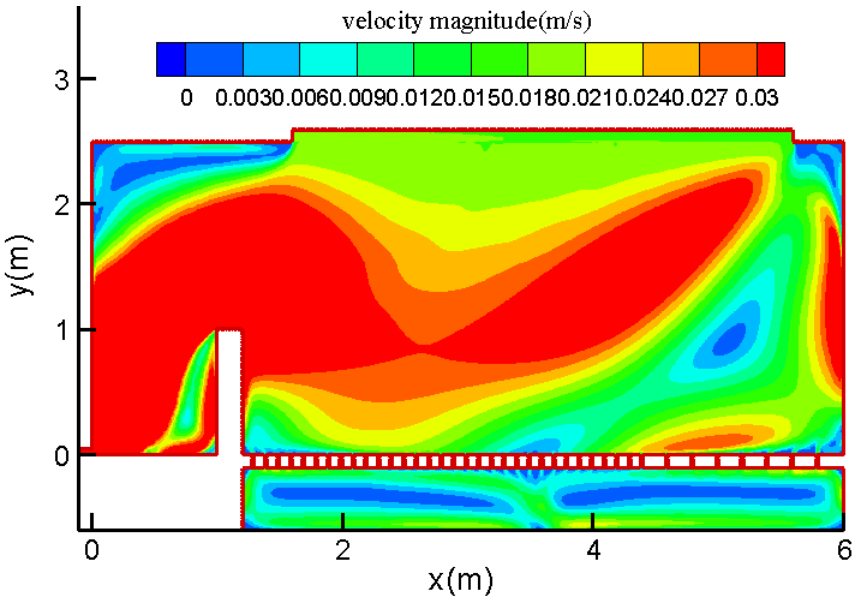

(c) Slatted floor Type C

Figure D.3 velocity distribution of different slatted floor types for diffusive ceiling ventilation system at 15ACH

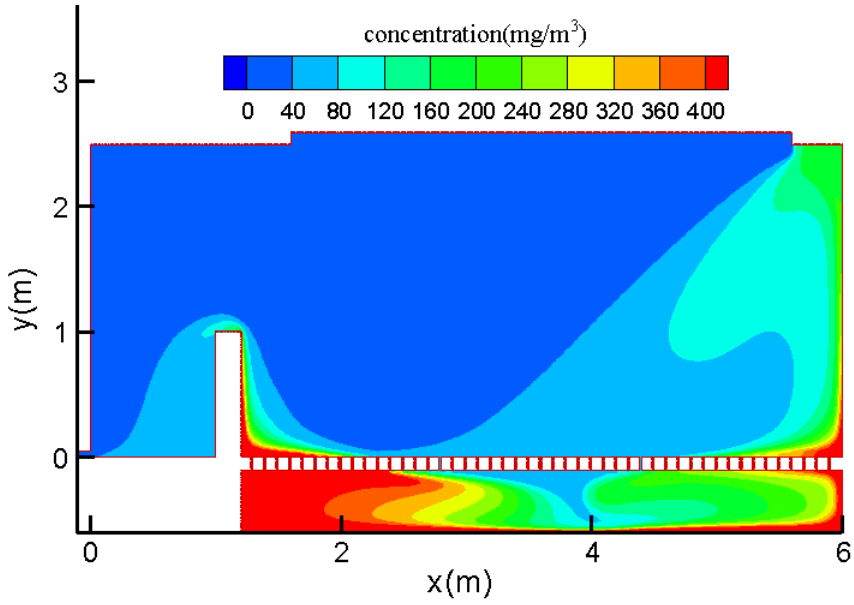

(a) Slatted floor Type A

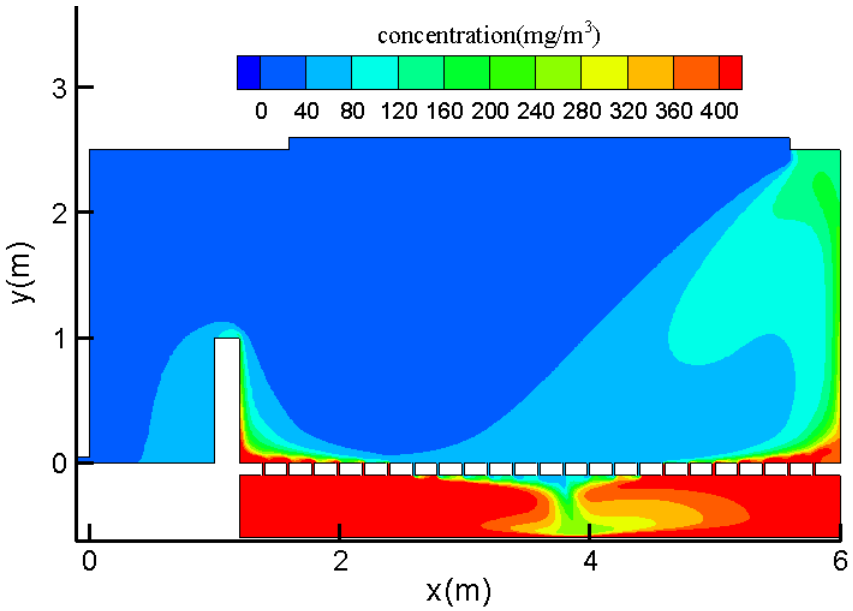

(b) Slatted floor Type B

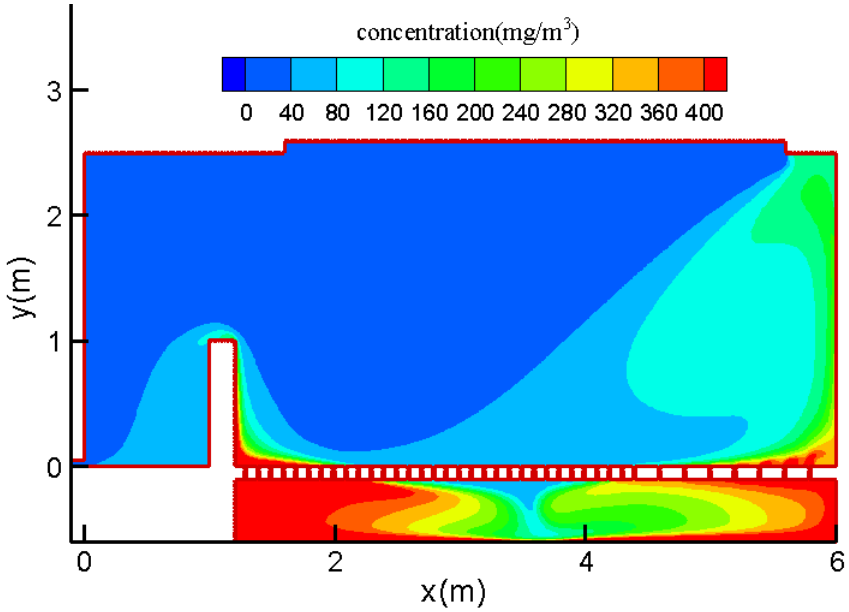

(c) Slatted floor Type C

Figure D.4 Concentration distribution of different slatted floor types for diffusive ventilation system at 15ACH

D.2 Velocity distribution of different ventilation rates for mixing ventilation system type I

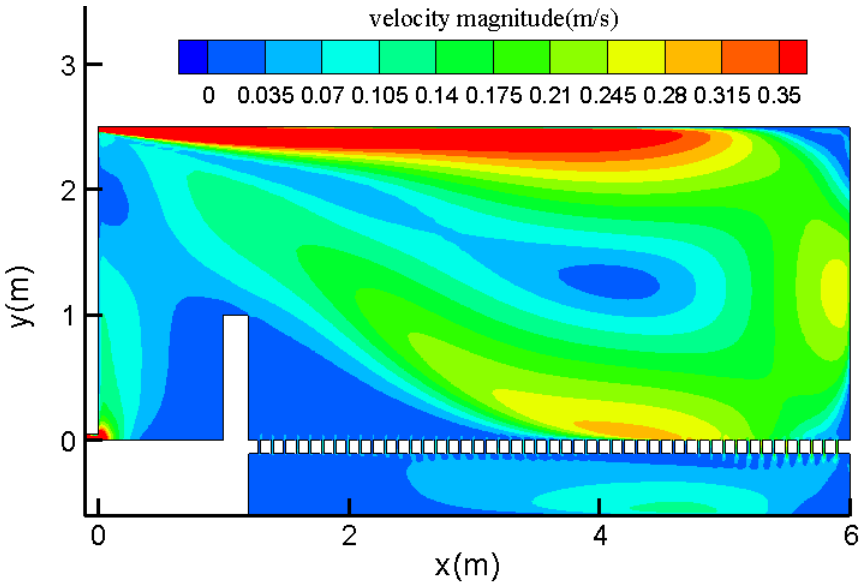

(a) N=9ACH

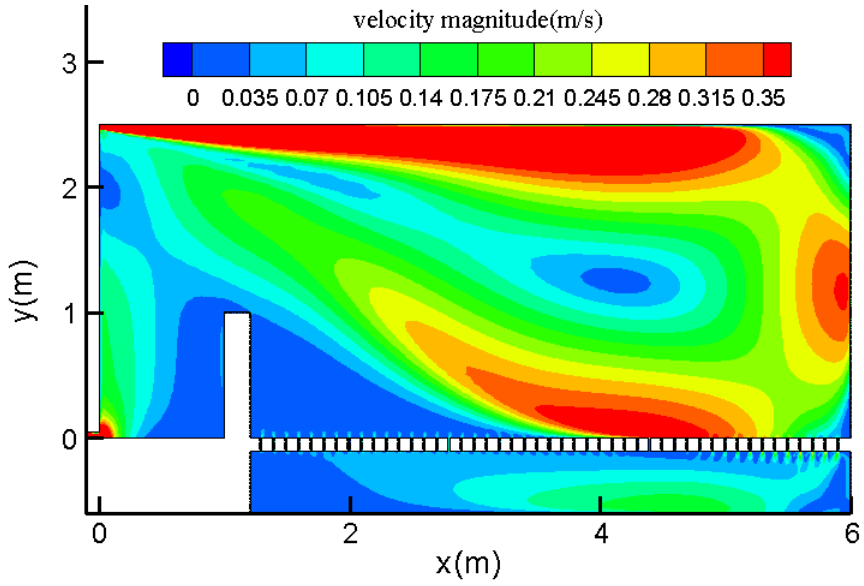

(b) N=12ACH

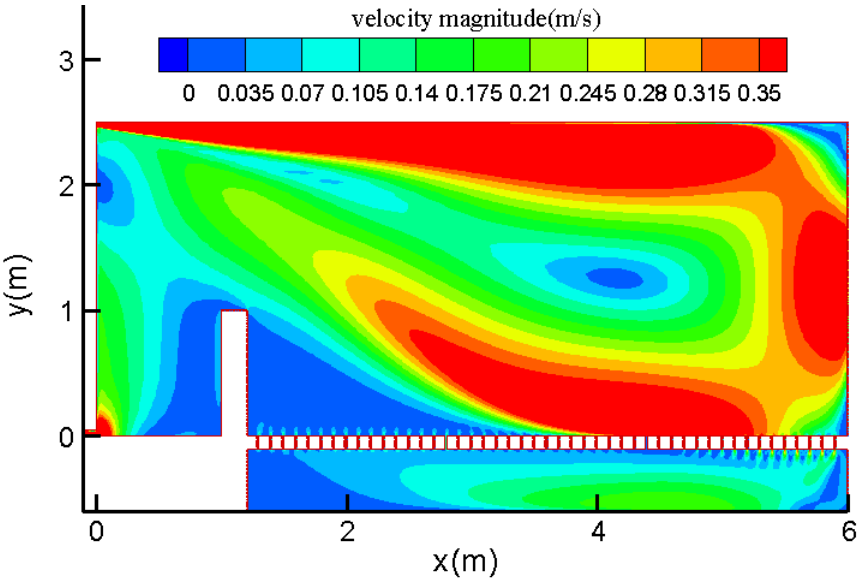

(c) N=15ACH

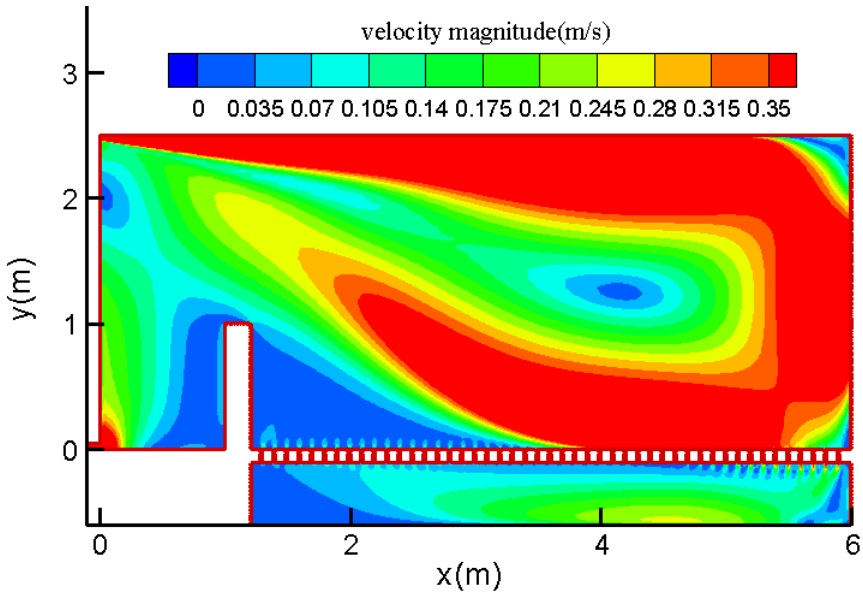

(d) N=18ACH

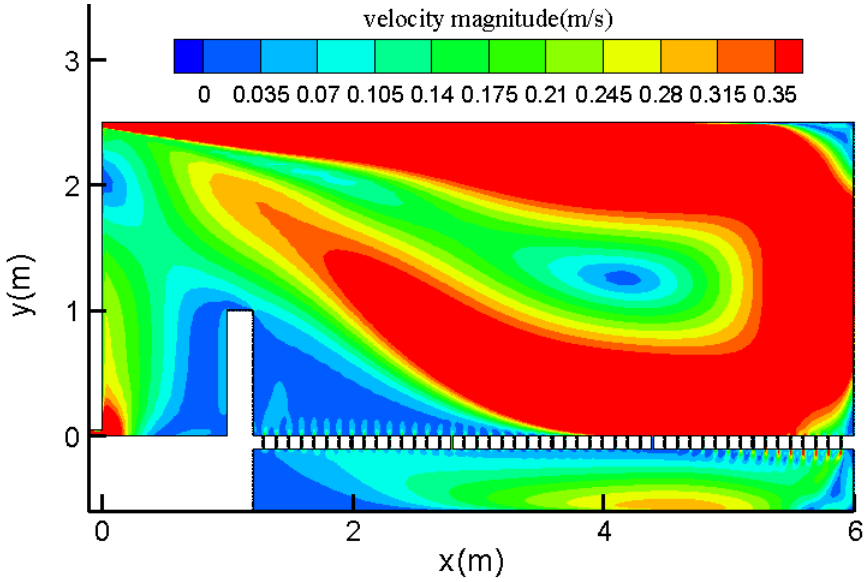

(e) N=21ACH

Figure D.5 Velocity distribution of different ventilation rate under mixing ventilation system type I

D.3 Velocity distribution of slatted floor type A under different ventilation systems

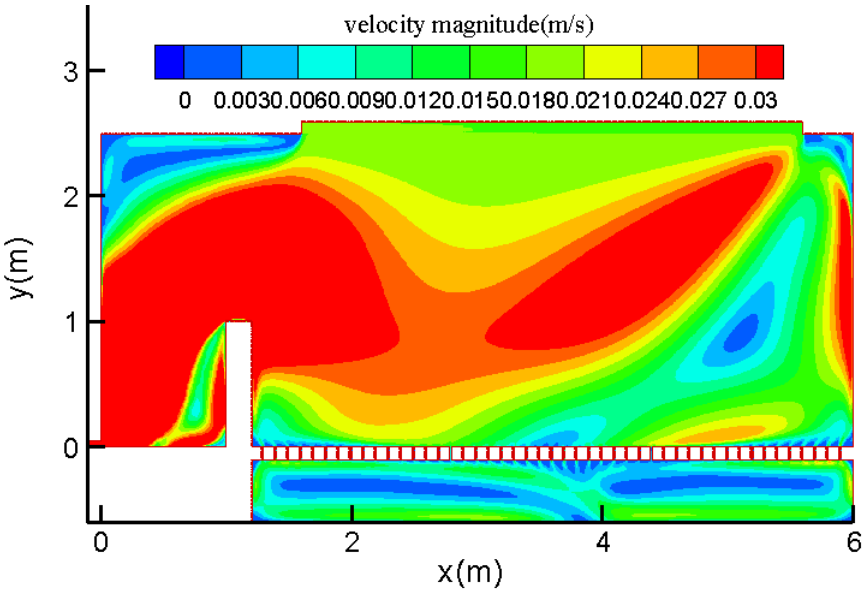

(a) Diffusive ceiling ventilation system

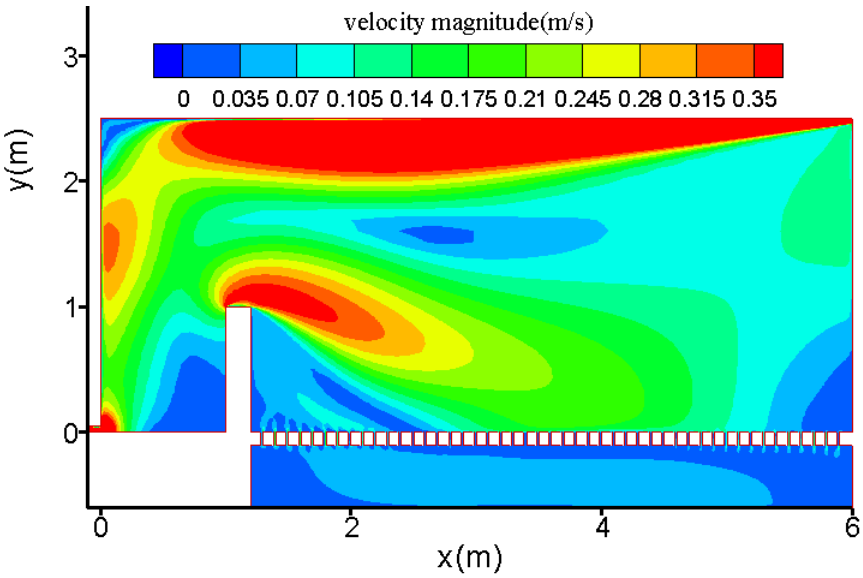

(b) Mixing ventilation system type II

Figure D.6 Velocity distribution of slatted type A under different ventilation systems at 15ACH

Reference

Aarnink A.J.A., Elzing A., 1998. Dynamic model for ammonia volatilization in housing with partially slatted floors for fattening pigs. Livestock Production Science, 53, 153-169.

Anderson G.A., Smith R.J., Bundy D.S.,Hammond E.G., 1987. Model to predict gaseous contaminants in swine confinement buildings. Journal of Agricultural Engineering Research, 37, 235-253.

Arogo J., Zhang R.H., Riskowski G.L., Christianson L.L., Day D.L., 1999. Mass transfer coefficient of ammonia in liquid swine manure and aqueous solutions. Journal of Agricultural Engineering Research, 73(1), 77-86.

Beutier D. and Renon H., 1978. Representation of Nh3-H2s-H2o, Nh3-Co2-H2o, and Nh3-So2-H2o Vapor-Liquid-Equilibria. Industrial & Engineering Chemistry Process Design and Development, 17(3), 220-230.

Bjerg B., Morsing S., Svidt K., Zhang G., 1999. Three-dimensional airflow in a livestock test room with two-dimensional boundary conditions. Journal of Agricultural Engineering Research, 74, 267-274.

Bjerg B., Svidt K., Zhang G., Morsing S., 2000. The effects of pen partitions and thermal pig simulators on airflow in a livestock test room. Journal of Agricultural Engineering Research, 77(3), 317-326.

Bjerg B., Svidt K., Zhang G., Morsing S., Johnsen J.O., 2002. Modeling of air inlets in CFD prediction of airflow in ventilated animal houses. Computers and electronics in agriculture, 34, 223-235.

Bjerg B., Zhang G., Kai P., 2008. Porous Media as Boundary Condition for Air Inlet, Slatted Floor and Animal Occupied Zone in Numerical Simulation of Airflow in a Pig Unit. In Agricultural & Biosystems Engineering for a Sustainable World – Proceedings of AgEng2008 International Conference on Agricultural Engineering, 23-25 June 2008, Crete, Greece. Paper No. OP-1520 on Proceeding CD.

Bird B.R., Stewart W.E., Lightfoot E.E., 1960. Transport Phenomena. John Wiley & Sons, Inc.

Chaoui H., Montes F., Rotz C.A., Richard T.L., 2009. Volatile ammonia fraction and flux thin layers of buffered ammonium solution and dairy cattle manure. Transactions of the ASABE, 52(5), 1695-1706.

Chen Q., 2009. Ventilation performance prediction for buildings: A method overview and recent applications. Building and Environment, 44, 848-858.

Choi K., Albright L.D., Timmons M.B., 1988. An application of the $k-\varepsilon$ turbulence model to predict air distribution in a slot ventilated enclosure. Transactions of the ASAE, 31, 1804-1814.

Choi K., Albright L.D., Timmons M.B., 1990. An application of the $k-\varepsilon$ turbulence model to predict how a rectangular obstacle in a slot ventilated enclosure affects airflow. Transactions of ASAE, 33, 274-281.

Cussler E. L. Diffusion: mass transfer in fluid systems. Cambridge University Press, 1985.

Cortus E.L., Lemay S.P., Barber E.M., Hill G.A., Godbout S., 2008. A dynamic model of ammonia emission from urine puddles. Biosystems Engineering, 99, 390-402.

Davison A.W., Cape J.N., 2003. Atmospheric nitrogen compounds-issues related to agricultural systems. Environmental International, 29, 181-187.

DPP, 2007. Annual Report 2007, Danish Pig Production Research Development. ISBN: 87-91460-09-3.

Erisman J.W., Bleeker A., Hensen A., Vermeulen A., 2008. Agricultural air quality in Europe and the future perspectives. Atmospheric Environment, 42, 3209-3217.

Fluent 6.3 User's guide, 2006. Fluent Inc.

Griffing E.M., Overcash M., Westerman P., 2007. A review of gaseous ammonia emissions from slurry pits in pig production systems. Biosystme Engineering, 97, 295-312.

Hales J. M. and Drewes D. R., 1979. Solubility of Ammonia in Water at Low Concentrations. Atmospheric Environment, 13(8), 1133-1147.

Harral B.B., Boon C.R., 1997. Comparison of Predicted and Measured Air Flow Patterns in a Mechanically Ventilated Livestock Building without Animals. Journal of Agricultural Engineering Research, 66, 221-228.

Hoff S.J., Janni K.A., Jacobson L.D., 1992. Three-dimensional buoyant turbulent flows in a scaled model, slot-ventilated, livestock confinement facility. Transactions of ASAE, 35(2), 671-686.

Hoff S. J., Li L., Tsao L., 1995. Simulated and measured effect of rectangular obstructions on carbon dioxide gas dispersion in a scaled swine building. Transactions of ASAE, 38(5), 1519-1532.

Hudson N., Ayoko G.A., 2008. Odour sampling. 2. Comparison of physical and aerodynamic characteristics of sampling devices: A review. Bioresource Technology, 99, 3993-4007.

Hudson N., Ayoko G.A., Dunlop M., Duperouzel D., Burrell D., Bell K., Gallagher E., Nicholas P., Heinrich N., 2009. Comparison of odour emission rates measured from various sources using two sampling devices. Bioresource Technology, 100, 118-124.

Kays W.M., rawford M.E. Convective heat and mass transfer. Fourth edition, 2005, McGraw-Hill book company.

Loubet B., Cellier P., Flura D., Genermont S., 1994a. An evaluation of the wind tunnel technique for estimating ammonia volatilization from land—part 1: analysis and improvement of accuracy. Journal of Agricultural Engineering Research, 72, 71-82.

Loubet B., Cellier P., Genermont S., Flura D., 1994b. An evaluation of the wind tunnel technique for estimating ammonia volatilization from land—part 2: influence of the tunnel on transfer processes. Journal of Agricultural Engineering Research, 72, 83-92.

Lynch J. A. and Kerchner M., 2005. The National Atmospheric Deposition Program: 25 years of monitoring in support of science and policy: An ammonia workshop: the state of science and future needs. Environmental Pollution, 135(3), 343-346.

Menter F.R., 1994. Two-equation eddy-viscosity turbulence models for engineering applications. Journal of AIAA, 32(8), 1598-1605.

Montes F., Rotz C.A., Chaoui H., 2009. Process Modeling of Ammonia Volatilizationo from Ammonium Solution and Manure Surfaces: A Review with Recommended Models. Transactions of the ASABE, 52(5), 1707-1719.

Mortimer R.G., 2008. Physical Chemistry, third edition. Elsevier Academic Press.

Ni J., 1998. Emission of carbon dioxide and ammonia from mechanically ventilated pig house. PhD thesis, Catholic University of Leuven.

Ni J.Q., 1999. Mechanistic models of ammonia release from liquid manure: a review. Journal of Agricultural Engineering Research, 72, 1-17.

Ni J., Hendriks J., Vinckier C., Coenegrachts J., 2000. Development and validation of a dynamic mathematical model of ammonia release in pig house. Environment International, 26, 105-115.

Nielsen P.V. (ed.), Allard F., Awbi H.B., Davidson L., Schaalin A., 2007. Computational Fluid Dynamics in Ventilation Design. REHVA Guidebook No.10, Forssa, Finland.

Norton T., Sun D., Grant J., Fallon R., Dodd V., 2007. Applications of computational fluid dynamics (CFD) in the modeling and design of ventilation systems in the agricultural industry: A review. Bioresource Technology, 98, 2386-2414.

NRC, 2003. Air Emissions from Animal Feeding Operations: Current Knowledge, Future Needs. Ad Hoc Committee on Air Emissions from Animal Feeding Operations, Committee on Animal Nutrition, National Research Council, 241pp.

Olesen J.E., Sommer S.G., 1993. Modeling effects of wind speed and surface cover on ammonia volatilization from stored pig slurry. Atmospheric Environment, 27A(16), 2567-2574.

Patek J., Klomfar J., 1995. Simple functions for fast calculations of selected thermodynamic properties of the ammoina-water system. International Journal of Refrigerator, 18(4), 228-234.

Phillips V.R., Scholtens R., Lee D.S., Garland J.A., Sneath R.W., 2000. A Review of Methods for Measuring Emission Rates of Ammonia from Livestock Buildings and Slurry or Manure Stores, Part 1: Assessment of Basic Approaches. Journal of Agricultural Engineering Research, 77(4), 355-364.

Portejoie S., Martinez J., Guiziou F., Coste C.M., 2003. Effect of covering pig slurry stores on the ammonia emission processes. Bioresource Technology, 87, 199-207.

Radom K., Blainey D., Blainey J., Danuser B., Iversen M., Monso E., Opravil U., Weber C., Nowak D., 1999. Respiratory symptoms in European pig farmers. In: International Symposium on Dust Control in Animal Production Facilities. Aarhus, Denmark.

Rong L., Nielsen P.V., Zhang G., 2009. Effects of airflow and liquid temperature on ammonia mass transfer above an emission surface: Experimental study on emission rate. Bioresource Technology, 100, 4654-4661.

Rong L., Nielsen P.V., Tong G., Ravn P., Zhang G., 2008. Computational fluid dynamics study on the influence of airflow patterns on carbon dioxide distribution in a scaled livestock building. In Agricultural & Biosystems Engineering for a Sustainable World – Proceedings of AgEng2008 International Conference on Agricultural Engineering, 23-25 June 2008, Crete, Greece. Paper No. OP-1190 on Proceeding CD.

Said M.N.A., Jouini D.B., Plett E.G., 1993. Influence of turbulence parameters at supply inlet on room air diffusion. ASME winter annual meeting, New Orleans, USA.

Sala O.E., Chapin Ⅲ F.S., Armesto J.J., et al., 2000. Global biodiversity scenarios for the year 2100. Science, 287, 1770-1774.

Schlichting H., 1979. Boundary layer theory, seventh edition, McGraw-Hill Book Company.

Seedorf J., Hartung J., 1999. Survey of ammonia concentrations in livestock buildings. Journal of Agricultural Science, Cambridge 133, 433-437.

Shah S.B., Westerman P.W., Arogo J., 2006. Measuring Ammonia Concentrations and Emissions from Agricultural Land and Liquid Surfaces: A Review. Journal of the Air & Waste Management Association, 56, 945-960.

Sharma, N., Chaudhry, K.K., Chalapati Ral, C.V., 2005. Air pollution dispersion studies through environmental wind tunnel (EWT) investigations: a review. Journal of Scientific and Industrial Research 64, 549–559.

Sissom L.E., Pitts D.R., 1972. Elements of Transport Phenomena. McGraw-Hill, Inc.

Smith R.J., Dalton P.A., 1999. Environmental odours from Australian piggeries. Environmental Engineering Conference, Auckland, New Aealand, 10-14 July.

Smith R.J., Watts P.J., 1994a. Determination of odour emission rates from cattles feedlots—part1: a review. Journal of Agricultural Engineering Research, 57, 145-155.

Smith R.J., Watts P.J., 1994b. Determination of odour emission rates from cattles feedlots — part 2: evaluation of two wind tunnels of different size. Journal of Agricultural Engineering Research, 58, 231-240.

Smith R.J., 1993. Dispersion of odours from ground level agricultural sources. Journal of Agricultural Engineering Research, 54, 187-200.

Soerensen D.N., Nielsen P.V., 2003. Quality control of computational fluid dynamics in indoor environments. Indoor Air, 13, 2-17.

Staudinger J., Roberts P.V., 1996. A critical review of Henry's law constants for environmental applications. Critical Reviews in Environmental Science and Technilogy. 26(3), 205-297.

Staudinger J., Roberts P.V., 2001. A critical compilation of Henry's law constant temperature dependence relations for organic compounds in dilute aquesous solutions. Chemosphere, 44(4), 561-576.

Sun H., Keener H., Deng W., 2004. Development and validation of 3-D CFD models to simulate airflow and ammonia distribution in a high-rise hog building during summer and winter conditions. Agricultural Engineering International: the CIGR Journal of Science Research and Development. Manuscript BC 04 004. Vol. Ⅵ.

Sun H., Stowell R., Keener H., Elwell D., Michel F., 2002. Two-dimensional computational fluid dynamics modeling of air velocity and ammonia distribution in a high rise hog building. Transaction of the ASAE, 45, 1559-1568.

Topp C., 1999. Diffusion and Evaporation-Controlled Emission in Ventilated Rooms. PhD thesis, Aalborg University.

Van der Peet-Schwering C.M.C., Aarnink A.J.A., Rom H.B., Dourmad J.Y., 1999. Ammonia emissions from pig houses in the Netherlands, Denmark and France. Livestock Production Science, 58, 265-269.

Van Wagenberg A.V., Bjerg B., Bot G.P.A., 2004. Measurements and simulation of climatic conditions in the animal occupied zone in a door ventilated room for piglets. Agricultural Engineering International: the CIGR Journal of Scientific Research and Development, Manuscript BC 03 020, Vol Ⅵ.

Wilcox D.C., 2004. Turbulence Modeling for CFD. DCW Industries, Inc.

Yang X.D., 1999. Study of Building Material Emissions and Indoor Air Quality. PhD thesis, MIT.

Ye, Z.Y., Zhang, G.Q., Li, B.M., Stroem, J.S., Tong, G.H., Dahl, P.J., 2008. Influence of airflow and liquid properties on the mass transfer coefficient of ammonia in aqueous solutions. Biosystems Engineering, 100(3), 422-434.

Ye Z., Zhang G., Seo I.-H., Kai P. Saha C.K., Wang C., Li B., 2009. Airflow characteristics at the surface of manure in a storage pit affected by ventilation rate, floor slat opening and headspace height. Biosystems Engineering, 104, 97-105.

Zhang Y., Wu Shiang-Yuh, Krishnan S., Wang K., Queen A., Aneja V.P., Arya S.P., 2008. Modeling agricultural air quality: Current status, major challenges and outlook. Atmospheric Environment, 42, 3218-3237.

Nomenclature

A	Emission surface area(m^2)
$c_{0,g}$, c_0	Concentration in the bulk gas phase(kg/m^3)
c	Concentration(kg/m^3)
c_i	Concentration at the inlet(kg/m^3)
c_r	Concentration at the outlet(kg/m^3)
$c_{w,g}$	Concentration on the emission surface(kg/m^3)
$c_{w,l}$	Concentration in the liquid phase through liquid-gas interface(kg/m^3)
$c_{0.l}$	Concentration in the bulk liquid(kg/m^3)
D_a	Diffusive coefficient of ammonia in the air(m^2/s)
E	Emission rate(kg/s)
E_{CFD}	Ammonia emission rate achieved from CFD simulation(kg/s)
E_{Exp}	Ammonia emission rate achieved from measurements(kg/s)
ERR	Ratio of ammonia emission rate between simulated and measured results
$\sum v$	Molecular volumes
h_c	Mass transfer coefficient(m/s)
J	Mass flux($kg/m^2.s$)
k	Turbulent kinetic energy(J/kg)
K_d	Dissociation constant(-)
K_a	Association constant(-)
K_h	Henry's law constant(-)
L	Characteristic length(m)
M_{air}	Molecular weight of air(g/mol)
M_{NH_3}	Molecular weight of NH_3
m_x	Ammonia mass fraction in the liquid(-)
m_y	Ammonia mass fraction in the air(-)
Δp	Pressure drop over the porous media(Pa)
p	Ammonia partition pressure in the air(atm)
Q	Airflow rate(m^3/s)
R_1	Internal resistance coefficient for porous media
R_2	Viscous resistance coefficient for porous media

Re_L	Reynolds number(-)
Sc	Schmidt number(-)
Sh	Sherwood number(-)
S_Φ	Source term for Φ
T	Ammonium solution temperature(K)
T_{air}	Temperature of the air(℃)
T_{liquid}	Temperature of the liquid(℃)
Tu	Turbulence intensity(-)
u	Velocity component in main flow direction(m/s)
u_*	Friction velocity(m/s)
u_{center}	Velocity in the center of the wind tunnel(m/s)
u_i	Time-averaged velocity component(m/s)
u'	Velocity fluctuation(m/s)
u^+	Dimensionless velocity(-)
v	Velocity through the porous media(m/s)
x	Co-ordinate(m)
x_i , x_j	Co-ordinate(m)
y	Co-ordinate(m)
y^+	Dimensionless distance(-)

Greek symbols

$\delta_{(x)}$	Concentration boundary layer (m)
δ	Velocity boundary layer thickness(m)
δ_D	Concentration boundary layer thickness(m)
Φ	Representatives of time-averaged velocity component, turbulent kinetic energy, dissipation of turbulent kinetic energy, specific dissipation rate, species, temperature
Γ_Φ	Effective diffusion coefficient for Φ
μ	Dynamic viscosity(kg/m.s)
ρ	Density(kg/m^3)
τ	Time(s)
τ_w	Wall shear stree(N/m^2)

Abbreviations

CFD	Computational Fluid Dynamics
DNS	Direct Numerical Simulation
HLC	Henry's Law Constant
LES	Large Eddy Simulation
RANS	Reynolds-Averaged Navier-Stokes
RNG	Renormalization Group
SST	Shear Stress Transport
VLE	Vapor-Liquid Equilibrium

ISSN 1901-7294
DCE Thesis No. 25